REEF DISSOLUTION

Rates and mechanisms of coral dissolution by bioeroding sponges and reef communities

Alice Emma Webb

Members of the reading committee:
Dr. J.M. de Goeij, University of Amsterdam
Dr. J.-P. Gattuso, University Pierre et Marie Curie-Paris 6
Prof. dr. J.B.M. Middelburg, Utrecht University
Prof. dr. J.W.F. Reumer, Utrecht University
Dr. K. Soetaert, NIOZ Royal Netherlands Institute for Sea Research (NWO)

Funding for this project was provided by the Netherlands Organization for Scientific Research (NWO2g Grants 858.14.021 and 858.14.022)

Cover design Robin Tumoine and Alice Webb
Printed by Ipskamp
ISBN: 978-94-028-1684-6

Reef Dissolution

Rates and mechanisms of coral dissolution by bioeroding sponges and reef communities

Het oplossende rif

Snelheden en mechanismen van het oplossen van koraalriffen door boorsponzen en rifgemeenschappen

(met een samenvatting in het Nederlands)

Proefschrift
ter verkrijging van de graad van doctor aan de
Universiteit Utrecht
op gezag van de
rector magnificus, prof.dr. H.R.B.M. Kummeling,
ingevolge het besluit van het college voor promoties
in het openbaar te verdedigen op
vrijdag 4 oktober 2019 des middags te 12.45 uur

door

Alice Emma Webb

geboren op 3 augustus 1988
te Rennes, Frankrijk

Promotor
Prof. dr. G.-J. Reichart

Co-promotors
Dr. L.J. de Nooijer
Dr. F.C. van Duyl

Contents

Chapter 1

General Introduction

'The errors and the dreams of science have been numerous. We have had the flints on the upper chalk formation attempted to be accounted for as the coprolites of whales; the 16^{th} and 17^{th} century gives us the wonderful story of the goose which developed from barnacles, and now we have a 'burrowing or boring sponge'.' (Waller 1871)

{*As seawater transits across a coral reef, it has a certain composition of ions, inorganic and organic carbon and nutrients that reef inhabitants utilise to build their soft and hard tissues. From these basic ingredients and the assistance of the sun, corals and many other calcifiers build immense reef structures that support an extraordinary heterogeneity of marine organisms. Within these reefs, free-living as well as symbiotic algae, take up dissolved inorganic carbon from the water column by photosynthesis to produce oxygen and organic matter which serves as a source of energy to heterotrophic organisms on the reef. Ancillary to photosynthesis, dissolved inorganic carbon is utilised in combination with calcium ions by calcifying organisms to generate skeletons and shells which form the solid backbone of coral reefs. The immense variety of biomineralisers is balanced by an equally diverse community of organisms capable of dissolving them or breaking them down into smaller pieces. Euendolithic microorganisms such as cyanobacteria, algae and fungi actively penetrate into carbonate substrates by a series of chemically driven mechanisms while parrot fish scrape away coral structures by grazing freshly grown algae. Boring sponges choose for a combination of dissolution and mechanical chip removal to carve their way into coral skeleton. The long-term success of coral reefs depends on a positive balance of calcium carbonate production exceeding dissolution and erosion.*}

1 Climate change and ocean acidification

The unprecedented intensification of anthropogenic activity over the past centuries is having severe repercussions on the global climate (IPCC 2018). Rapid burning of fossil fuel reserves and deforestation are instigating an exponential rise in carbon dioxide (CO_2) emissions (Raupach et al., 2007). Since the industrial revolution, atmospheric CO_2 levels increased from approximately 280 to 410 ppm (for the most current measurements see: https://www.co2.earth/). While approximately a quarter of the released CO_2 is taken up by organisms, the majority remains in the atmosphere $[CO_2]$atm, causing the surface of the earth to heat up. Yet, another considerable fraction of anthropogenic emissions ($\sim$25%, which equals 2.2 Pg C year^{-1}) dissolves into the ocean (Sabine et al., 2004; Canadell et al., 2007). As this fraction of CO_2 enters the ocean, it reacts with the water to form carbonic acid. Subsequently, carbonic acid rapidly dissociates forming bicarbonate ions and protons, reducing the seawater pH (Raven et al., 2005) (Box 1). The accelerated dissolution of CO_2 in the past century has led today to an average decline by 0.1 pH units of surface ocean waters, which translates to a 30% rise in acidity (IPCC 2018). A further decrease of 0.3–0.4 pH units is expected if $[CO_2]$atm reaches 800 ppm, the projected end-of-century concentration according to the business-as-usual emission scenario of the Intergovernmental Panel

on Climate Change (IPCC). Under high-CO_2 conditions, carbonate ions are withdrawn from the pool that is available to biochemical cycles as the relative abundance of bicarbonate ions increases (Guinotte and Fabry, 2008; Doney et al., 2009; Hendriks et al., 2010). Consequently, the calcium carbonate ($CaCO_3$) saturation state decreases, which is generally believed to impair formation of shells and skeletons by calcifying organisms (Kleypas et al., 2005; Doney et al., 2009 and references therein). On an ecosystem level, the effects of ocean acidification may be the most pronounced on coral reefs (Kleypas et al., 1999; Langdon et al., 2000; Hoegh-Guldberg et al., 2007; Kleypas and Yates, 2009; Hughes et al., 2017).

Box 1 - Ocean acidification (OA)

$CO_2 + H_2O \leftrightarrow H_2CO_3$	Diffusion of CO_2 into water (H_2O) results in the formation of carbonic acid (H_2CO_3).
$H_2CO_3 \leftrightarrow H^+ + HCO_3^-$	Carbonic acid rapidly dissolves to form protons (H^+) and bicarbonate (HCO_3^-).
$CO_3^{2-} + H^+ \leftrightarrow HCO_3^-$	The available protons are neutralized by carbonate ions (CO_3^{2-}) which are naturally saturated in seawater therewith forming more bicarbonate.
$CO_2 + H_2O + CO_3^{2-} \leftrightarrow 2HCO_3^-$	Net reaction.

2 Coral reef ecosystems

Coral reefs are exceptionally diverse and rich ecosystems, typically found in shallow (sub)tropical waters between latitudes 30°S and 30°N (Connell, 1978; Reaka-Kudla, 1997; Spalding et al., 2001). The complex physical topography created by calcifying stony corals underpins (by large) these hotspots of biodiversity (Odum and Odum, 1955; Grigg et al., 1984). The structural framework promotes complex ecosystem functioning and niche partitioning which supports this extraordinary heterogeneity of associated biota. Although the large limestone structures that form the fundament of a coral reef represents only less than one percent of the sea floor, they provide a home to almost one third of all marine species (Mcallister, 1991; Spalding and Grenfell, 1997). These rich ecosystems provide nutrition and income to tens of millions of people through fisheries, tourism and protection of the coastline (Smith, 1978; Cesar

et al., 2003; Spalding et al., 2017). As such, coral reefs are indispensable to the world we live in today. However, they are currently deteriorating at a catastrophic rate due to a variety of pressures associated with increased anthropogenic activity on both a global and local scale (Gardner et al., 2003; Jackson et al., 2014). The impact of the exponential increase of greenhouse gas concentrations and its effects on the global climate evidently impact coral reefs as well (Pandolfi et al., 2003; Wilkinson, 2004). The reduced carbonate ion availability caused by ocean acidification affects precipitation of $CaCO_3$ by corals (Gattuso et al., 1998; Pandolfi et al., 2011; Dove et al., 2013). Ancillary to this, warming of surface waters is compromising the symbiosis of corals and photosynthetic zooxanthellae, causing frequent occurrence of region-wide mass bleaching and mortality of corals (e.g. Glynn, 1996; Hoegh-Guldberg, 1999; Dove and Hoegh-Guldberg, 2006; Eakin et al., 2010; Grottoli et al., 2014; Hughes et al., 2017).

While reef degradation is a worldwide phenomenon, the declining trend appears most prominent in the western Atlantic. Throughout the Caribbean and Gulf of Mexico, local stressors intensify the impact of global change on the ecological status of reefs. Factors including overharvesting of fish and declining water quality greatly reduce coral resilience towards bleaching or diseases (Jackson et al., 2001; Hughes et al., 2003; Knowlton and Jackson, 2008; Vega Thurber et al., 2014). Since coral reefs thrive in oligotrophic conditions, the addition of nutrients and organic matter through untreated sewage and terrestrial run-off reduces their competitive advantage over other sessile reef organisms (Hughes, 1994; Fabricius, 2005). This can be ascribed to increased local pressure associated with the unprecedented human population expansion in the region. Since the 1950s, the total population in the Caribbean has more than doubled (Guzman et al., 2006). In addition, Caribbean surface water is significantly impacted by discharge from the major rivers like the Amazon and Orinoco. This is exacerbated by the basin-like morphological and hydrological features that then promote the retention of polluted and eutrophied water within the Caribbean basin (Roff and Mumby, 2012).

Present Caribbean reefs bear very little resemblance in configuration with those existing pre-1980s, in terms of benthic composition, coral cover and structural complexity (De Bakker et al., 2017). Opportunistic organisms, such as algae, sponges and benthic cyanobacteria can more rapidly convert available sustenance into biomass which has resulted in a considerable increase in their abundance under eutrophic conditions. The evident decline in coral cover and the deviation from historical species configuration with a dominance of reef-building species, as well as the recognised impacts of ongoing ocean acidification and eutrophication on calcification and bioerosion processes (Schönberg et al., 2017; Webb et al., 2017, 2019), are likely to drastically reduced the biogenic calcifying capacity of these reefs. In-situ benthic metabolism

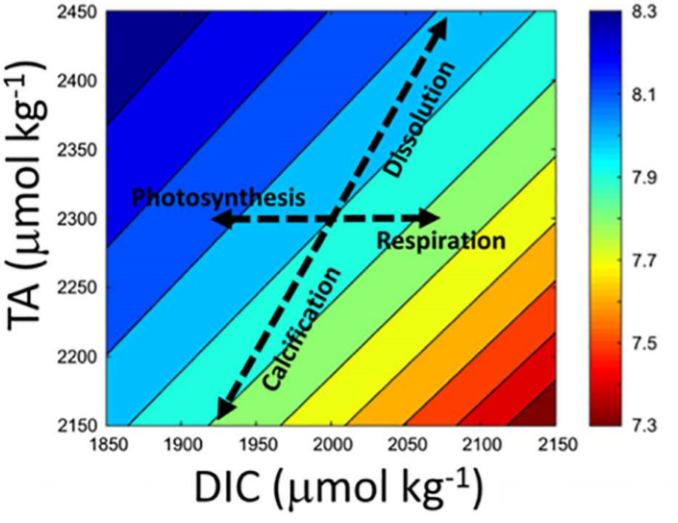

Figure 1: Dominant metabolic processes on coral reefs and their influence on seawater A_T, DIC and pH (Cyronak et al., 2018).

measurements, i.e. net community calcification (NCC) and net community production (NCP), are used as important indicators of reef status (Koweek et al., 2015). Reef communities are active components in their biogeochemical environments, manipulating the availability of various inorganic and organic resources via calcification, primary production and respiration (Anthony et al., 2011; Albright et al., 2015). Dissolved inorganic carbon (DIC) and alkalinity (A_T) changes in sea water over a coral reef point to the relative contribution from different metabolic processes (figure 1). Understanding the impacts of changes in benthic composition and seawater conditions on coral reef metabolism, as well as the effects of oean acidification is critical in predicting a reef's future ability to accrete $CaCO_3$.

3 Bioerosion by excavating sponges

Bioerosion on coral reefs is illustrated by the destruction of carbonate ($CaCO_3$) substrate by various marine organisms (Neumann and Jan, 1966). On undisturbed reefs, a delicate balance exists between carbonate accretion and erosion, where bioerosion plays a considerable role in shaping the reef and producing vast amounts of sand (Glynn and Manzello, 2015). Currently, however, it appears that altered reef conditions are tipping this interaction on many reefs in favour of bioerosion (Wisshak et

al., 2014; Schönberg et al., 2017). On Caribbean reefs, excavating sponges (figure 2) are often the dominant macroboring organisms (Rützler, 2002). These macroborers respond positively, in both their eroding capacity and their abundance, to eutrophication, ocean acidification and the rising sea water temperatures (Wisshak et al., 2014; Achlatis et al., 2017; Webb et al., 2017). Nevertheless, bioeroding sponges are, at present, relatively understudied compared to other reef organisms. Excavating sponges have significant ecological and biogeochemical effects on coral reef habitat as they break down calcium carbonate structures by a combination of dissolution and mechanical chip removal system in a manner analogous to a mining operation (figure 3) which can result in the production of up to 30% of the sediment on a coral reef (Rützler, 1975; Nava and Carballo, 2008; Carballo et al., 2017). Bioeroding sponges contribute substantially to the excavation of coral skeletons, accounting often for 40–70%, but incidentally up to >90% of macroborer activity on coral reefs (Wisshak et al., 2012; Schönberg et al., 2017). It is hypothesised that specialised cells are able to reduce saturation state with respect to aragonite at the sponge-coral interface, resulting in dissolution of the coral's skeleton (Rützler and Rieger, 1973; Pomponi, 1977). Since the etching interface is not directly accessible for observations, investigating the underlying mechanisms by which these sponges dissolve $CaCO_3$ has proven to be challenging (Schönberg, 2008).

Figure 2: Three examples of Caribbean excavating sponges. From left to right: *Cliona caribbaea* (brown), *Siphonodictyon brevitubulatum* (yellow) and *Cliona delitrix* (orange).

Recent results have shown that boring rates increase with higher seawater pCO_2, suggesting that a reduced ambient saturation state directly lowers the energetic costs for the sponge to lower the saturation state in which the aragonite skeleton dissolves (Fang et al., 2013; Wisshak et al., 2013; Webb et al., 2017). Despite the expected increase of sponge bioerosion impact on coral reefs with on-going ocean acidification, the mechanistic link between environmental conditions and bioerosion rates remains unknown. Production of acids is thought to be ultimately responsible for $CaCO_3$

dissolution. Hatch (1980) suggested that excavation by sponges involves a localized modification of the $CaCO_3$ solubility equilibrium. Furthermore, there is evidence for the presence of the enzyme carbonic anhydrase at the sponge-coral interface, which could facilitate the transport of H^+ across membranes or provide an optimum pH for other chemical processes involving, for instance, calcium chelators (Hatch, 1980). The unknowns in excavating sponge's biology and its sensitivity to ongoing climate change, form the basis of the research presented in this thesis.

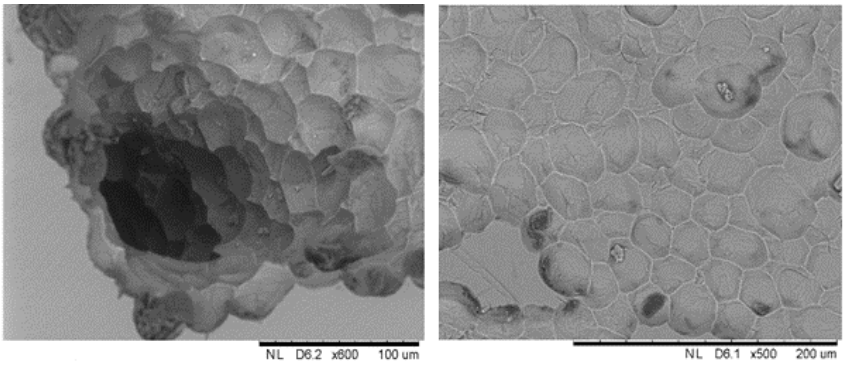

Figure 3: Scanning electron microscope images of calcite excavated by *Cliona varians*. Both images depict excavated channels lined with characteristic pits that remain after the chips are removed.

4 Synopsis

The overarching aim of this thesis is to quantify and understand the accretion and loss terms of coral reef communities with a focus on the interactions of anthropogenic ocean acidification and eutrophication with bioerosion by coral excavating sponges. To this end, the underlying mechanisms of $CaCO_3$ chemical dissolution by excavating sponges was investigated (chapters II and III), as well as the combined effect of ocean acidification and eutrophication on bioerosion rates (chapters III and IV). Chemical dissolution was then assessed at the reef community level, in situ and tackled questions regarding net community calcification and net community production of various community assemblages found in both pristine and degraded areas (chapters V and VI).

Chapter II 'pH Regulation and Tissue Coordination Pathways Promote Calcium Carbonate Bioerosion by Excavating Sponges' identifies the main physiological mechanisms by which sponge *Cliona* spp. promotes dissolution of coral skeleton. Although

a localised modification of the $CaCO_3$ solubility equilibrium at the sponge/coral interface was proposed in the early 80s, this had not yet been investigated successfully. Growing sponges on Icelandic spar (calcite) and the use of fluorescence microscopy made it possible to visualise the underlying mechanisms promoting $CaCO_3$ dissolution.

Chapter III 'Diurnal Variability in Carbonic Anhydrase Activity for $CaCO_3$ Dissolution by Excavating Sponges' addresses the role of carbonic anhydrase in chemical dissolution by excavating sponges. Several of the most competitive boring sponges harbour the same endosymbiotic dinoflagellate zooxanthellae as corals. Although bioerosion is the natural counterpart of accretion, these symbionts appear to play a role in both light enhanced calcification and bioerosion. As carbonic anhydrase (CA) enzymes greatly increase the speed of the reversible reaction $H_2O + CO_2 \leftrightarrow H^+ + HCO_3^-$ and have been detected abundantly associated with etching processes at the sponge-coral interface, they are thought to play a central role in the dissolution of $CaCO_3$ by excavating sponges. In this chapter, the activity of carbonic anhydrase is blocked in various pCO_2 ranges during the day and at night to provide an assessment of CA involvement in chemical dissolution by boring sponges.

Chapter IV 'Combined Effects of Experimental Acidification and Eutrophication on Reef Sponge Bioerosion Rates' assesses environmental control on bioerosion rates of *Cliona* spp. in controlled, laboratory experiments. The impacts of increased pCO_2 combined with nutrients and organic loading in surface waters on coral calcification have been repeately reported, however the synergetic effects on bioerosion are poorly studied. As the long term success of tropical coral reefs depends largely on the balance between constructive (calcification nd cementation) and destructive forces (mechanical-chemical degradation), understanding the combined effects of global and local pressures on the antagonist of calcification, i.e. dissolution, are essential. In this study, *Cliona caribbaea*, a photosymbiont-bearing excavating sponge widely distributed in Caribbean reef habitats, was exposed to a range of pCO_2 concentrations, as well as different eutrophication levels.

Chapter V 'In-situ incubation of a coral patch for community-scale assessment of metabolic and chemical processes on a reef slope' investigates in situ diurnal trends of CO_2 system parameters (dissolved inorganic carbon, total alkalinity), dissolved oxygen, and nutrients (phosphate, nitrate, nitrite, and ammonium) on a 20 m deep coral reef patch offshore from the island of Saba, Dutch Caribbean by means of tent incubations. The reef in this area is located on a steep incline from the heights of Saba toward the ∼500 m deep stretch between the island and the Saba Bank carbonate platform. Coral reefs around Saba harbour a relatively rich diversity of marine species and is considered one of the more pristine sites in the context of the

wider Caribbean. Comprehensive monitoring of the abovementioned fluxes allows for subsequent quantification of integrated whole community coral reef metabolic processes (net community calcification (NCC) and production (NCP)) in a highly hydrodynamic environment.

Chapter VI 'Carbonate dissolution mediated by key benthic communities on a degrading coral reef' explores benthic metabolic rates across five different benthic assemblages over diurnal cycles using small underwater tent like incubations. Present Caribbean reefs bear very little resemblance in configuration with reefs pre-1980s, in terms of benthic composition, coral cover and structural complexity. Areas covered by sand, rubble, cyanobacteria, excavating sponges, turf and macroalgae have increased at the expense of coral. In this chapter, benthic metabolic rates are quantified in situ across benthic assemblages that currently characterized shallow Caribbean reef substrate.

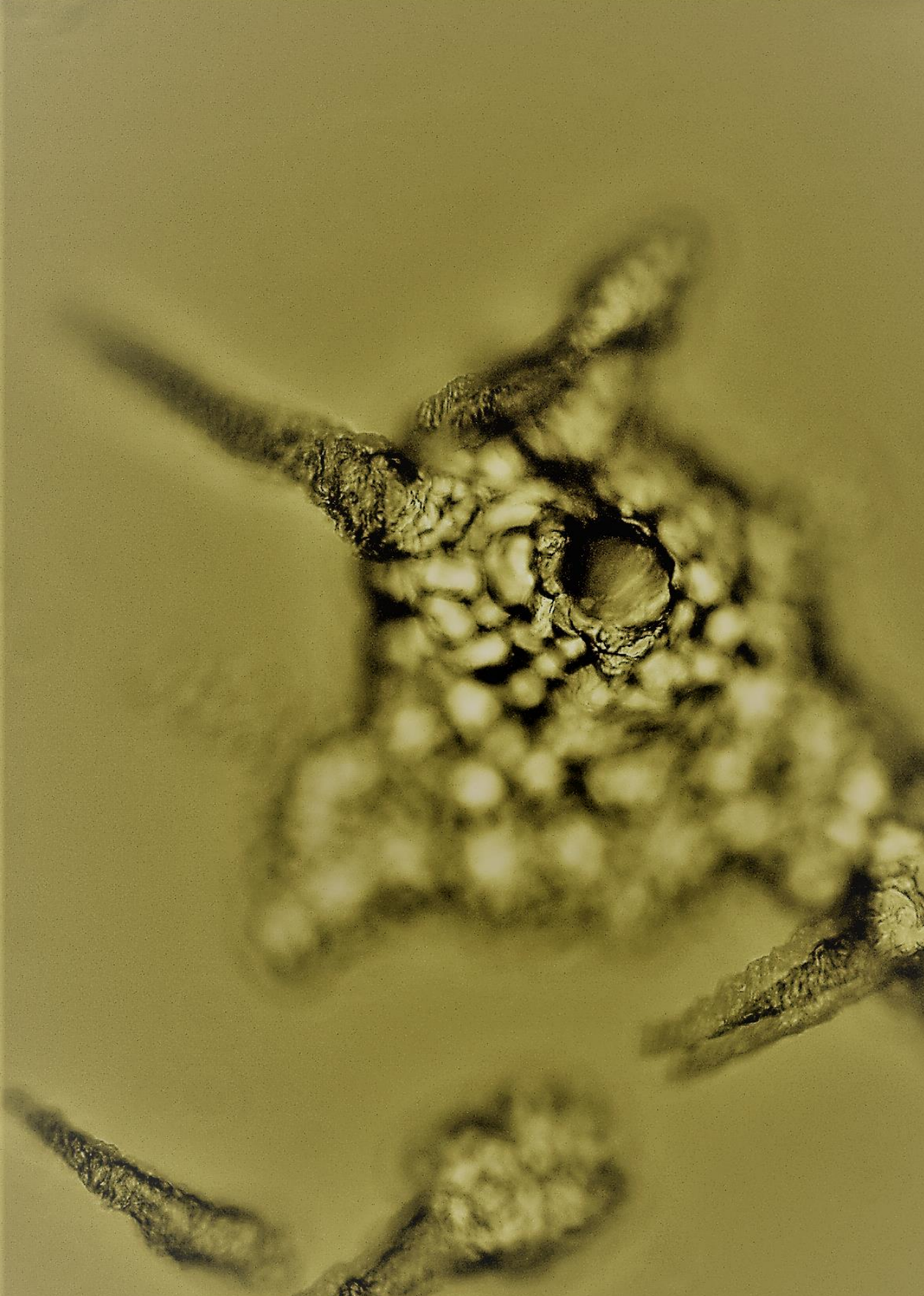

Chapter 2

pH Regulation and Tissue Coordination Pathways Promote Calcium Carbonate Bioerosion by Excavating Sponges

Alice E. Webb, Shirley A. Pomponi, Fleur C. van Duyl, Gert-Jan Reichart, Lennart J. de Nooijer

Webb et al. 2019, Scientific Reports 9, 1:758

Abstract

Coral reefs are threatened by a multitude of environmental and biotic influences. Among these, excavating sponges raise particular concern since they bore into coral skeleton forming extensive cavities which lead to weakening and loss of reef structures. Sponge bioerosion is achieved by a combination of chemical dissolution and mechanical chip removal and ocean acidification has been shown to accelerate bioerosion rates. However, despite the ecological relevance of sponge bioerosion, the exact chemical conditions in which dissolution takes place and how chips are removed remain elusive. Using fluorescence microscopy, we show that intracellular pH is lower at etching sites compared to ambient seawater and the sponge's tissue. This is realised through the extension of filopodia filled with low intracellular pH vesicles suggesting that protons are actively transported into this microenvironment to promote $CaCO_3$ dissolution. Furthermore, fusiform myocyte-like cells forming reticulated pathways were localised at the interface between calcite and sponge. Such cells may be used by sponges to contract a conductive pathway to remove chips possibly instigated by excess Ca^{2+} at the boring site. The mechanism underlying $CaCO_3$ dissolution by sponges provides new insight into how environmental conditions can enhance dissolution and improves predictions of future rates of coral dissolution due to sponge activity.

1 Introduction

Boring sponges excavate and grow into calcium carbonate substrates with their activity leading to significant marine carbonate erosion (Rützler, 2002; Zundelevich et al., 2007; Schönberg and Ortiz, 2008). In coral reef environments, bioerosion leads to significant loss of reef structures and may tip the balance between production and erosion in favour of the latter (Perry et al., 2014; Murphy et al., 2016).

Bioerosion by excavating sponges is achieved by a combination of chemical dissolution and mechanical chip removal (Nasonov, 1924; Rützler and Rieger, 1973; Pomponi, 1980). It is hypothesised that specialised cells are able to reduce saturation state with respect to aragonite at the sponge-coral interface, resulting in dissolution of the coral's skeleton (Hatch, 1980). Since the etching interface is not directly accessible for observations, investigating the underlying mechanisms by which these sponges dissolve $CaCO_3$ has proven to be challenging. Recent results showed that boring rates increase with higher seawater pCO_2 (Wisshak et al., 2012; Duckworth and Peterson, 2013; Fang et al., 2014; Wisshak et al., 2014; Schönberg et al., 2017; Webb et al., 2017), suggesting that a reduced ambient saturation state directly lowers the energetic costs for the sponge to lower the saturation state in which the aragonite skeleton is dissolved. Despite the expected increase of sponge bioerosion impact

on coral reefs with on-going ocean acidification, the mechanistic link between environmental conditions and bioerosion rates remains unknown. Production of acids is thought to be ultimately responsible for $CaCO_3$ dissolution (Hancock, 1849; Cotte, 1902; Warburton, 1958). Hatch (1980) suggested that excavation by sponges involves a localized modification of the $CaCO_3$ solubility equilibrium. Furthermore, Hatch (1980) provided evidence for the presence of the enzyme carbonic anhydrase at the sponge-coral interface, which could facilitate the transport of H^+ across membranes or provide an optimum pH for other chemical processes involving, for instance, calcium chelators. Sullivan et al. (1986) demonstrated the presence of such calcium chelators in *Siphonodictyon coralliphagum* (Rützler, 1971) and described the dissolution process as a cycle in which calcium chelators release protons in exchange for calcium ions at the etching site and release calcium ions to the water outside the sponge in exchange for protons. This proposed pathway implies that a reduction of pH at the sponge-substrate interface would form the basis of sponge chemical erosion. However, a direct characterization of the conditions during aragonite dissolution is necessary to confirm that this mechanism is adopted by excavating sponges.

Here we investigate the cell physiological and chemical conditions at the dissolution interface of the sponge *Cliona varians* (Duchassaing De Fonbressin and Michelotti, 1864) by applying a pH fluorescent probe and subsequent visualization of pH at the etching site with fluorescence microscopy.

2 Materials and methods

2.1 Sample collection and growth conditions.

Samples from 5 different *C. varians* sponges (figure 1) were collected off Summerland Key in the Florida Keys using a hammer and a chisel. Sponge samples (n=30) were placed in flow-through seawater raceways at the Mote Tropical Marine Laboratory in Summerland Key, attached to pieces of Iceland spar (3 to 4 cm^3) with plastic tie wraps, and subjected to a natural diurnal light cycle. They were kept in the flow-through raceways for one month to allow the cut surfaces to heal and attach to the Iceland spar. They were then transferred to Harbor Branch Oceanographic Institute (HBOI) at Florida Atlantic University, where they were placed in a recirculating seawater raceway in the aquaculture facility for 3 weeks before the experiment was started.

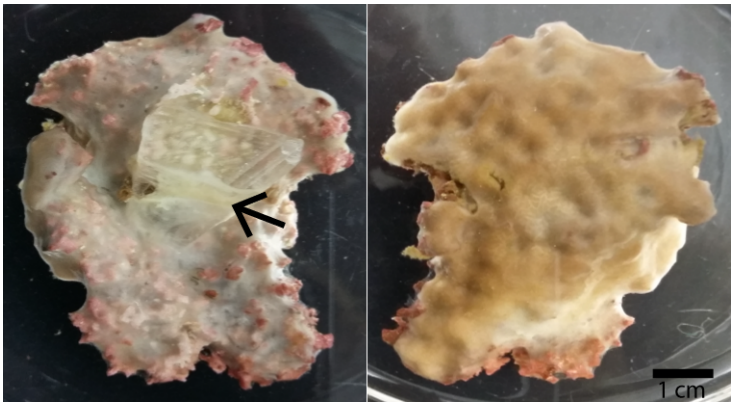

Figure 1: *Cliona varians* sample viewed from bottom (left panel) and top (right panel). Sponge has attached (arrow) to the piece of Iceland spar placed on its lower side.

2.2 Specimen preparation and staining.

Pieces of calcite (Iceland spar) in early stages of sponge bioerosion were detached from the 'mother sponge' (figure 1) and broken into smaller thin fragments with surface areas ranging from 0.10 to 0.25 cm^2 and with thickness of 0.1 to 0.2 cm. For each calcite piece, ∼10 fragments were collected and stained following a derived protocol for pHrodo™ Red and Green AM Intracellular pH Indicators based on protocols developed by the manufacturer (Life Technologies). This involved dilution of 10 µL of stain into 100 µL of PowerLoad concentrate, dilution of the resulting solution into 10 mL of filtered seawater and incubation of the sponge fragments in 2 ml of this solution for 1 hour. Finally, the sponge/calcite fragments were rinsed in filtered seawater, placed in a 24-well plate and immediately imaged.

2.3 Fluorescence Microscopy and Image Analysis.

Fluorescence and transmitted light imaging was performed on an Invitrogen™ EVOS™ FL Auto Imaging System. Fluorescence emission intensity was measured after illuminating the incubated tissue with different excitation wavelengths. The red channel of emission in all images represents pH and was obtained using the Texas Red light cube with excitation and emission maxima around 585 and 624 nm, respectively. The commercial pHrodo™ indicator and Intracellular pH Calibration Buffer Kit (Thermofisher) were used for intracellular pH determination and pH calibration, respectively.

(1) pHrodo™ Red Intracellular pH imaging.

To assess intracellular pH, the fluorogenic intracellular pHrodo™ Red probe was utilized. pHrodo™ Red is weakly fluorescent at neutral pH but increasingly fluorescent as pH decreases. This reagent allows quantification of cellular cytosolic pH in the range of 4-9 with a pKa of ∼6.5 and excitation/emission optima of 560/585 nm. To obtain absolute pH values, a pH calibration curve was produced using an Intracellular pH Calibration Buffer Kit. Modification of pHrodo™ with AM ester groups results in an uncharged molecule that can permeate cell membranes. Once inside the cell, the lipophilic blocking groups are cleaved by nonspecific esterases, resulting in a compound that is retained within the intracellular space.

(2) Intracellular pH Calibration Buffer Kit.

The Intracellular pH Calibration Buffer Kit enables the quantification of intracellular pH when used in conjunction with pHrodo™ Red AM. It includes four pH calibration buffers (pH 4.5, 5.5, 6.5, and 7.5), as well as valinomycin and nigericin, which are used to equilibrate the pH inside and outside of cells. After staining dissociated cells (1×106 cells/ml) from *C. varians* with pHrodo™ Red AM and detemining the fluorescence intensity under experimental conditions, cells were re-suspended in one of the calibration buffers and fluorescence intensity was measured again. This was performed in duplicate for each buffer to produce a calibration curve allowing translation of the sponge's fluorescent images into pictures showing the internal pH distribution.

2.4 Image processing for the calibration curve.

The calibration curve was produced using the programming environment R.3.4.3 (R Core Team, 2017). Each image is imported in R as a pixel matrix. Each given pixel has an intensity value between 0 and 1, corresponding to a luminosity scale from dark to light. Each image was corrected for background noise and excess luminescence due to potential leakage of the buffers out of the cells and superposition of the fluorescence signal. This was achieved by approximately removing the 1st and 4th quartile of the data, corresponding to 43% of the pixels from the original image (the removal of the data's 4^{st} quartile led to an overestimation of pixels belonging to excess luminescence and was corrected for visually). The average pixel luminescence from each image was subsequently used to generate a calibration curve showing a significant linear relationship ($R^2 = 0.98$, $p<0.0001$) between intracellular pH and relative pixel fluorescence (and its variability: figure 2).

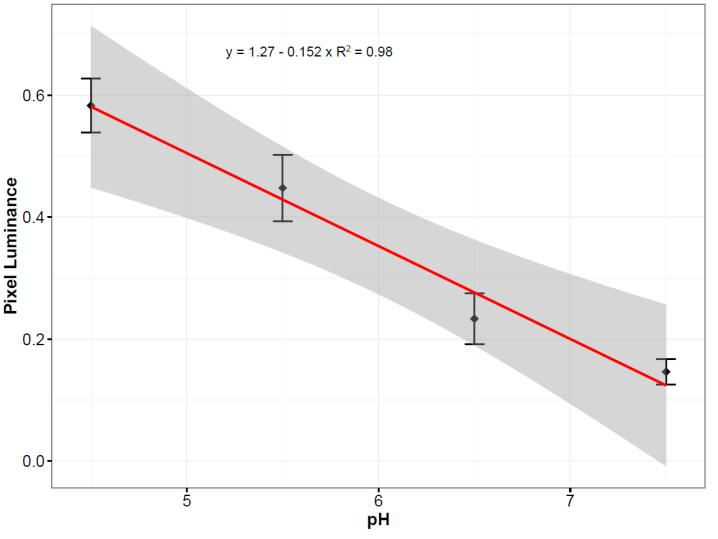

Figure 2: Calibration curve for intracellular pH in *C. varians* pixel luminescence intensity after removal of 1^{st} and 4^{st} quartiles. Error bars represent standard deviation derived from the variability in all pixels for the images taken. Uncertainty (grey envelope) surrounding the linear regression curve represents the 95% confidence intervals.

3 Results and Discussion

Iceland spar crystals containing tissue of *C. varians* that grew into the calcite were carefully detached from the "mother sponge". This exposed a complex network of fibre-like interconnections as well as several circular perforations of the surface crystal face, filled with living tissue. Scanning electron microscopy exposed clear signs of bioerosion and calcite chips within the tissue (figure 3). Transmitted light microscopy revealed two dominant cell types (figure 4 & 5) with vesicular cytoplasm likely playing key roles in bioerosion. These two cell types have a distinct morphology and localization, which reflects their function and will be subsequently discussed in light of previous descriptions on their role in chip production and removal (Pomponi, 1980; Rützler and Rieger, 1973).

3.1 Myocyte-like cells forming tissue coordinating pathways.

At locations adjoining excavating activity, elongated fusiform cells, measuring between 25 to 80 µm in length and 2 to 5 µm in diameter, with a relatively vesicular cytoplasm (figure 4a), are found forming bundles that resemble pathway connections

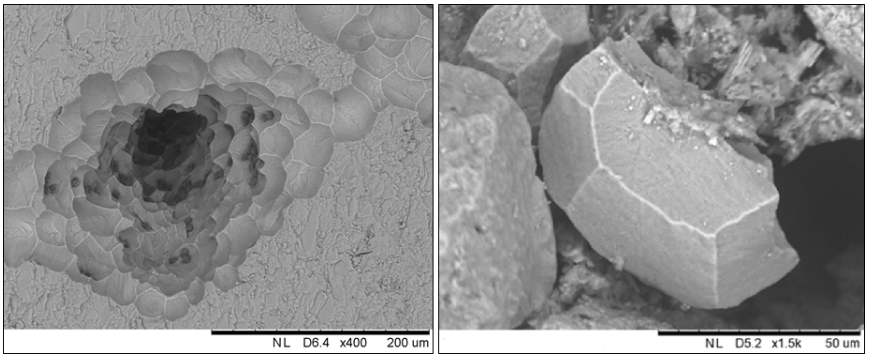

Figure 3: Scanning electron microscope images of calcite excavated by *C. varians*. The top panel depicts an excavated channel lined with characteristic pits that remain after the chips are removed; the bottom panel shows a chip with its distinctive orthogonal carved shape.

(figure 4b & 4c). Their overall appearance (e.g., figure 4c) resembles the organization of vertebrate muscle fibres, and hence may represent the mobile fusiform collencytes observed by Rützler and Rieger (1973).

We suggest that these cells may be actinocytes/myocytes (Bagby, 1966; Prosser, 1967; Leys, 2015) capable of directed transport of the chips formed in the dissolution pits through coordinated tissue contraction, although such cells have not yet been identified in excavating sponges. It should be noted that Grant (1826) created the new genus *Cliona* in reference to the high frequency of contractions of *Cliona celata*. Furthermore, De Ceccatty (1974) describes a comparable type of fixed tissue coordination pathway in the sponges *Tethya*, *Hippospongia*, and *Euspongia* that is formed through connections and bundles between muscle-like cells from the same unit structure. De Ceccatty (1974) argues that this system is based on the capacity of cells to construct a structurally defined pathway in order to promote direct exchanges from one cell to another. In the same species, electron microscopy images illustrate tight membrane appositions between adjacent cells and transfer of vesicles from cell to cell (De Ceccatty, 1966).

The exclusive organization of the *C. varians* cells into bundles connecting the boring pits with the rest of the sponge (figure 4d) indicates that they are instrumental to the transport of chips out of the excavated pit and into an excurrent canal. The role of these cells in chip removal is almost a priori given the fact that the formed chips have to be transported away from the bottom of the boring pits (figure 4) and hence must pass these myocyte-like cells before entering the excurrent canal.

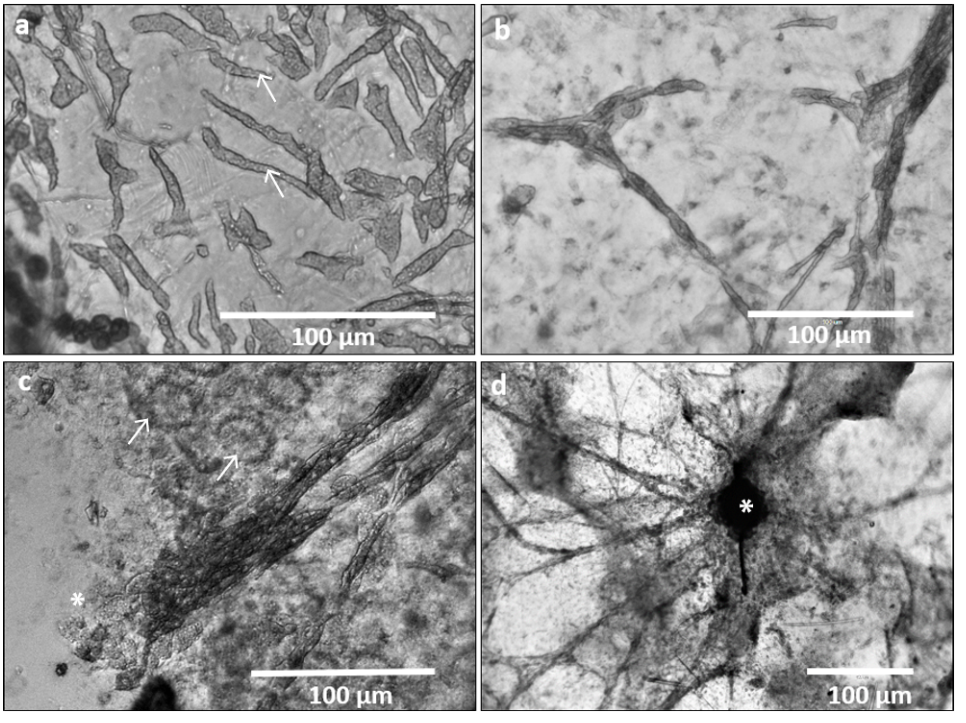

Figure 4: Transmitted light images of cells of *C. varians* organised in bundles and networks responsible for chip transport. (a) Elongated cells with vesicular cytoplasm merge into muscle-like pathways (b, c, & d) spreading from pits where excavation happens. Note etching cells (*) in the lower left of (c) in contact with the elongated cell network and choanocyte chambers (arrows) in the upper part of (c). In (d), the fibre-like network is organised around a boring pit (*).

3.2 Etching cells

Etching cells are the second dominant cell type present at the sponge/calcite interface. Their morphology changes to correspond with their ultimate function: the dissolution of calcium carbonate. Initially, they appear as club-like cells of archeocyte origin with a prominent nucleus and cytoplasm with a vesicular appearance (figure 5a). To penetrate the carbonate substrate, several thread-like filopodia originate from the cell body (figure 5b & 5c) and ramify to partly fuse again forming cytoplasmic sheets (figure 5b, 5c & 5d). The filopodia form a basket-shaped meshwork corresponding in size to the substratum chips they surround. Previous research also showed networks of thread-like pseudopodia originating from club-like cells and based on their morphology inferred that they were likely responsible for $CaCO_3$ dissolution (Cotte, 1902; Nasonov, 1924; Warburton, 1958; Rützler and Rieger, 1973). Many etching cells with their accompanying processes in this study were observed in a disintegrating stage. This collapse of cells has also been observed previously (Rützler and Rieger, 1973; Pomponi, 1977) and appears to be linked to the penetration of the filopodial extensions into the substrate. The cell disintegration stage hence appears to be a function of filopodial growth. Etching cells are very vesicular in appearance (figure 5a) which may be linked to the flocculent secretory product within the filopodia described by Rützler and Rieger (1973). This product was assumed to be contained within vesicles that would be subsequently emptied into a cytoplasmic sac. In the present study, no flocculent material inside the filopodia was observed using transmitted light microscopy but this may be due to the limited spatial resolution of our method. Fluorescence microscopy imaging, however, revealed low pH vesicles in the filopodia (see section 3.3). The tissue composition and configuration around and inside burrowing tunnels formed by this excavating sponge is an indication of how dynamic the etching process is. It appears that etching cells are being continuously formed and discarded, filling every crack and cavity to ensure sponge growth and dissolution of the $CaCO_3$ substratum.

3.3 pH reduction at sponge/substrate interface

Visualization of pH inside the sponge tissue revealed that the intracellular pH within the filopodial extensions approximates 5 during carbonate dissolution, while non-bioeroding tissue approximates a pH higher than 7 (representing the upper limit of our approach). The observed lowered pH is consistent with a study using microsensors measurements where pH was found to decrease continuously as a function of tissue depth towards the substrate (Schönberg, 2008). However, results from the latter study showed a rather modest pH change throughout the sponge tissue compared to

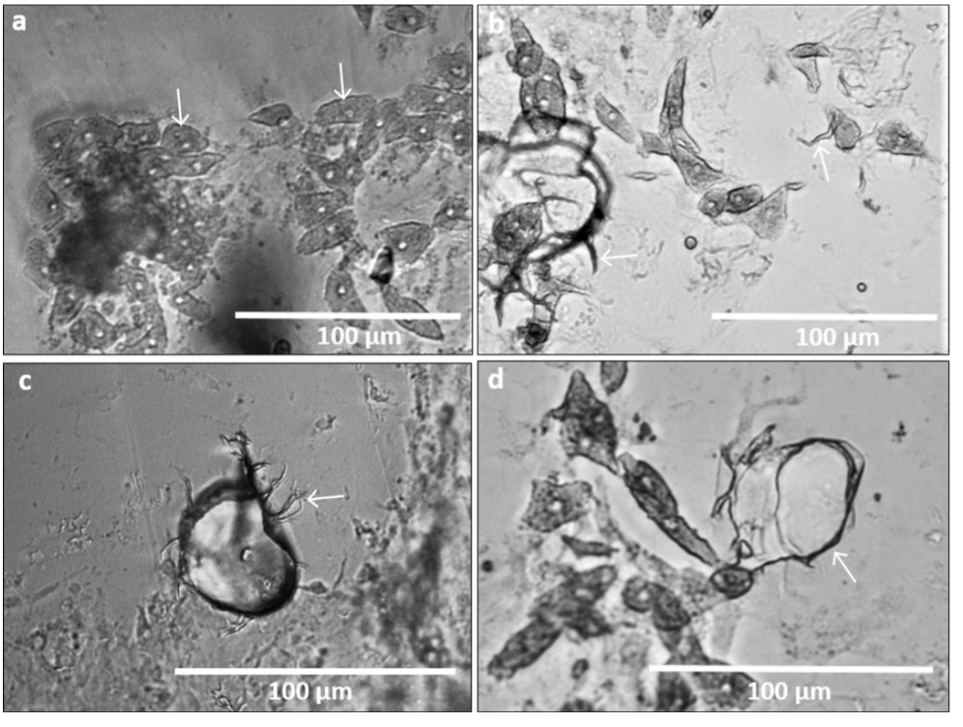

Figure 5: Transmitted light images of *C. varians* etching cells (a, arrows) and accompanying filopodia (b, c & d). (a) Club-like etching cells (arrows) with prominent nuclei and vesicular cytoplasm. The cells are located around two initial boring pits. (b) On the right, a filopodium is extruding from an etching cell (arrow). On the left, the filopodia network is developing and outlines of chips can be distinguished. (c) Formation of a chip by extending filopodia (arrow). (d) Filopodial extensions emanating from an etching cells and merging to form cytoplasmic sheets engulfing a calcite chip.

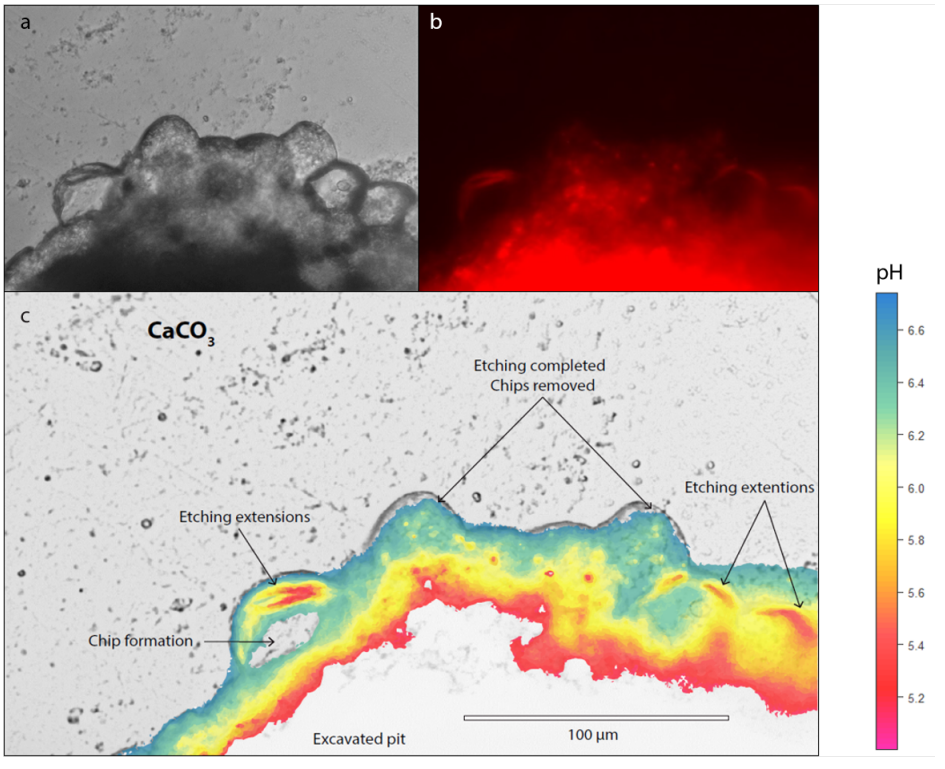

Figure 6: Low pH in etching filopodia in sponge excavated pit exposed after detachment of a piece of bioeroded calcite from the "mother sponge". (a)Transmitted light image showing etching filopodia carving out chips on the leading edge of a bored channel in the substratum. (b) Z-stack imaging of the same area; red fluorescence represents pH below neutral. (c) Processed image using the fluorescence intensity/pH calibration (figure 2) showing low pH in etching filopodia that are carving chips from an excavation pit. Due to the detachment from the "mother sponge", most tissue around the pit was removed, however, a large fraction of cells within etched crevices remained, enabling exclusive visualization of the etching filopodia. The high fluorescence levels in the centre of the pit are due to the superposition of cells causing additive fluorescence and were therefore dismissed from further analysis.

the present study. The discrepancy between previously published and present observations may primarily reflect positioning of the microsensors as the site of dissolution is very restricted and not easily accessible. Fluorescent dyes are more suited to show changes at the actual interface. Our results suggest that *C. varians* locally reduce the pH at the etching site in order to dissolve calcite (Icelandic spar), we infer that the same process applies to aragonite (coral skeleton). At high magnification, it is clear that the lowest pH values are confined to filopodia of the etching cells protruding around the chips (figure 6). Figure 6c illustrates the active formation of 3 chips (one on the left, and two on the right). Other visible grooves are filled with cells, but no etching filopodia are discernible. We suggest that the lack of etching at these locations indicates that chip etching in these areas was completed; chips have been removed and cells only recently recolonised this space, probably reorganizing for the next phase of chip excavation. The low pH inside the filopodia appears to reside in numerous subcellular vesicles (figure 7b, 7c & 7d) which are consistently spaced in concentric rings within the inner space of the filopodia networks. These low pH vesicles observed in the filopodia are comparable to what Rützler and Rieger (1973) refers to as a flocculent secretory product extending into the filopodia. We propose that vesicles discharge their contents in the cytoplasmic sheets, enabling the filopodia to penetrate the substrate. The absence of vesicles in figure 6 is likely due to vesicles having just discharged their content and dissolution neutralising the low-pH fluid.

To estimate whether the vesicles within the filopodia can be fully responsible for the volume of aragonite that is dissolved around one chip, the fluorescent images and obtained intra-vesicle pH values can be combined and compared to the calculated proton budget involved in aragonite dissolution. Assuming vesicles have a pH of ∼5, the concentration of protons in a given number of vesicles with an estimated volume can be translated to the maximum volume of $CaCO_3$ that can be dissolved (figure. 8). To do so we assume that the chip can be approximated by half of a sphere, with a diameter of 40 µm (the approximate average of observed excavated pits; see e.g. figure. 6), the filopodia's width is on average 0.4 µm and 3 % of the chip is dissolved (Rützler and Rieger, 1973). Based on these parameters, we estimate the amount of $CaCO_3$ dissolved for each individual chip to equal 2.8 × 10-11 mol. The $[H^+]$ present in each vesicle of pH 5 is equal to 1 × 10-5 ml L^{-1}. Assuming vesicles take up the entire volume of the filopodia and each vesicle has a volume of 0.01 μm^3 (diameter = 0.3 µm and a length equalling the radius of the semi sphere), a total of ∼105 vesicles can be squeezed in the filopodia surrounding the chip. These vesicles can therefore only provide 1 × 10-17 ml of protons for dissolution at one time. However, this number is already an overestimation as filopodia form intricate networks around chips and do not cover the entirety of the chip walls. In addition, although figure 7 depicts tightly

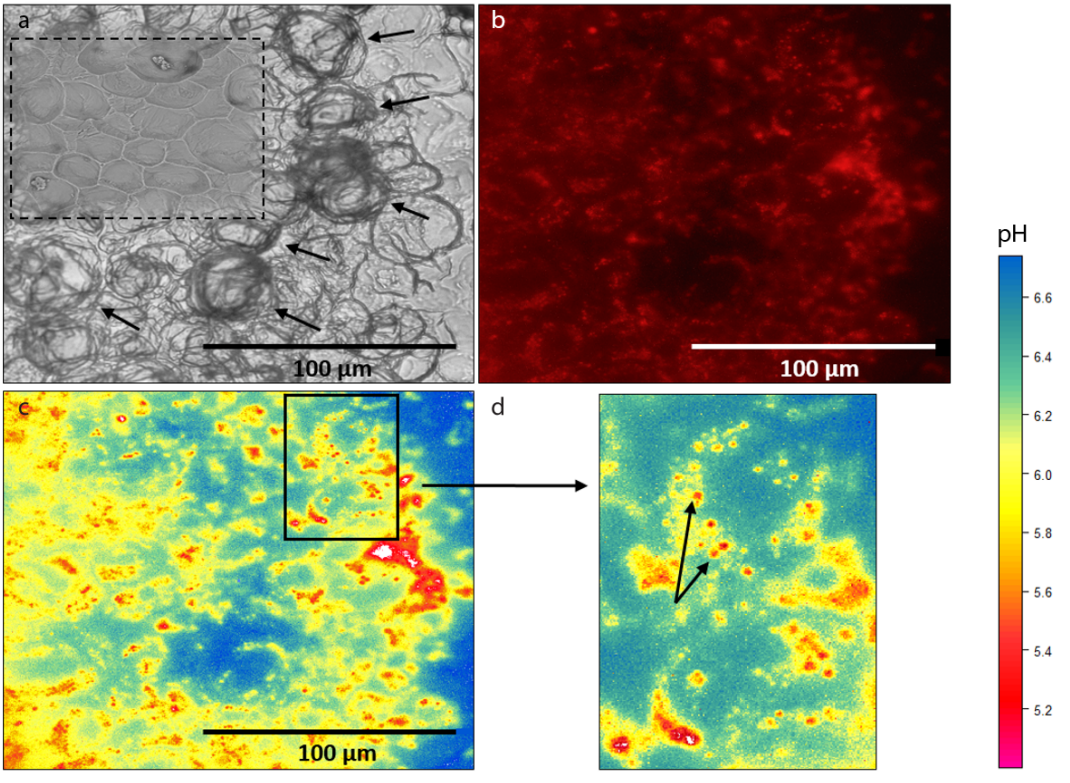

Figure 7: Low-pH vesicles within etching filopodia located at the bottom of an excavated pit viewed from the top. (a) Transmitted light image of etching filopodia indicated by black arrows and corresponding SEM image (top left) of excavated chip pits without etching filopodia (dashed square). (b) Z-stack imaging of the same area, where red fluorescence represents low pH, showing numerous vesicles with low pH following the outline of etching filopodia. (c) Processed image with pH quantification showing lower pH within vesicles with detail enlarged in (d).

packed vesicles within the filopodia, they do not appear to be filling the complete volume of the filopodia. If the etching process is completely achieved by exocytosis of low-pH vesicles, a continuous influx of vesicles and/or a constant replacement of filopodia and etching cells would be necessary. A single delivery of an acidic fluid would dissolve some $CaCO_3$, but also be neutralized by the release of carbonate ions. Therefore, the low pH values observed at the etching sites need to be maintained over time and likely require active pumping and a continuous flux of protons.

3.4 Conceptual model for sponge excavation of calcium carbonates

The overall observations and interpretations from the present study form the basis of an improved conceptual model for sponge bioerosion. Our results clearly demonstrate that a decrease in pH is actively created at the sponge/substrate interface. The high $[H^+]$ at this site is achieved through delivery of low-pH vesicles by the etching cells (figure 7) and leads to dissolution of the $CaCO_3$ (here calcite) and subsequent disintegration of the filopodia. Dissolution of calcite neutralizes the released protons and elevates pH, after which the increased concentrations of Ca^{2+} and HCO_3^- are removed before new acidic vesicles are emptied at the sponge-calcite interface. The manner and the speed in which Ca^{2+} and HCO_3^- ions are transported away from the site of dissolution will inherently determine the speed at which $CaCO_3$ can be dissolved.

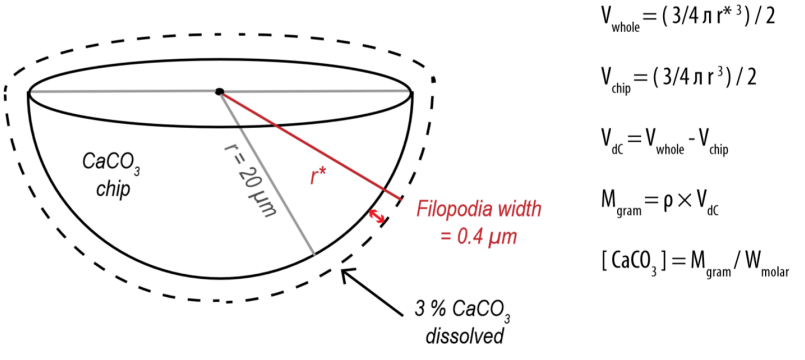

Figure 8: Chip schematic where V_{dC} is the volume of dissolved $CaCO_3$, V_{whole} is the volume of the chip plus the volume of dissolved $CaCO_3$, V_{chip} is the volume of the chip, M_{gram} is the mass of $CaCO_3$ dissolved, p is the density of aragonite and W_{molar} the molecular mass of $CaCO_3$.

However, these processes remain to be investigated. Research on euendolithic phototrophic cyanobacteria demonstrated that microbial excavation is achieved through active intracellular Ca^{2+} transport (Guida and Garcia-Pichel, 2016). Calcium chelators and a suite of proteins are known to bind calcium, and could hence be the origin of an active calcium flux from the substrate into the sponge's cytoplasm. The protein proteoglycan is known to play a key role in the aggregation of dissociated sponge cells where calcium mediates the process by acting as an intracellular messenger (Dunham et al., 1983). When studying secondary metabolites, Sullivan et al. (1986) demonstrated the presence of calcium chelators in *Siphonodictyon coralliphagum* (Rützler, 1971). Various siphonodictyals of this sponge were able to bind calcium ions and lower their activity in the solution. The authors displayed the potential reaction as a cycle in which the chelator molecule releases $[H^+]$ and receives calcium ions at the site of dissolution, then releases calcium into the water column in exchange for a new $[H^+]$ ion. In this pathway, a lowering of pH at the sponge/substrate interface must occur and this process would be affected by changes in seawater conditions such as an increase in pCO_2 (Fang et al., 2013; Webb et al., 2017). However, the mechanism involved in transporting ions from the site of active dissolution to the water column remains unclear.

Guida and Garcia-Pichel (2016) showed that long range transport of Ca^{2+} is mediated by calcium ATPases or channels through cells. A specialised cell was identified accumulating calcium at concentrations more than 500-fold compared to concentrations found in other cyanobacteria. The authors suggest that these cells permit fast calcium flow at nontoxic concentrations through undifferentiated cells by providing temporary storage for excess calcium before final excretion to the outside medium. Calcium is known to play an important role for tissue contraction in marine sponges where cell to cell communication is used for tissue coordination (De Ceccatty, 1971; Lorenz et al., 1996). The network of muscle-like cells that was observed on the calcite after removal of the "mother sponge" (figure 4) may provide a pathway for the intracellular transport of calcium ions out of the sponge and into the water column, similar to how muscle cells contract when triggered by an increase in intracellular Ca^{2+}. We propose a working model for sponge dissolution of calcium carbonate (figure 9) where protons are received in exchange for calcium ions (potentially via calcium chelators) at the water-sponge interface. Protons are moved through the sponge via the transport cells until reaching the etching cells. They are then incorporated in vesicles (pH $\sim$5) that travel towards filopodia. Subsequently, the vesicles discharge their contents through exocytosis, which leads simultaneously to the dissolution of calcium carbonate and disintegration of the etching cell. The new space is then rapidly colonised by new filopodia, and the process continues. An efficient way to flush out HCO_3^- would

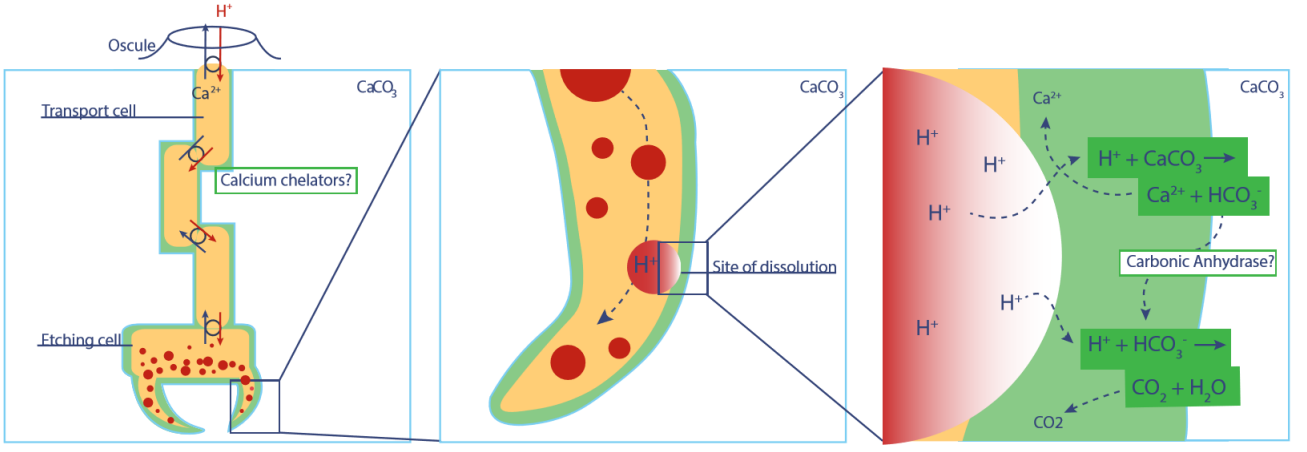

Figure 9: Working model for chemical dissolution of calcium carbonate by an excavating sponge. Protons are received in exchange for calcium ions (potentially via calcium chelators) at the water sponge interface. Protons are moved through the sponge via the transport cells until reaching the etching cells. They are then incorporated in vesicles (pH 4 to 5), which travel towards filopodia. Subsequently, the vesicles discharge their content through exocytosis, which leads simultaneously to the dissolution of calcium carbonate and disintegration of the etching cell. The new space is then rapidly colonised by new filopodia and so on. Newly freed bicarbonate ions are converted to CO_2, a reaction made faster with carbonic anhydrase enzymes, which passively diffuses out of the sponge.

be to convert it to carbon dioxide so it can simply diffuse out of the sponge. Carbonic anhydrase enzymes have been located in great number around etching processes (Pomponi, 1980) and may accelerate this conversion.

Conclusions

These results show that $CaCO_3$ dissolution by the excavating sponge *Cliona varians* is associated with the production of low pH vesicles in the filopodia of etching cells responsible for chip formation. These vesicles are transported within the etching cells towards the site of dissolution where they are emptied and create undersaturated conditions. The resulting high concentration of calcium at the sponge-calcite interface is hypothesized to be reduced by transport of calcium ions away from the site of dissolution, possibly directly balancing the flux of protons towards this site. The cells that connect the etching cells to the rest of the sponge tissue have a distinct morphology that is in line with transport of Ca^{2+} away from the site of dissolution. These findings reveal for the first time the basic mechanism by which excavating sponges dissolve calcium carbonate: the dependency of these sponges on the production of protons for $CaCO_3$ dissolution may provide an explanation for the observed positive relationship between seawater pCO_2 and dissolution rates (Wisshak et al., 2012; Fang et al., 2013; Wisshak et al., 2014; Webb et al., 2017).

Acknowledgements

We would like to thank the Mote Marine Laboratory, International Center for Coral Reef Restoration and Research for hosting part of the experiment and particularly Dr. David Vaughan for his support. Megan Conkling and Stephanie Munroe are gratefully thanked for their field and lab assistance. We also thank Prof Dennis Webb for sharing his insights on the matter. Support was provided by the National Oceanic and Atmospheric Administration, Office of Ocean Exploration and Research, award number NA14OAR4320260. This work is supported by the Gravitation grant NESSC from the Dutch Ministry of Education, Culture and Science. External funding for this project was provided by the Netherlands Organization for Scientific Research (NWO2g grants 858.14.021 and 858.14.022).

Chapter 3

Diurnal Variability in Carbonic Anhydrase Activity for $CaCO_3$ Dissolution by Excavating Sponges

Alice E. Webb, Didier M. de Bakker, Steven M.A.C. van Heuven, Fleur C. van Duyl, Gert-Jan Reichart, Lennart J. de Nooijer

Under review in the Journal of Experimental Biology

Abstract

Excavating sponges have significant ecological and biogeochemical effects on coral reef communities as they bore into coral skeleton using a combination of chemical dissolution and mechanical chip removal. Their bioerosion rates have been found to respond positively to ocean acidification, warming and eutrophication. Several of the most competitive boring sponges harbor the same endosymbiotic dinoflagellate zooxanthellae as corals. Although bioerosion is the natural counterpart of accretion, these symbionts appear to play a role in both light enhanced calcification and bioerosion. As carbonic anhydrase (CA) enzymes greatly increase the speed of the reversible reaction $H_2O + CO_2 \leftrightarrow H^+ + HCO_3^-$ and have been detected abundantly associated with etching processes at the sponge-coral interface, they are thought to play a central role in the dissolution of $CaCO_3$ by excavating sponges. Here we determine the role of carbonic anhydrase in chemical dissolution by *Cliona caribbaea*, a zooxanthellae bearing species and *Suberea flavolivescens*, a species that does not host algal symbionts. We blocked the activity of carbonic anhydrase in experiments with various controlled pCO_2 ranges during the day and at night to provide an assessment of CA involvement in chemical dissolution by boring sponges. The effect of CA inhibition on chemical bioerosion is found to be comparable across pCO_2 ranges, however, day and night effects are opposite. We show a decrease in dissolution rates at night across sponge types, which attests to the important role of CA at night compared to day time. We suggest that in the dark, increased CA activity may promote outward diffusion of the additional DIC, which is the result of dissolution, in the form of CO_2. During the day, the CO_2 gradient is enhanced by symbiont photosynthesis which promotes diffusion of CO_2 out of the dissolution site, resulting in higher bioerosion rates.

1 Introduction

Excavating sponges from the family *Clionidae* (Gray, 1867) are abundant and common inhabitants of coral reef communities (Chaves-Fonnegra and Zea, 2011; Schönberg et al., 2017). They have significant ecological and biogeochemical effects on these communities as they disintegrate calcium carbonate structures by a combination of dissolution and mechanical chip removal (Zundelevich et al., 2007; De Bakker et al., 2018) which is shown to accelerate with ocean acidification (Fang et al., 2013; Wisshak et al., 2013; Schönberg et al., 2017; Webb et al., 2017). Bioeroding sponges contribute substantially to the excavation of coral skeletons, accounting often for 40–70% and up to 90% of macroborer activity on coral reefs (Wisshak et al., 2012; Schönberg et al., 2017). Locally, this activity and the accompanying production of aragonite chips can contribute up to 30% to the sediment on a coral reef (Rützler,

1975; Nava and Carballo, 2008; Carballo et al., 2017). Although sponges in the family *Clionidae* contribute substantially to coral erosion, most of them house the same photosymbiotic dinoflagellates of the genus *Symbiodinium* as their coral substrates that contribute to the counterpart of bioerosion, accretion (Hill, 1996; Schönberg, 2000). The *Symbiodiniaceae*-hosting clionids are referred to as the "*Cliona viridis*" species complex (Schönberg, 2000). Interestingly, these intracellular dinoflagellates seem to be responsible for light-enhanced calcification as well as light-enhanced bioerosion, which may indicate that these zooxanthellae aid both these opposite processes, production as well as dissolution of $CaCO_3$ (Hill, 1996; Webb et al., 2017). Compared to its role in calcification, the mechanism by which photosynthesis affects dissolution is still elusive. Photosynthesis of the symbiont may supply carbon-rich photosynthetic compounds to the sponge, thereby providing energy to etching cells. Alternatively, symbionts may provide oxygen for the sponge's mitochondria and thereby a more acidic environment through net CO_2 production (Achlatis et al., 2019). CO_2 uptake by symbionts would theoretically cause local pH within the sponge to increase, making conditions for $CaCO_3$ dissolution less favorable. However, as most of the dinoflagellate cells migrate to the surface layer of the sponge by day, dissolution and photosynthesis become spatially separated, which may explain their coexistence in spite of their opposite effects (Schönberg and Suwa, 2007; Achlatis et al., 2019). In addition, the creation of a microenvironment with a distinct chemistry (Rützler and Rieger, 1973; Pomponi, 1977; Schönberg et al., 2017) suggests strict control by etching cells over the carbonate chemistry at the dissolution site (Webb et al., 2019). The etching process involves the production of low pH vesicles and shifting solubility equilibria at the interface between the coral skeleton and the sponge (Webb et al., 2019). As carbonic anhydrase enzymes greatly increase the speed of the reversible reaction $H_2O + CO_2 \leftrightarrow H^+ + HCO_3^-$ and have been observed abundantly around etching processes at the sponge-coral interface (Hatch, 1980; Pomponi, 1980), they are thought to play a central role in dissolution of $CaCO_3$ by excavating sponges.

CA is known to be involved in $CaCO_3$ precipitation by many calcifiers such as corals (Furla et al., 2000; Moya et al., 2008; Tansik et al., 2017) and bivalves (Miyamoto et al., 2002) among others. The exact role CA plays in enhancing aragonite dissolution by excavating sponges in unclear but it is hypothesized that it may facilitate the transport of H^+ across membranes and/or provides an optimum pH for the activity of chelating agents (e.g. calcium chelators) and enzymes responsible for the breakdown of the organic matrix (Hatch, 1980; Pomponi, 1980).

This study aims at determining the role of carbonic anhydrase in chemical dissolution by excavating sponges. As dissolution rates have been shown to be light-enhanced and increase in high CO_2 environments, we block the activity of carbonic anhydrase

in two sponge species: *Cliona caribbaea* (Carter 1882) and *Suberea flavolivescens*, of which the latter does not host *Symbiodinium* and the effect of this inhibition is tested as a function of pCO_2 during the day, as well as during night.

2 Materials and methods

2.1 Study area and sample collection

Bioeroding sponge specimens were retrieved from dead coral substrate found between 5 and 15 m depth at the leeward side of Curaçao (southern Caribbean) during February 2017. Samples were collected at Snake Bay (12°8'N, 68°59'W), Piscadera Bay (12°7'N, 68°58' W) and Directors Bay (12°3'N, 68°51'W) using an air drill and hole saw (inner diameter: 45 mm). The retrieved sponges were transported submerged in ambient sea water to large flow-through aquaria in the research facilities of the Carmabi Research Station. Cores were gently cleaned and left to acclimatize and recover for 1 week, during which full tissue regeneration was observed. Samples of similar dimension consisting of dead coral skeleton which were not infested by bioeroding sponges, served as control substrate.

Two excavating sponge species were collected including a gallery-forming species: *Cliona caribbaea* and a network forming species: *Suberea flavolivescens*. *C. caribbaea* lives in symbiosis with photosynthetic dinoflagellates of the family *Symbiodiniaceae*, whereas no algal symbionts have been recorded in *S. flavolivescens* (De Bakker et al., 2018). In total, 18 cores were collected including 6 containing *S. flavolivescens* and 12 with *C. caribbaea*. To determine chemical bioerosion rates, net respiration and production during daytime and nighttime, they were placed in closed 0.5 L polycarbonate incubators, for 1 hour, with inbuilt stirrers. Chambers were submerged in aquaria to prevent temperature fluctuations during the incubations. Two cores were placed in each chamber which was sealed air-tight to avoid gas exchange with the external environment. Temperature (°C) and oxygen concentration (mg L^{-1}) were monitored continuously over the course of the incubation using a PreSens O_2 sensor (Fibox 4, PSt3). Samples for alkalinity (~250 mL), pH (~30 mL) and nutrient concentrations (PO_4^{3-}, NH_4^+, NO_2^-, NO_3^-) were collected at the start and the end of each run.

2.2 Sample analysis

Analyses for A_T were performed within 2 hours following sampling using spectrophotometrically guided single-step acid titration (Liu et al., 2015). This optical titration procedure has a remarkable high precision (± 0.7 μmol kg^{-1}) allowing the detection of minor (<5 µmol kg^{-1}) alkalinity fluctuations. A_T was measured immediately upon

sample collection. To compensate for a drift in A_T over the course of the experimental period, certified reference material (CRM; supplied by Dr. A. Dickson, Scripps Institution of Oceanography) was analyzed every 20 samples. Sample pH was measured using an automated spectrophotometric pH measurement system with precision on the order of 0.004 pH units (Clayton and Byrne, 1993; Liu et al., 2011). Other carbonate system parameters were calculated from A_T and pH using the package 'seacarb' in the programming environment R 3.3.2 (R Core Team, 2013). Samples for dissolved inorganic macronutrients ($NO_2^- + NO_3^-$, PO_4^{3-} and NH_4^+) were prepared by dispensing sampled water through 0.8/0.2 μm Acrodisk filters into 5 ml pony vials, and subsequently stored at -20°C upon analysis at NIOZ on a QuAAtro continuous flow analyser (SEAL Analytical, GmbH, Norderstedt, Germany) following GO-SHIP protocol (Hydes et al., 2010).

2.3 Inorganic carbon scenarios

Incubations were carried out in three scenarios, all of which had a similar total inorganic carbon concentration (DIC), but varied in their relative pCO_2, HCO_3^- and CO_3^{2-} concentrations (table 1). Target pCO_2 concentrations were adjusted by adding to ambient seawater calculated amounts of either NaOH or HCL. Ranges of pCO_2 concentrations were aimed to include a pre-industrial scenario (280 µatm), an ambient scenario (400 µatm), and a 'business-as-usual' CO_2 emission scenario (1050 µatm). However, as seawater carbonate chemistry was altered using chemicals rather than bubbling CO_2 in the seawater (Riebesell et al., 2011), we refrain from discussing the results in the context of future climate change scenarios.

2.4 Carbonic anhydrase inhibitor and symbiont impairment

For each scenario, three additional incubations were carried out within the presence of the CA-inhibitor acetazolamide (AZ). AZ is a membrane-impermeable inhibitor that has been previously used to assess extracellular CA activity in a wide variety of marine macrophytes (Björk et al., 1997; Uku and Björk, 2005; Moroney et al., 1985; Chen and Gao, 2004). An inhibitor stock solution was prepared by dissolving sodium acetazolamide in filtered sea water (20 mM) and adjusting the pH by addition of HCl (0.1 M) to that of the sea water system for each respective scenario. Incubations were performed parallel to those for which no inhibitor was added. For *C. caribbaea*, 6 of the 12 cores were placed in the dark, in a flow through tank for 2 weeks prior to the start of the incubation period in order to bleach them from most of their symbionts (pers. com. Malcolm Hill). The sponges became white after a few hours due to migration of the symbionts deeper into the tissue (Schönberg and Suwa, 2007) and stayed white for

the remainder of the experimental period. Once all the incubations were carried out, the dinoflagellates in the tissues of both *C. caribbaea* and *C. caribbaea*-bleached were quantified and compared. To isolate the sponge tissue from the coral skeleton, cores were dissolved in acid (2 M HCl). The liberated sponge tissue was then cut in small pieces and pressed through a compress to dissociate the cells. Five subsamples for each sponge sample were then placed on a haemocytometer to determine the symbiont density.

For each sponge type, incubations were carried out in triplicates in each pCO_2 scenario, with and without AZ during the day and the night resulting in a total of 108 (3x3x3x2x2) incubations. To investigate CA activity further, 24 (4x6)additional incubations were carried out for each pCO_2 scenario, during day and night at twice the AZ (40 mM) concentration (+ an extra 5 incubation to check the spread of *C. caribbaea* dissolution rates during the day and 3 extra at night for *S. flavolivescens*).

2.5 Net dissolution rates

Chemical bioerosion was quantified using the alkalinity anomaly technique (Smith et al., 1975; Chisholm and Gattuso, 1991), which involves measuring the changes in A_T (μmol kg^{-1}) associated with dissolution in seawater during 1h incubation periods. and correcting for changes in the concentrations of ammonium, nitrate and phosphate (Jacques and Pilson, 1980; Wisshak et al., 2013). Release of nutrients during respiration decreases A_T (or increases A_T for net release of NH_4^+), confounding the interpretation of changes in A_T to represent $CaCO_3$ dissolution only. Following common protocol, we corrected measured A_T for nutrient release and the amount of dissolved calcium carbonate [$\Delta M(CaCO_3)$, in μg] was calculated using Equation (1) (Zundelevich et al., 2007; Nava and Carballo, 2008):

$$\Delta M(CaCO_3) = 0.5 \times [\Delta A_T + \Delta PO_4 - \Delta NH_4 + \Delta(NO_3 + NO_2)] \times V_{SW} \times \rho SW \times 100$$

Where ΔA_T is the increase in A_T over the incubation period associated with dissolution, V_{SW} is the volume of seawater in the incubation chamber and ρSW is local seawater density. The multiplication factor "100" represents the molecular mass of $CaCO_3$.

2.6 Net respiration rates

Net respiration was quantified from ΔDIC which was calculated from pH and A_T using the package 'seacarb" in the programming environment R 3.3.2 (R Core Team,

2013). The contributions of net respiration to the observed concentrations of DIC were calculated as follows:

$\Delta A_T{}^{diss} = \Delta A_T{}^{obscNC}$ ..... change in A_T due to diss or calci
$\Delta A_T{}^{resp} = 0$ ..... change in A_T due to resp or photo
$\Delta DIC^{diss} = \Delta A_T{}^{obscNC}/2$ ..... change in DIC due to diss or calci
$\Delta DIC^{resp} = \Delta DIC^{obsc} - \Delta DIC^{diss}$ ..... change in DIC due to resp or photo

2.7 Statistical analysis

All statistical analyses were performed using the programming environment R 3.3.2 (R Core Team, 2013). Rates and residuals were tested for normality and homoscedasticity using the Shapiro-Wilk and Levene's test, respectively. Chemical bioeorsion rates were sqrt (x + a) transformed to meet normality assumptions. Subsequently, they were analyzed by means of a 3 × 3 × 2 × 2 crossed analysis of variance (ANOVA) with 4 categorical factors (pCO_2, light, sponge type, AZ) including three pCO_2 scenarios (low, ambient, and high), two light levels (day and night), three sponge types (*C. caribbaea*, *C. caribbaea*-bleached and *S. flavolivescens*) and two acetazolamide (with and without AZ) levels, respectively. Net respiration rates were analysed using a 3-way ANOVA with 3 categorical factors (pCO_2, light, sponge type). As the main factor AZ (2 levels: 'With' or 'Without') did not have a significant effect on net respiration and did not show any interaction with any other factor, it was pooled from the 4-way ANOVA to render the analysis more robust. Chemical bioerosion rates across different AZ concentrations were analysed by means of a 2 × 3 × 3 ANOVA with 3 categorical factors including light, sponge type and AZ concentration (3 levels: '0 mM', '20 mM', and '40 mM'). In the case of significant interactive effects, Post hoc tests (Tukey HSD with Bonferroni correction) were applied to explore differences between multiple group means and determine the effect of a factor at each level of the other.

3 Results

The inorganic carbon chemistry in low, ambient and high pCO_2 scenarios were significantly different from each other ($p < 0.001$), both with and without the addition of the inhibitor (table 1). Some discrepancies occurred within each scenario due to both the addition of AZ and the daily variation in ambient water chemistry. The addition of AZ caused the bicarbonate ion concentration to increase significantly by ∼70 µmol $kgSW^{-1}$ on average in each scenario. The increase in A_T as well as DIC with AZ addition are explained by the latter. The main effect of AZ on pCO_2 was not

Table 1: Carbonate chemistry parameters in µmol kgSW^{-1} of the 3 scenarios: low pCO_2, ambient and high pCO_2 with and without the addition of acetazolamide (AZ).

Scenarios	AZ	A_T*	DIC *	pH_{meas}	pCO_2	HCO_3*	CO_3	ΩAr
Low	−	2507±2	2055±8	8.20±0.01	277±8	1726±13	321±5	5.1±0.1
	+	2613±5	2136±6	8.20±0.02	311±18	1800±25	323±10	5.1±0.1
Ambient	−	2383±12	2045±15	8.00±0.02	399±15	1794±18	241±5	3.8±0.1
	+	248±5	2139±9	8.00±0.01	426±11	1880±12	248 ±3	3.9±0.1
High	−	2157±2	2053±8	7.60±0.01	1211±120	1929±10	92±4	1.5±0.1
	+	2263±5	2138±16	7.60±0.04	1133±61	2001±21	100±9	1.6 ± 0.1

[1] Carbonate parameters that changed significantly with addition of AZ are marked with a '*'.

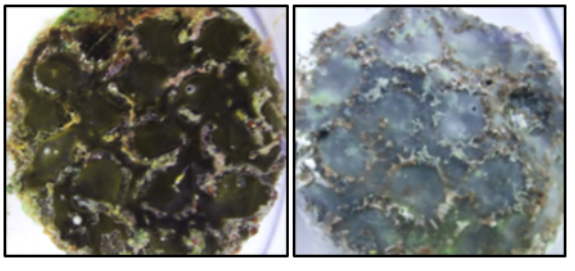

Figure 1: *C. caribbaea* (left) and *C. caribbaea*-bleached (right) cores.

significant. Initial pH and pCO_2 varied significantly with light (p=0.02 and p=0.01 respectively).

Symbiont densities were on average 78% lower in cores of *C. caribbaea*-bleached than in *C. caribbaea*. Remaining symbionts were all located deep within the tissue, explaining the discoloration of the sponge (figure 1). The main effect of scenarios, light, sponge type and AZ on dissolution rates were all significant (figure 2, table 2). In addition an interaction between the effects of AZ and light was present, as well as between the effects of pCO_2 scenarios and sponge types, and between sponge type and light (table 2). The addition of AZ appears to affect dissolution rates differently during day and night.

A post hoc pairwise comparison revealed that the significant differences in impact of AZ between day and night mostly occurred for the *Cliona* species (also bleached). During day-time, dissolution rates increased with the addition of AZ while at night-time, the addition of the AZ appears to inhibit part of the chemical bioerosion (figure 2). A post hoc pairwise comparison revealed that the effect of light on dissolution rates by *S. flavolivescens* was not significant unlike the *C. caribbaea* and *C. carib-*

baea-bleached.

Doubling the AZ concentration (to 40 mM) still enhances day-time dissolution rates although the average rates decreased slightly (not significant, table 3) compared to treatments with 20 mM AZ for all sponge types (figure 3). The highest AZ concentration further inhibited night dissolution rates in *C. caribbaea* and bleached *C. caribbaea* but not in *S. flavolivescens*. The effects of light and sponge type on dissolution rates are significant and although the main effect of different AZ concentrations is found to be non-significant, an interaction between the effects of light and AZ is revealed (table 3). A post hoc pairwise comparison revealed that the effect of AZ is inversed at day and at night. For all types of sponges, dissolution rates decreased significantly at night with increased AZ concentration. Net respiration rates increased significantly at night for *C. caribbaea* in every pCO_2 scenarios (figure 4). Increase in pCO_2 caused a significant decrease in net respiration during the day for *C. caribbaea*. Although a slight decrease in average net respiration was observed with addition of AZ for all sponge types, it did not significantly affected respiration rates. In accordance with net respiration, net dissolved oxygen evolution decreased significantly at night for *C. caribbaea* in every pCO_2 scenarios (table S1). However no clear pattern could be identified across pCO_2 ranges nor with or without the addition of AZ.

4 Discussion

4.1 CO_2 enhanced chemical bioerosion

Enhanced pCO_2 has an overall positive effect on erosion rates (figure 2), which is in line with previously published effects of higher pCO_2 on sponge erosion rates (Wisshak et al., 2012; Fang et al., 2013; Wisshak et al., 2013; Schönberg et al., 2017; Webb et al., 2017). Although dissolution rates were found to be comparable to literature (De Bakker et al., 2018), current dissolution rates will not be discussed in the context of ocean acidification as seawater carbonate chemistry was not altered in an ecological relevant way (Riebesell et al., 2011). Over the ranges tested here, higher pCO_2 caused the largest increase in dissolution rates. Although, the mechanism responsible for higher dissolution rates at increased pCO_2 is unclear, it likely involves a) a reduced effort by etching cells to decrease ΩAg below 1 (Webb et al., 2019), b) an increase in proton availability to dissolve aragonite and c) an increase in energy delivered to etching cells due to enhanced photosynthesis (Hill, 1996; Schönberg et al., 2017; Achlatis et al., 2018). However, as enhanced day and night dissolution rates become comparable at high pCO_2 irrespective of the species, the positive effects of enhanced photosynthesis on dissolution rates appear to become negligible.

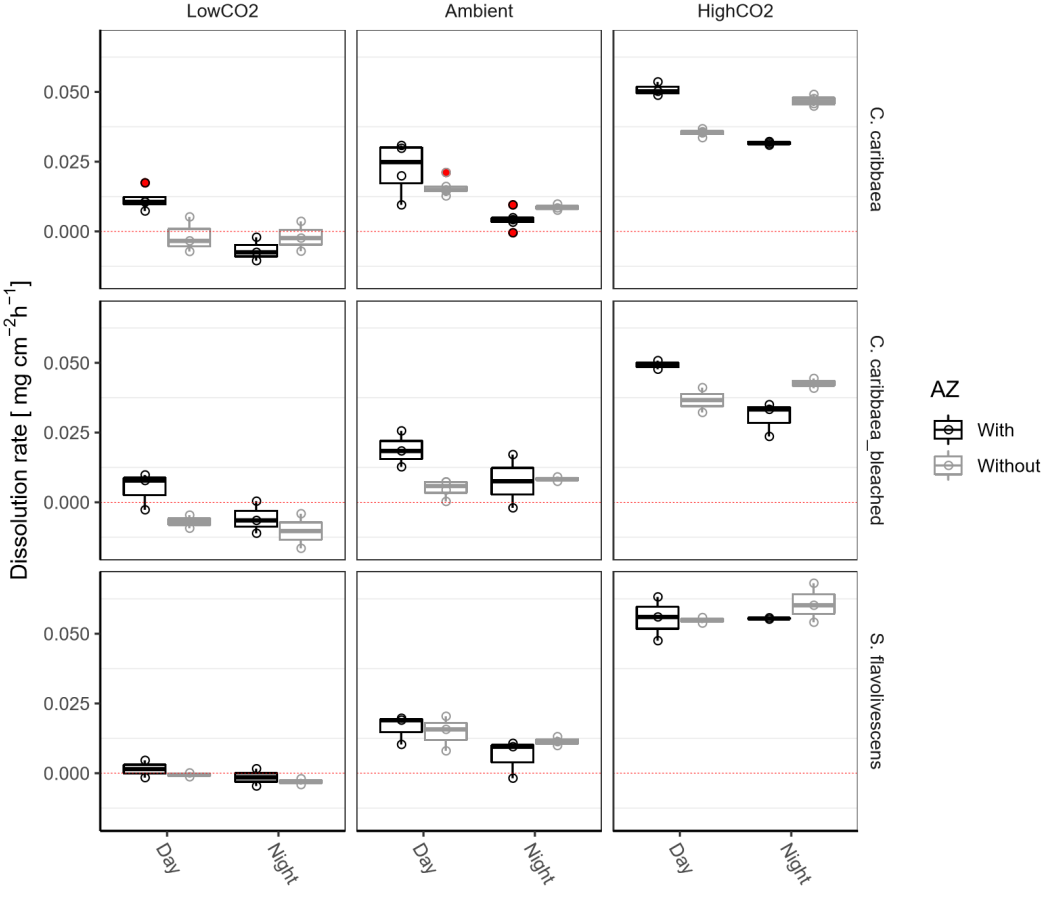

Figure 2: Boxplots of chemical bioerosion rates by *C. caribbaea*,*C. caribbaea*-bleached and *S. flavolivescens* under LowCO_2, AmbientCO_2 and HighCO_2 scenarios with and without acetazolamide (AZ) during day and night incubations. Outliers are in red.

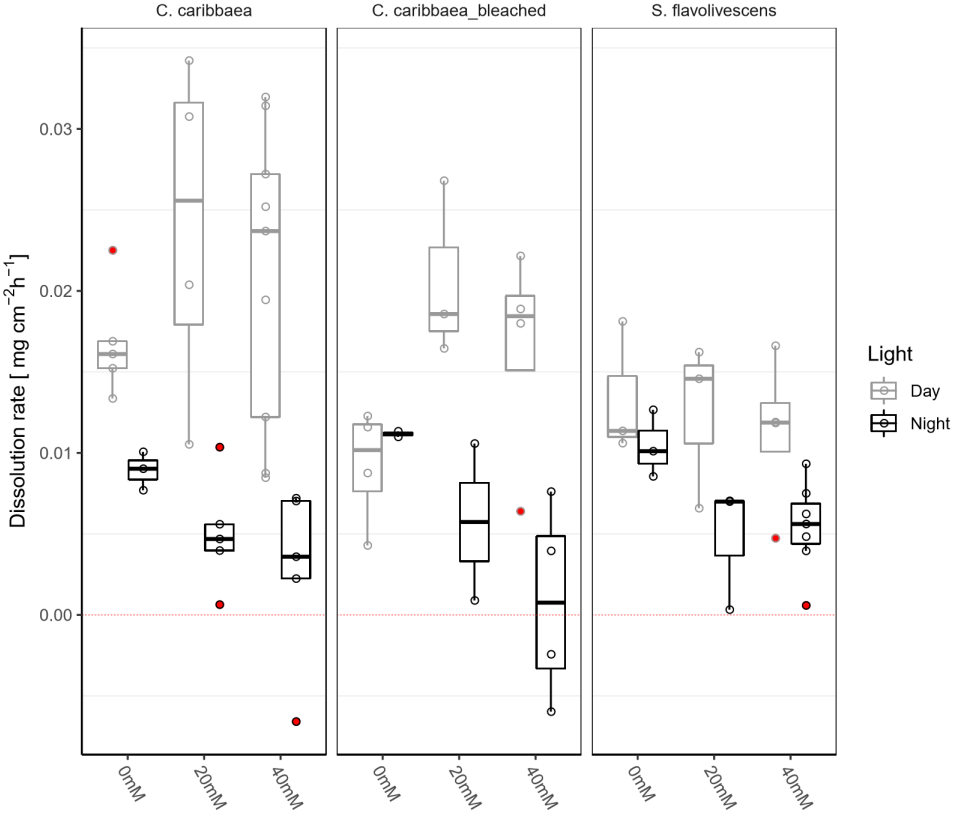

Figure 3: Boxplots of chemical bioerosion rates by *C. caribbaea*, *C. caribbaea*-bleached and *S. flavolivescens* under 3 different concentrations of acetazolamide (AZ: 0, 20 and 40 mM) at ambient pCO_2. Outliers are in red.

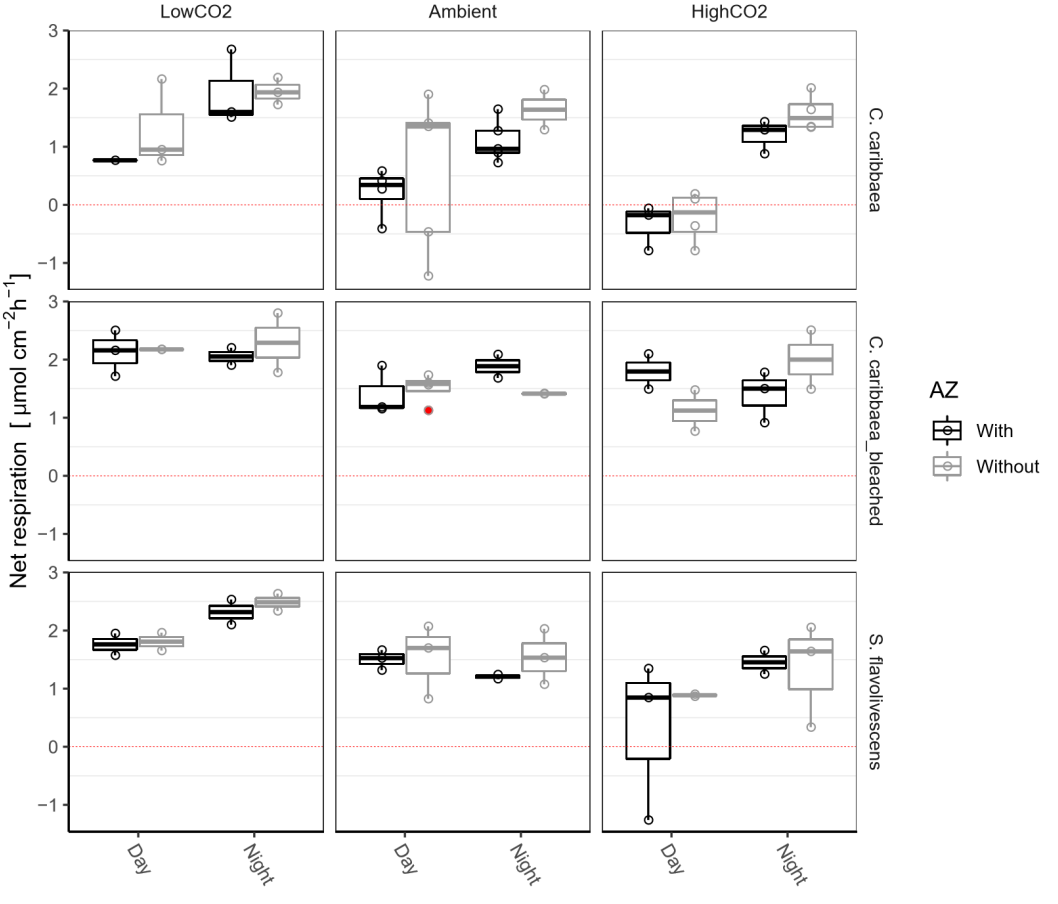

Figure 4: Boxplots of net respiration rates by *C. caribbaea*, *C. caribbaea*-bleached and *S. flavolivescens* under scenarios LowCO_2, AmbienCO_2 and HighCO_2 with and without acetazolamide (AZ). Outliers are in red.

Table 2: 4-way ANOVA and 3-way ANOVAs with chemical bioerosion rates and net respiration rates as dependent factors and pCO_2 scenarios, sponge type, light and acetazolamide (AZ) concentrations as independent categorical factors.

	df	SS	MS	F value	P value
Dissolution Rates ~ pCO_2 * Light * Sponge * AZ					
Scenario	2	0.257	0.129	409.765	**<0.001**
Light	1	0.011	0.011	34.907	**<0.001**
Sponge	2	0.006	0.003	8.76	**<0.001**
AZ	1	0.001	0.001	4.51	**0.037**
Scenario:Light	2	0.002	0.001	3.611	**0.032**
Scenario:Sponge	4	0.004	0.001	2.85	**0.03**
Light:Sponge	2	0.002	0.001	2.48	0.091
Scenario:AZ	2	0.002	0.001	2.895	0.062
Light:AZ	1	0.009	0.009	29.065	**<0.001**
Sponge:AZ	2	0.002	0.001	3.006	0.056
Scenario:Light:Sponge	4	0.002	0.0003	0.805	0.526
Scenario:Light:AZ	2	0.0003	0.0002	0.576	0.565
Scenario:Sponge:AZ	4	0.001	0.0002	0.617	0.652
Light:Sponge:AZ	2	0.001	0.001	2.213	0.117
Scenario:Light:Sponge:AZ	4	0.001	0.0002	0.788	0.537
Residuals	69	0.022	0.0003		
Dissolution Rates ~ Light * Sponge * AZ concentration					
Light	1	0.002	0.002	67.587	**<0.001**
Sponge	2	0.0002	0.0001	2.981	0.059
AZ concentration	2	0.00004	0.00002	0.51	0.603
Light:Sponge	2	0.0003	0.0002	4.849	**0.011**
Light:AZ concentration	2	0.0004	0.0002	5.762	**0.005**
Sponge:AZ concentration	4	0.0001	0.00002	0.593	0.669
Light:Sponge:AZ concentration	4	0.0001	0.00002	0.706	0.592
Residuals	55	0.002	0.00003		
Net respiration Rates ~ pCO_2 * Light * Sponge					
Scenario	2	11.031	5.516	20.21	**<0.001**
Light	1	11.534	11.534	42.261	**<0.001**
Sponge	2	14.31	7.155	26.217	**<0.001**
Scenario:Light	2	2.90	1.45	5.312	**0.007**
Scenario:Sponge	4	1.366	0.341	1.251	0.297
Light:Sponge	2	3.006	1.503	5.508	**0.006**
Scenario:Light:Sponge	4	0.925	0.231	0.847	0.45
Residuals	75	20.469	0.273		

4.2 Light enhanced chemical bioerosion

At ambient pCO_2, chemical dissolution rates are enhanced on average by 40% during daytime compared to night time. These results are comparable with rates from previous studies (Hill, 1996; Fang et al., 2013; Webb et al., 2017). Chemical bioerosion rates of bleached *C. caribbaea* were not enhanced during day-time compared to night at ambient pCO_2, which attests to the lessened activity of the diminished symbiont numbers. In addition, increased net respiration rates during the day for bleached *C. caribbaea* is also in line with the reduced photosynthesis by the symbionts.

The cause for light-enhanced dissolution rates remains elusive but previous research suggest that the symbionts provide additional energy to etching cells which stimulate chemical dissolution during the day (eg. Hill, 1996). Using a tracer experiment, (Weisz et al., 2010) found strong evidence of a transfer of carbon from zooxanthellae to their *Cliona* sponge hosts. More recently, Achlatis et al. (2018) showed translocation of labelled organic nutrients from *Symbiodinium* to the *Symbiodinium*-hosting sponge cells, and occasionally to other sponge cells. This supports the potential metabolic interaction between the sponge and dinoflagellates.

DIC is a substrate for both photosynthesis and chemical bioerosion. The chemical species used (HCO_3^- or CO_2), the provenance of this species (metabolic or external) and the mode of transport (active versus passive) are not fully known for both mechanisms regarding excavating sponges. We make the case that the fact that both corals and bioeroding sponges regulate their carbonate chemistry to precipitate or dissolve $CaCO_3$ and both harbour dinoflagellates of genus Symbiodinium may suggests that symbionts are benefiting not only from protection but also from the chemical products of calcification or dissolution.

4.3 CA involvement in bioerosion

Combining results, we found no interaction between pCO_2 scenarios and CA inhibition (table 3), indicating that the inhibitor has similar effect on chemical bioerosion across pCO_2 ranges. The effects of carbonic anhydrase inhibitor on chemical bioerosion rates by excavating sponges differ between day-time and night-time. Dissolution rates at night decrease significantly with AZ addition (figure 2 & 3), unlike day dissolution rates which increase with the addition of the CA inhibitor. The recorded decrease in dissolution rates at night across sponge types suggest a relatively important effect of CA activity at night compared to day time. This is comparable to results from experiments with corals (Goreau, 1959; Furla et al., 2000; Moya et al., 2008), where effects of carbonic anhydrase inhibitor on calcification were found to be higher in the dark than in the light. Moya (2008) found an up-regulation of the coral CA gene

during the night and suggested this was a mechanism to cope with night acidosis by removing protons produced by the calcification process at a faster rate. In light, protons are titrated by the alkaline environment due to photosynthesis facilitating CO_2 diffusion out of the calcification site. Whereas at night, enhanced protonation of bicarbonate ions facilitates CO_2 diffusion away from the site of calcification.

It is interesting to note that, in the *C. caribbaea* species, the inhibitor has a comparable effect at night as exclusion of light, both causing a fall of about 30 to 40% in the dissolution rate. This suggests that, as far as their potentiating effect on the dissolution rate is concerned, the action of carbonic anhydrase and that of photosynthesizing zooxanthellae are similar (Goreau, 1959).

4.4 Possible mechanisms and implications

As chemical bioerosion can still continue under dark conditions and in presence of AZ, it suggests that neither the enzyme nor the symbiotic algae determine the basic $CaCO_3$ dissolution reaction, but that they can exert a strong influence on its integrated rate. Whatever the mechanism underlying enhanced chemical bioerosion, the rate of $CaCO_3$ dissolution depends on a) the rate at which protons are provided to the etching site (Webb et al., 2019) and simultaneously b) the rate at which the 'waste' products (i.e. Ca^{2+} and DIC) are removed from this site, as the buildup of these compounds would increase saturation state and hamper ongoing dissolution. Depending on the pH, the carbonate ions originating from carbonate dissolution are converted to bicarbonate ions and CO_2, with the ratio between the two depending on the $[H^+]$ (and hence delivery of protons into the etching site) and the rate of DIC removal from the etching site. An efficient way to remove the DIC would be through passive diffusion of uncharged CO_2 molecules (not unlike the process by which corals remove unwanted protons from the calcification site (Moya et al., 2008)), which is promoted by maintaining a gradient in CO_2 over the boundary separating the etching site from the rest of the sponge's tissue (figure 5). Carbonic anhydrases may help diffusion by promoting the protonation of bicarbonate to form CO_2, which would explain why inhibiting CA activity decreases erosion rates (figure 1 & 2).

During the day, the uptake of CO_2 by the symbionts likely intensifies the pCO_2 gradient between etching site and sponge's interior, hence promoting removal of carbonate ions from the etching space and stimulating dissolution rates. Alternatively, once out of the etching site, CA may also be involved in the conversion of CO_2 into HCO_3^-, preventing CO_2 back-diffusion and provide symbionts with metabolic HCO_3^-, still intensifying the gradient. Zooxanthellae have been shown to be able to take both DIC sources (Goiran et al., 1996; Furla et al., 2000; Leggat et al., 2002). Although symbionts likely stimulate dissolution during the day by providing energy

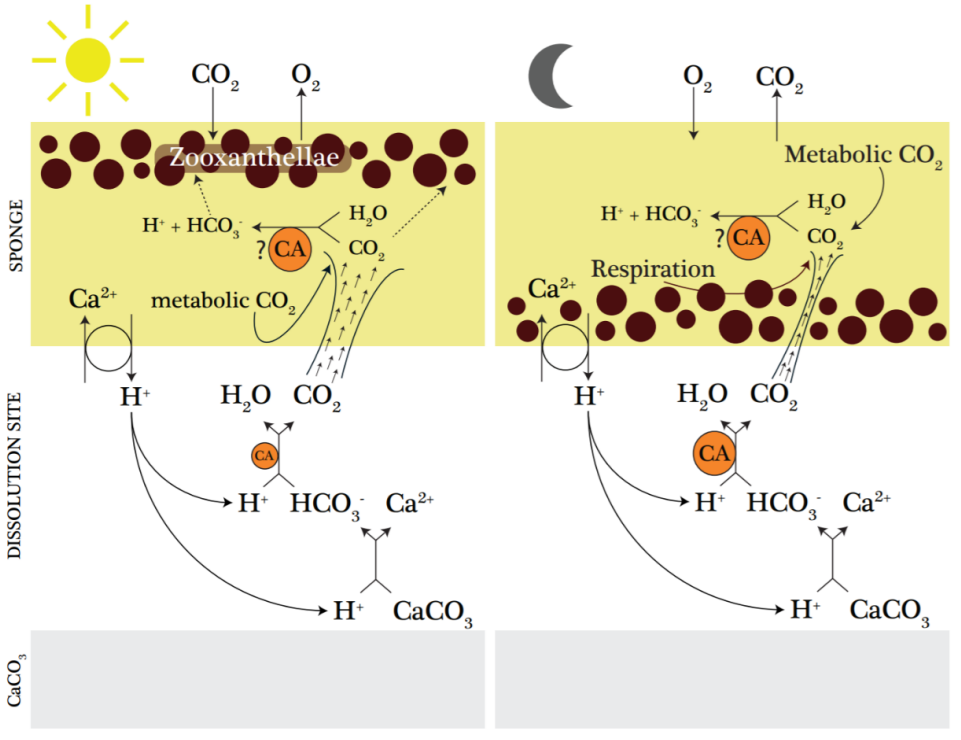

Figure 5: Working model for the diurnal variability in carbonic anhydrase activity in chemical dissolution by excavating sponges. Brown circle represent Zooxanthellae which photosynthesise during the day and respire during the night. Protons are received in exchange for calcium ions at the dissolution site. Dissolution of $CaCO_3$ puts bicarbonate ions in solution which are converted to CO_2 and passively diffuses out of the sponge. This reaction is made faster with carbonic anhydrase enzymes. During the day, due to uptake of CO_2 or HCO_3^- by symbionts, the natural gradient is favourable to CO_2 diffusion out of the etching site and so CA activity (in orange) is minor. Whereas at night, the high CO_2 concentration within the sponge tissue due to symbiont + sponge respiration (here metabolic CO_2) causes the diffusion gradient to be lessened. CA activity is enhanced within the etching site to promote CO_2 diffusion. Once out of the etching site, CA may also be involved in the conversion of CO_2 into HCO_3^-, preventing CO_2 back-diffusion and provide symbionts with metabolic HCO_3^-, still intensifying the gradient.

to the sponge (Achlatis et al. 2018), we hypothesize that additionally, the symbionts' activity increase the rate at which dissolution products are removed from the etching site. Since day and night dissolution rates are comparable at high pCO_2 (Webb et al., 2017), we also hypothesize that the pCO_2 gradient cannot be intensified further, even

with enhanced photosynthesis, as in the sponge tissue pCO_2 concentrations are too high. At high pCO_2, faster dissolution rates are likely the result from the reduced ΩAg, with less protons being required to dissolve calcium carbonate.

4.5 CA involvement at night

At night-time, the pCO_2 gradient between etching site and the sponge tissue decreases since the symbionts respire and produce, rather than consume, CO_2. Increased CA activity at night hence speeds up protonation of bicarbonate ions, enabling CO_2 to diffuse out of the etching area (figure 5). This explains why inhibiting CA decreases dissolution rates of *C. caribbaea* at night. Concerning *S. flavolivescens*, a decrease in dissolution rates during day and night times is expected as this sponge has no algal symbionts. Although a decrease at night was observed, dissolution rates during the day did not change significantly with the addition of CA inhibitor. *S. flavolivescens* is an understudied excavating sponge and only recently found on Curaçao (De Bakker et al., 2018). Although thought to have no algal symbionts, it may still harbour low densities of Symbiodinium or photosynthetic cyanobacteria which would explain the reduced CA activity during the day. However, *S. flavolivescens* did not exhibit enhanced day + AZ dissolution rates unlike *C. caribbaea* irrespective of the pCO_2 and symbiont impairment which in turn suggests that *S. flavolivescens* does not harbour the same symbionts.

4.6 CA involvement during the day

Although the addition of AZ impacted dissolution rates differently between day and night irrespective of the species and the pCO_2 scenario, AZ did not impact *S. flavolivescens* during the day (at all AZ concentrations tested here). This suggest a minor role of CA in chemical bioerosion for *S. flavolivescens* during the day. The AZ-enhanced dissolution rates observed during the day for *C. caribbaea* seem to be irrespective of the condition and activity of the symbionts, as dissolution rates for both bleached and non-bleached *C. caribbaea* become comparable with the addition of AZ. Although a large number of replicates were used, experimental biases cannot be entirely rejected. Previous literature reported events of AZ being moderately cell permeable (Teppema et al., 2006) which may have impacted other holobiont metabolic processes and enhanced chemical bioerosion during the day. The significant [HCO_3^-] increase ($\sim$70 µmol $kgSW^{-1}$ on average in all scenarios) may also have impacted our results. Bicarbonate has previously been shown to have a stimulatory effect on CA activity (Müller et al., 2013). However, the availability of bicarbonate ions is already high compared to pCO_2 scenario and unlikely to be a limitation factor for photo-

synthesis. Initial conjecture explaining day AZ-enhanced dissolution rates includes enhancement of photosynthesis. The addition of the CA inhibitor may have caused zooxanthellae in low abundance in *C. caribbaea*_bleached to maximised CO_2 uptake. Indeed, the slight (non-significant) decrease in net respiration for *C. caribbaea* with addition of AZ (figure 5) across pCO_2 scenarios could attest to the enhancement of photosynthesis. However, if the CO_2 intake of symbionts was also amplified in bleached *C. caribbaea* with AZ addition, a similar decrease in net respiration would be expected which is not observed. In addition, O_2 profiles do not attest to an increase in net production with the addition of AZ (table S1). This suggests that the presence of these algal symbionts, irrespective of their numbers or activity, may enhance $CaCO_3$ dissolution rates of the host, which is inhibited by the action of the carbonic anhydrase enzyme. Zooxanthellae may exert a general stimulant effect on the host's metabolism, mediated through a vitamin or hormone-like factor (Goreau, 1959).

Recent work on symbionts in coral by Tansik et al. (2017) suggests host regulation of DIC delivery to the symbionts. They recorded very low DIC half saturation constant for photosynthesis and high levels of internal carbonic anhydrase activity, implying that symbionts exist in a carbon scarce environment and invest a great deal of energy in concentrating carbon at the site of photosynthesis. As *C. caribbaea* symbionts are located intracellularly and DIC is a substrate for both photosynthesis and chemical bioerosion, we tentatively infer that also here host cells might exert control over DIC delivery to the symbiont. This control may involve external CA and blocking its activity would impact the host's control on DIC delivery.

Conclusion

To conclude, the carbonate anhydrase enzyme is involved in chemical bioerosion processes by excavating sponges. This is the first report to show diurnal variability in the effect of carbonic anhydrase activity for $CaCO_3$ dissolution. The decrease dissolution rates at night across sponge type suggests a relatively important role of CA activity at night compared to day time. We propose that similarly to coral, dark-enhanced CA activity in sponges may promote diffusion of dissolution waste products in the form of CO_2. The increase in dissolution rates during the day with the addition of CA inhibitor is unexpected and requires further research to provide a clear understanding.

Aknowledgements

We would like to thank the Carmabi research station and particularly Dr. Mark Vermeij for his support and facilitating the fieldwork on Curaçao. Lisanne van den Bogaart is gratefully thanked for field and lab assistance. We also wish to thank Jasper de Goeij for lending us some equipment. We extend our sincere gratitude to Karel Bakker and Sharyn Ossebaar for analysing nutrient samples.

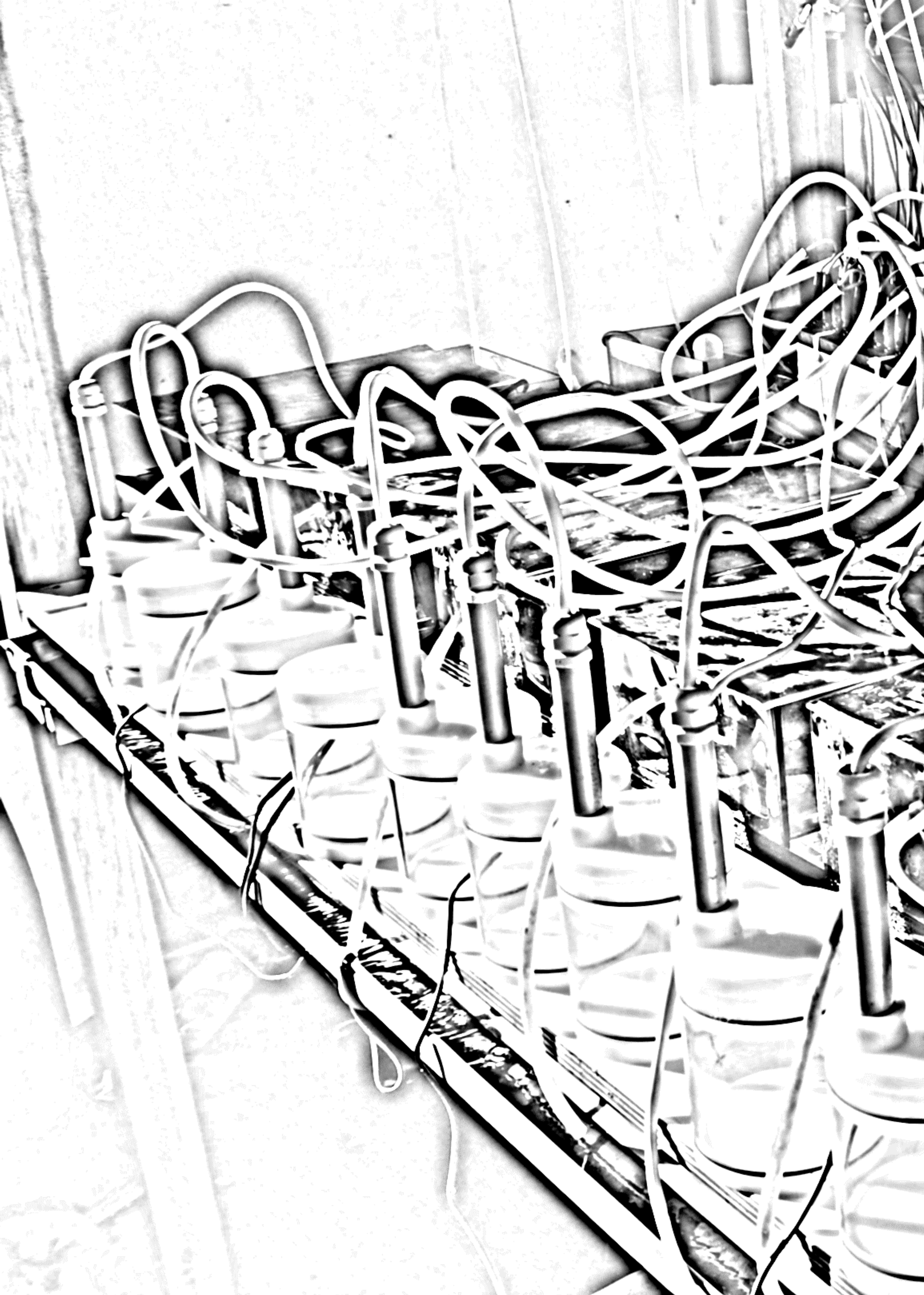

Chapter 4

Combined Effects of Experimental Acidification and Eutrophication on Reef Sponge Bioerosion Rates

Alice E. Webb, Steven M.A.C. van Heuven, Didier M. de Bakker, Fleur C. van Duyl, Gert-Jan Reichart, Lennart J. de Nooijer

Webb et al. 2017, Frontiers of Marine Science 4:311

Abstract

Health of tropical coral reefs depends largely on the balance between constructive (calcification and cementation) and destructive forces (mechanical - chemical degradation). Gradual increase in dissolved CO_2 and the resulting decrease in carbonate ion concentration ("ocean acidification") in ocean surface water may tip the balance toward net mass loss for many reefs. Enhanced nutrients and organic loading in surface waters ("eutrophication"), may increase the susceptibility of coral reef and near shore environments to ocean acidification. The impacts of these processes on coral calcification have been repeatedly reported, however the synergetic effects on bioerosion rates by sponges are poorly studied. Erosion by excavating sponges is achieved by a combination of chemical dissolution and mechanical chip removal. In this study, *Cliona caribbaea*, a photosymbiont-bearing excavating sponge widely distributed in Caribbean reef habitats, was exposed to a range of CO_2 concentrations, as well as different eutrophication levels. Total bioerosion rates, estimated from changes in buoyant weights over 1 week, increased significantly with pCO_2 but not with eutrophication. Observed chemical bioerosion rates were positively affected by both pCO_2 and eutrophication but no interaction was revealed. Net photosynthetic activity was enhanced with rising pCO_2 but not with increasing eutrophication levels. These results indicate that an increase in organic matter and nutrient renders sponge bioerosion less dependent on autotrophic products. At low and ambient pCO_2, day-time chemical rates were ∼50% higher than those observed at night-time. A switch was observed in bioerosion under higher pCO_2 levels, with night-time chemical bioerosion rates becoming comparable or even higher than day-time rates. We suggest that the difference in rates between day and night at low and ambient pCO_2 indicates that the benefit of acquired energy from photosynthetic activity surpasses the positive effect of increased pCO_2 levels at night due to holobiont respiration. This implies that excavation must cost cellular energy, by processes, such as ATP usage for active Ca^{2+} and/or active proton pumping. Additionally, competition for dissolved inorganic carbon species may occur between bioerosion and photosynthetic activity by the symbionts. Either way, the observed changing role of symbionts in bioerosion can be attributed to enhanced photosynthetic activity at high pCO_2 levels.

1 Introduction

The ocean serves as the largest sink of anthropogenic CO_2 on earth after the atmosphere itself. Since the beginning of the industrial revolution, it has taken up ∼28% of the emitted anthropogenic CO_2 (Le Quéré et al., 2015). The cumulative uptake of atmospheric carbon dioxide by the ocean has increased the total marine inorganic

carbon concentration, reduced pH and consequently decreased the $CaCO_3$ saturation state. Together, these effects are termed ocean acidification (OA) and it is predicted that average surface ocean $CaCO_3$ saturation state will have decreased by 25–50% at the end of the current century, depending on the emission scenario (Hoegh-Guldberg et al., 2007; Gattuso and Hansson, 2011; Veron, 2011).

Eutrophication, caused by increasing release of nutrients and organic material in surface waters, represents an additional threat to near-shore and coral reef environments. Recent studies have shown that local anthropogenic disturbances, such as nutrient and organic rich run-offs from agriculture and coastal development, as well as the input of poorly treated waste waters (Gast et al., 1999; Lapointe and Mallin, 2011; Govers et al., 2014) have caused the average pCO_2 of coral reefs to increase $\sim$ 3.5 fold faster throughout the globe over the past 20 years compared to the open ocean. This is suggested to be caused by a shift in the metabolic balance of coral reef ecosystems (Cai et al., 2011; Cyronak et al., 2014; Yeakel et al., 2015). Such anthropogenic input also promotes growth of opportunistic organisms, such as sponges, macroalgae, turf algae and/or benthic cyanobacteria (Holmes et al., 2000; Kuffner and Paul, 2001; Gorgula and Connell, 2004; Vermeij et al., 2010), potentially resulting also in major shifts in benthic community compositions (Hughes, 1994; Bruno et al., 2009; De Bakker et al., 2017).

Reef bioerosion by sponges and other bioeroding organisms (Wisshak and Tapanila, 2008) plays an important role in regulating the carbonate budget of coral reefs (Perry et al., 2014). Although the negative effects of OA on production of $CaCO_3$ (calcification) by corals are widely documented (Gattuso et al., 1998; Kleypas and Langdon, 2006; Hoegh-Guldberg et al., 2007; Pandolfi et al., 2011; Dove et al., 2013), its impact on biologically induced carbonate dissolution and mechanical destruction have been understudied (Zundelevich et al., 2007; Fang et al., 2013; Wisshak et al., 2014; Enochs et al., 2015; Schönberg et al., 2017) and has so far not been quantified in combination with eutrophication.

Bioeroding sponges contribute between 60 and 90% of total macroborer activity on coral reefs and their (surface-normalized) erosion rates have been found to equal and even surpass calcification rates of hermatypic corals (Macgeachy and Stearn, 1976; Edinger and Risk, 2000; Carballo et al., 2008; Perry et al., 2014). Bioeroding sponges use a combination of chemical dissolution and mechanical $CaCO_3$ chip removal to erode coral substrate (Nasonov, 1924; Rützler and Rieger, 1973; Pomponi, 1980). It is hypothesized that specialized cells of the bioeroding sponges are able to lower the pH at selected sites to promote controlled aragonite dissolution, thereby creating cavities in which the sponge grows. The mechanisms by which sponges dissolve carbonate has however remained elusive since this etching interface is not directly accessible.

Several of the most competitive bioeroding sponges harbor endosymbiotic dinoflagellates zooxanthellae and this symbiosis has been shown to enhance bioerosion in light (Hill, 1996; Fang et al., 2016). This raises the question further as to how symbionts enhance bioerosion. Geochemically, this is paradoxical because the autotrophic symbionts would tend to increase pH and enhance carbonate precipitation rather than dissolution (Garcia-Pichel et al., 2010).

If the chemical composition of the fluid at these sites is related to that of seawater, a reduction in ambient saturation state may lower energetic costs for the sponge to create a microenvironment that is undersaturated for $CaCO_3$, in which the aragonite skeleton may subsequently dissolve and chips are dislodged. Schönberg (2008) provided a first glimpse of a pH gradient toward the etching sites using micro-sensors which may indicate that sponges do indeed alter the chemistry at the site of bioerosion. Although the underlying physiological and mechanical processes employed by the sponges to erode are currently unknown, a number of studies have shown that an increase inpCO_2 of the ambient water results in increased bioerosion rates (Wisshak et al., 2012, 2013; Duckworth and Peterson, 2013; Fang et al., 2013), suggesting that changes in seawater chemistry directly affect the saturation state at the site where the coral aragonite is dissolved.

Since eutrophication may increase effects of OA in coastal waters, we here assess the potential combined effects on bioerosion rates (both chemical and mechanical) of the sponge *Cliona caribbaea* Carter, 1882. *C. caribbaea* is found abundantly in the Caribbean and is a representative of the "*Cliona viridis* species complex," including clionaids that form a symbiosis with the dinoflagellates of the genus *Symbiodinium* (Schönberg, 2000). These photosynthetic symbionts (zooxanthellae) provide sponges with a significant fraction of their carbon and energy via photosynthesis (Weisz et al., 2010; Fang et al., 2014). Since this affects diurnal patterns in the holobiont metabolism (Freeman and Thacker, 2011), bioerosion rates by *C. caribbaea* were determined at day and night.

2 Materials and methods

2.1 Sample collection

In December 2015, samples containing the bioeroding sponge *Cliona caribbaea* were retrieved from dead coral substrate (*Diploria* spp.), found at a water depth between 3 and 5 meters (S= 34 and T= 28°C) at the leeward side of the island of St. Eustatius, Caribbean Netherlands (17.4890°N, 62.9736° W). Annual mean seawater temperature is 27.6°C and varies from 26.1°C in Feb-Mar to 28.2°C in Sept-Oct. Samples were

collected using an air drill and hole saw (inner diameter: 40 mm) and transported submerged in ambient SW to an on-shore CO_2-controlled experimental set-up. The sponge-infested cores were placed in large flow-through tanks (50 L) for 1 week to allow them to recover from collection and transport. Samples of coral skeleton without bioeroding sponges served as control substrate for the incubations. Collected cores were brushed delicately with a soft brush to remove any non-sponge organisms. The experiment lasted 1 week from December 23 to December 30 2015, excluding acclimatization to the various pCO_2 scenarios, which was performed gradually over 6 days from the December 17 to December 22. Each core was photographed at the start (before acclimatization) and at the end of the experiment to assess physical variations throughout the experiment. In addition, fluorescein was released near the ostia half way through the experiment to make sure cores were still filtering.

2.2 Experimental setup

Sand-filtered nearshore seawater was continuously supplied to four 200-L barrels in which the pCO_2 of the water was maintained at four different levels. Water from each of the four barrels was continuously pumped into nine aquaria of 12 L each, resulting in a total of 36 aquaria distributed across three tables (A, B and C). Three different levels of dissolved organic and inorganic matter concentrations were maintained in three sets of three aquaria within each pCO_2 scenario (Figure 1). All aquaria received an irradiance at levels and spectral quality similar to in-situ conditions, as provided by sunlight passing through Marine Blue filters (#131; Lee filters), and neutral density shading cloth. The aquaria were placed in a 5 cm high flow-through bath of seawater to minimize temperature fluctuations.

Carbonate chemistry of the water in the four barrels was manipulated using a feedback control system developed in-house, consisting of a central xCO_2 sensor (LICOR Inc. model LI-7000), CO_2 injectors, CO_2 scrubbers and a control computer. In each barrel, water was adjusted to desired pCO_2 concentration via air perturbation continuously pumped at high flow ($\sim$25 L^{-1} min) through a sparger located at the bottom of the barrel to ensure rapid air-sea pCO_2 equilibration. Air from the four treatment barrels was sequentially sampled and analyzed for xCO_2. Measurements of xCO_2 (in ppm) were converted to pCO_2 (in µatm) by accounting for average hydrostatic pressure after bubble injection, water temperature and salinity and the humidity of the measurement gas stream following Dickson et al. (2007). Additionally, a zero-standard and ambient air were regularly measured to allow approximate drift-free operation. The measured pCO_2 levels were compared by a central computer system to set points and adjusted by either (i) injecting small amount of pure CO_2 into the circulated headspace air or (ii) recirculating the air through large soda lime-filled CO_2

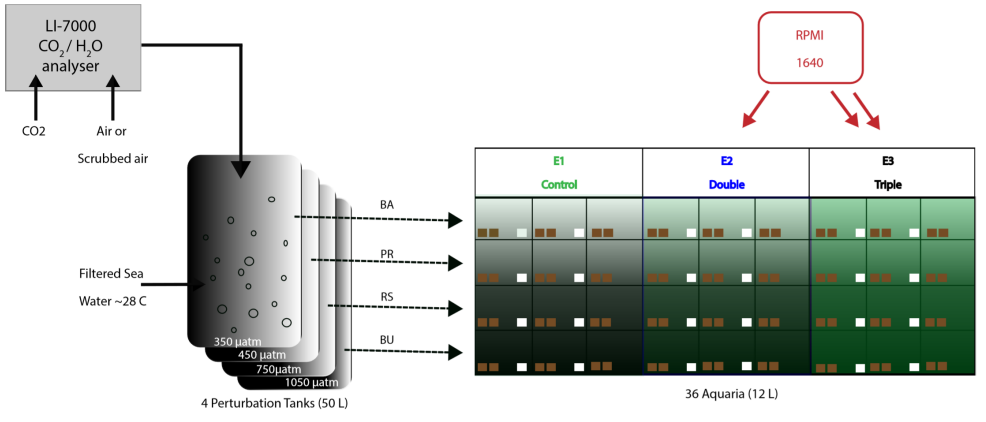

Figure 1: Experimental setup consisting of four large barrels in which the pCO_2 (4 levels) is manipulated and controlled through a central CO_2 sensor. From every barrel water is pumped into 9 aquaria (12 L each). Of these 9 two groups of 3 aquaria were supplied with additional dissolved organic carbon (E1: green, E2: blue, E3: black) using peristaltic pumps. Pumps ran at different speed between E2 and E3 to deliver different concentration of RPMI. Each of the 36 aquaria contained 2 sponge bearing coral cores (brown squares) and 24 aquaria contained control cores (white squares).

cartridges to remove CO_2. The system allowed treatment and delivery of ~50 liters of water per hour. The four treatments included a pre-industrial scenario (PI; 280 µatm), a present-day scenario (PD; 410 µatm), and two concentrations based on scenarios for potential future atmospheres predicted for 2100 (Solomon et al., 2007): one based on a 'reduced' CO_2 emission scenario (RE; 750 µatm) and one based on a 'business-as-usual' CO_2 emission scenario (BU; 1050 µatm). Reported pCO_2 is valid for the culturing temperature (i.e., slightly cooler than the treatment barrels), and estimated to be accurate to within 10 µatm.

Different amounts of dissolved organic and inorganic material were supplied from stock solutions by two 12-channel peristaltic pumps. Roswell Park Memorial Institute (RPMI) 1640 medium was used as the eutrophication supplement. RPMI is a well-known culture medium and it has been used as a growth enhancer on *C. crambe* sponge explants (Camacho et al., 2006). It contains sugars, inorganic salts, amino acids and vitamins and was used to simulate different levels of eutrophication in the aquaria.

The experiment aimed to provide multiples (1x, 2x, 3x) of the natural near-shore

labile DOC concentrations. Labile DOC represents the portion of the total DOC pool on which sponges can feed, here ∼20% of ∼80 µmol kg^{-1} (van Duyl and Gast, 2001; De Goeij and Van Duyl, 2007). Treatments were E1: control labile DOC conditions (i.e., only ∼16 µmol kg^{-1} natural labile DOC), E2: double labile DOC conditions (natural DOC + 16 µmol kg^{-1} DOC as RPMI1640) and E3: triple labile DOC conditions (natural + 32 µmol kg^{-1} RPMI 1640).

In total, 72 sponge-bearing cores and 24 control cores were collected and distributed evenly over the 12 scenarios, resulting in 2 sponge-bearing cores per aquarium and 2 control cores per scenario. Cores from increased-pCO_2 scenarios were exposed to gradually increasing pCO_2 over one week, ending with the desired pCO_2 for that treatment. Addition of RPMI started as scenarios reached their desired pCO_2 concentration. Subsequently, sponges were left to acclimatize to their respective carbon dioxide and eutrophication levels for a week prior to the incubations. Cores were placed in closed 0.5 L polycarbonate incubators with inbuilt stirrers in their respective aquaria to keep at constant temperature. Each incubation contained two cores and lasted 6 hours to determine chemical bioerosion rates (see 2.5). The optimum incubation time was determined through trials of 2, 4, 6 and 8 hours. Although 6 hours was considered the best fit to capture the alkalinity gradient caused by chemical bioerosion, it must be noted that sponges placed in 0.5 L of standing water for more than 1 hour would experience lack of food and reduced amounts of oxygen (especially at night) over time. At the end of each incubation, cores were returned to their aquaria.

2.3 Data collection

Temperature and irradiance of the water in the aquaria were recorded every 10 min by 6 HOBO® Pendant UA-002-64 light and temperature loggers and 2 calibrated Odyssey PAR sensors (Dataflow Systems, X, Y), respectively. Salinity was recorded daily in each aquarium using a salinometer (VWR CO310). Oxygen was recorded using a PreSens O_2 sensor (Fibox 4, PSt3) after each incubation. Throughout the experiment, every other day around noon, water samples were taken from each treatment to monitor carbonate chemistry, DOC and nutrients. Samples for alkalinity (A_T) and dissolved inorganic carbon (DIC) were collected into 250 ml borosilicate bottles and poisoned with 50 % saturated $HgCl_2$ solution (final concentration 0.02 %) to arrest biological activity. DOC samples (30 ml) were collected in pre-combusted (550 °C) glass vials and acidified with 10 drops of concentrated HCl (37%). Both A_T and DIC were measured on a Versatile Instrument for the Determination of Titration Alkalinity (VINDTA) model 3C (Marianda GmbH, Kiel, Germany). Determination of A_T was by 'open cell' potentiometric acid titration (Mintrop et al., 2000; Dickson

et al., 2007) and DIC was measured coulometrically (Johnson et al., 1993; Dickson et al., 2007). Prevention of drift and a high accuracy for A_T and DIC were attained by analysis of certified reference material (CRM; supplied by Dr. A. Dickson, Scripps Institution of Oceanography) after every ∼20 samples. The full carbonate system state was calculated from the measured temperature, salinity, A_T and DIC using the Seacarb package (R-3.2.0) and using the dissociations constants preferred by Dickson and Millero (1987). Samples for determination of nitrate + nitrite, nitrite, phosphate and ammonium were filtered upon collection and stored frozen. Analyses for nutrients were carried out on a QuAAtro continuous flow analyzer (SEAL Analytical, GmbH, Norderstedt, Germany) following GO-SHIP protocol (Hydes et al., 2010). DOC analyses were performed with a total carbon analyzer (TOC-VPN, Shimadzu Corp., Kyoto, Japan).

2.4 Assessment of net respiration and photosynthesis rates

Observed changes in DIC and A_T are governed by the combination of respiration and carbonate dissolution and the associated reverse processes of photosynthesis and calcification. The individual contributions of respiration and carbonate dissolution can be disentangled by empirically adjusting observed ΔA_T for nutrient effects using the measured nutrient concentration buildup. Indeed, in the case of incubation experiments, all of the change in nutrient concentrations must originate from processes within the incubation chamber. Therefore, this method will result in an appropriate estimate of respiration/dissolution, making calculated bioerosion rates insensitive to errors in measured DIC. Additionally, it takes into account the effect of release of $NH4^+$ on measured A_T, which the vector deconvolution does not and cannot, due to the variable release stoichiometry of $NH4^+$.Calculations were carried out as follow:

Pretreatment:

$$\Delta A_T{}^{nutsreleasecorrected} = \Delta A_T{}^{obs} + \Delta PO_4 - \Delta NH_4 + \Delta(NO_3 + NO_2)$$

Relationships:

$\Delta A_T{}^{nutsreleasecorrected} = 2 \times \text{diss}$
$\Delta DIC^{obs} = 1 \times \text{diss} + 1 \times \text{resp}$

$\Delta A_T{}^{resp} = 0$ ..... change in A_T due to respiration
$\Delta A_T{}^{diss} = \Delta A_T{}^{obs}$ ..... change in A_T due to dissolution
$\Delta DIC^{resp} = \Delta DIC^{ob} - \Delta DIC^{diss}$ ..... change in DIC due to respiration

$\Delta DIC^{diss} = \Delta A_T{}^{obs}/2$ ..... change in DIC due to dissolution

ΔDIC^{resp} was then converted into net respiration rates which were used to estimate approximately net photosynthesis rates as follow:

$$P_{net} = \text{Night Resp}_{net} - \text{Day Resp}_{net}$$

This method assumes that sponge respiration is constant during the day and the night and that symbionts' intake an equal amount of DIC for photosynthesis that they produce during respiration.

2.5 Assessment of bioerosion rates

Total, chemical and mechanical bioerosion rates were quantified using three methods described below. Total bioerosion refers to the sum of both mechanical and chemical bioerosion. We expressed chemical and mechanical rates both in mg cm^{-2} $hour^{-1}$ (to distinguish rates between day and night) and in mg cm^{-2} day^{-1} (sum of day and night rates). Total bioerosion was expressed in mg cm^{-2} day^{-1} using both buoyant weight results and the sum of day and night results for chemical and mechanical bioerosion.

2.6 Chemical bioerosion

Chemical bioerosion was determined using the alkalinity anomaly technique (Smith et al., 1975; Chisholm and Gattuso, 1991) which involves measuring the change in A_T (µmol kg^{-1}) associated with dissolution in seawater during 6h incubation periods and correcting for changes in ammonium, nitrate and phosphate (Jacques and Pilson, 1980; Wisshak et al., 2013).The amount of mass of dissolved calcium carbonate ($\Delta M(CaCO_3)$, in µg) was calculated using Eq (1) (Zundelevich et al., 2007; Nava and Carballo, 2008):

$$\Delta M(CaCO_3) = 0.5 \times [\Delta A_T + \Delta PO_4 - \Delta NH_4 + \Delta(NO_3 + NO_2)] \times V_{SW} \times \rho SW \times 100 \quad (1)$$

Where ΔA_T is the increase in A_T over the incubation period associated with dissolution, V_{SW} is the volume (l) of seawater in the incubation chamber and ρSW is local seawater density (1.022 kg L^{-1}). The multiplication factor '100' represents the molecular mass of $CaCO_3$. The six hour incubations were carried out during both the day and at night, starting either two hours after sunrise and one hour after sunset, respectively. Subsamples were used for determination of A_T and DIC (250ml, single

sample), DOC (30 ml) and nutrient (5 ml) analysis from each chamber at the start and end of each incubation. Bioerosion rates are commonly expressed as mass of removed substrate per unit surface area of the removing organism per unit time. Rates were therefore converted to mg cm^{-2} h^{-1} by expressing the change in A_T per surface area of the sponge. Two surface areas of the sponge-bearing cores were determined, the upper circle and the healed surface around the sides of the core.

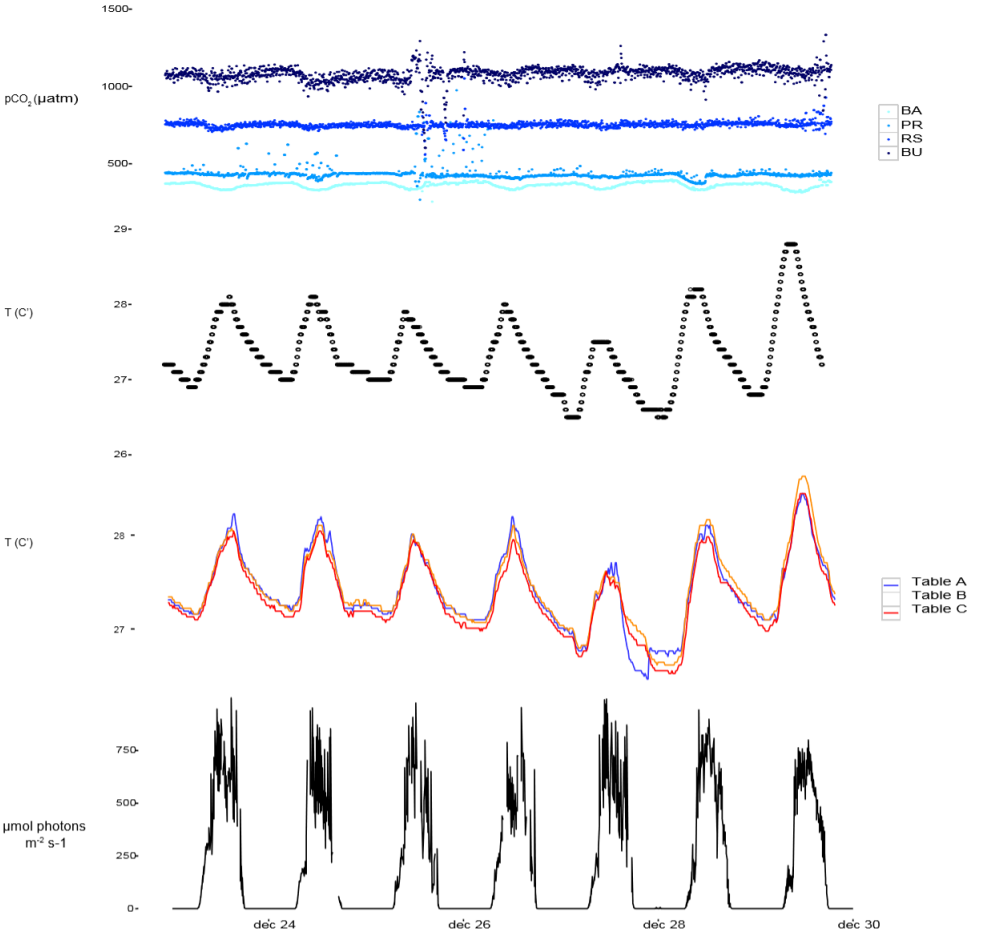

Figure 2: Temporal variability from December 23 to December 30 2015 of continuously monitored pCO_2 (a), temperature monitored in the barrels used for setting the pCO_2 experiments (b), temperature measured directly in aquaria from table A.B and C (c) and light throughout the 1 week experiment.

2.7 Mechanical bioerosion

Mechanical bioerosion was estimated by quantifying the $CaCO_3$ sediment produced by *C. caribbaea* during 6 hour incubations using the method described in Fang et al. (2013). All remaining incubation chamber seawater (∼150 mL) + sediment was collected and the chamber was rinsed with 100 mL water to retrieve any remaining chips. The water was then sieved over a 150 µm mesh to remove non-chip material and then filtered through a precombusted (550˚C, 3h) and pre-weighed GF/F glass microfiber filter (0.7 µm; Whatman). Filters were then combusted at 550˚C for 3 hours to remove any organic matter and re-weighed to determine the difference in weight and hence that of the sediment produced.

2.8 Total bioerosion

Total bioerosion (both mechanical and chemical) was estimated by the change in buoyant weight of the cores over the week of exposure to different pCO_2 and eutrophication scenarios (Fang et al., 2013). This method assumes organic components of the sponge to have a density equal to that of the ambient seawater (i.e., growth of the sponge will not change buoyant weight of the core). Both sponge cores and control cores were buoyant weighed using electronic scales with 0.1mg accuracy before and after the week's exposure to the various pCO_2 levels. The buoyant mass change of the cores was calibrated for seawater density and corrected for residual mass loss using the control cores.

2.9 Statistical Analysis

All statistical analysis were performed using the programming environment R 3.3.2 (R Core Team, 2013). Dependent variables acquired from incubation experiments were analyzed by means of an analysis of covariance (ANCOVA) with two categorical factors (Eutrophication, day/night) including three (E1, E2 and E3) and two (day and night) levels respectively and one continuous covariate (pCO_2). Total bioerosion rates acquired from buoyant weight measurements and net photosynthesis rates were analyzed by means of a 4 X 3 crossed analysis of variance (ANOVA) with two categorical factors (pCO_2, eutrophication) including four (BA, PR, RS and BU) and three (E1, E2 and E3) levels respectively. Normality and homoscedacity were confirmed using the Shapiro-Wilk and Levene's test respectively. If no significant two-way interactions were revealed, main effects were reported. In the case of significant interactive effects, Post Hoc tests (Tukey HSD with Bonferroni correction) were applied to determine the effect of a factor at each level of the other. In addition, linear regression models were performed, after confirming assumptions for residual normality and homoscedacity,

between pCO_2 (now as a continuous predictor variable) and chemical bioerosion rates for each eutrophication and time levels.

3 Results

3.1 Health

The sponge tissue damaged due to coring healed during the recovery session and started growing along the upper sides of the core throughout the experiment which indicated that sponges were healthy and recovering. Sponge color from the start to the end only varied very slightly, sponges in every treatment became a bit darker which may indicate a higher chlorophyll-a content in symbionts or an increase in symbiont abundance. Fluorescein injections revealed that sponges were still filtering half way through experiment.

3.2 Seawater variables

Over the course of the experiment, headspace pCO_2 in the four barrels remained sufficiently constant to warrant distinction between treatments (Figure 2, Table 1). Calculated mean pCO_2 values in the experimental aquaria were 362.5, 443.8, 755.9 and 1046.0 µatm under PI, PD, RE and BU. The pCO_2 levels in PI were on average 82.5 µatm higher than the intended pre-industrial pCO_2 levels. However, they remained significantly different from the present scenario and therefore the pre-industrial scenario will be termed "Below-ambient" (BA) in the following text. Sponge cores were exposed to natural variations in temperature and light which, however, proved to be minimal over the experimental period. The average experimental temperature was 27.63°C (min=25.81°C and max=29.75 °C) and the average light intensity registered inside the aquaria around midday was 562 ± 125.0 µmol photons m^{-2} s^{-1}.

Measured DIC and hence all calculated carbonate system parameters were found to vary significantly across the four OA scenarios (Table 1) and dissolved organic carbon (DOC), ammonium (NH_4) and phosphate (PO_4) concentrations were found to increase significantly across the eutrophication treatments (Table 2). Bioerosion, photosynthesis and respiration within incubations altered the carbonate chemistry of the water (Table 1). The pCO_2 concentrations increased and the pH and Ωaragonite decreased throughout all incubations. The change in pCO_2, pH and Ωaragonite was significantly different between pCO_2 scenarios and between day and night. In none of the incubations, Ωaragonite reached values below 1. Initial pCO_2 concentrations calculated from A_T and DIC at the beginning of each chamber incubation were found to increase slightly with addition of RPMI for each OA scenario. Accordingly, pH

Table 1: Seawater physical and carbonate chemistry parameters at the start (T_0) and the end (T_6) of incubation experiments, averaged (± standard deviation) over all incubations for each pCO_2 scenario.

Variables	Time	BA	PD	RE	BU
T_{barrel} [°C]		27.33±0.48	27.33±0.48	27.33±0.48	27.33±0.48
$T_{aquaria}$ [°C]		27.69±0.02	27.52±0.02	27.61±0.03	27.71±0.02
Salinity		34.1±0.2	34.1±0.2	34.1±0.2	34.1±0.2
${pCO_2}^{meas}$ [µatm]*		361.3±18.2	436.6±74.6	754.4±55.8	1081.4±60.2
A_T [µmol kg^{-1}]	T_0	2326.0±13.7	2323.9±29.9	2328.9±7.8	2323.7±15.2
	T_6	2365.7±34.4	2366.1±26.7	2679.2±11.5	2418.0±15.4
DIC [µmol kg^{-1}]	T_0	1979.2±44.1	2018.9±34.7	2129.1±32.5	2176.6±33.9
	T_6	2075.5±51.4	2099.5±50.7	2264.4±37.5	2337.8±48.8
${pCO_2}^{meas}$[µmol kg^{-1}]	T_0	362.5±72.9	443.8±110.2	755.87±149.4	1046.0±270.7
	T_6	490.5±105.2	559.2±132.5	1313.25±285.4	1640.5±335.7
pH^{calc}(total scale)*	T_0	8.1±0.07	8.0±0.08	7.8±0.07	7.69±0.10
	T_6	7.98±0.07	7.93±0.09	7.61±0.09	7.52±0.10
${HCO_3}^{-calc}$ [µmol kg^{-1}]*	T_0	1722.5±69.2	1787.13±61.30	1955.63±49.43	2026.7±52.0
	T_6	1850.7±71.5	1887.7±84.1	2124.2±49.8	2203.9±54.8
${CO_3}^{2-calc}$ [µmol kg^{-1}]*	T_0	247.06±27.99	219.93±32.65	153.3±21.24	122.07±25.67
	T_6	211.75±28.10	196.77±22.68	105.26±11.73	88.68±18.55
${\Omega_{calcite}}^{calc}$*	T_0	4.00±0.45	3.56±0.53	2.49±0.35	1.97±0.42
	T_6	3.43±0.46	3.18±0.64	1.70±0.33	1.43±0.30

[1] 'Below-ambient' (BA), 'Present-day' (PD), 'Reduced-emission' (RE) and 'Business-as-usual' (BU). Temperature, salinity, A_T and DIC were measured and used to calculate pH and the other carbonate system state parameters (indicated with superscript calc). The variable ${pCO_2}^{meas}$ represents the measured pCO_2 by the LICOR from the air space in the treatment barrels (after attaining the temperature of the aquaria), whereas ${pCO_2}^{calc}$ represents calculated pCO_2 from A_T and DIC measurements in the aquaria at the start of incubations averaged for each scenario.

[2] Significant difference across all OA scenarios marked with an asterix*.

Table 2: Initial (T0) and final (T6) DOC and nutrient concentrations averaged over all incubations (± standard deviation) for the three 'eutrophication' treatments: 'E1' (natural organic loading), 'E2' (double labile organic loading), 'E3' (triple labile organic loading).

Variables	Time	E1	E2	E3
DOC [µmol kg^{-1}]*	T_0	82 ± 4	96 ± 4	106 ± 13
	T_6	106 ± 12	122 ± 18	123 ± 19
NO_x [µmol kg^{-1}]	T_0	1.0 ± 0.4	1.0 ± 0.5	1.0 ± 0.5
	T_6	1.1 ± 0.5	1.1 ± 5	1.4 ± 0.8
NO_2 [µmol kg^{-1}]	T_0	0.1 ± 0.4	1.0 ± 0.5	1.0 ± 0.5
	T_6	0.2 ± 0.1	0.2 ± 0.1	0.3 ± 0.1
NH_4 [µmol kg^{-1}]	T_0	2.6 ± 0.3	3.4 ± 2.8	4.3 ± 4.1
	T_6	19.4 ± 12.1	24.6 ± 14.0	25.3 ± 11.8
PO_4 [µmol kg^{-1}]	T_0	0.01 ± 0.01	1.4 ± 0.9	2.9 ± 2.3
	T_6	0.5 ± 0.5	2.41 ± 1.0	4.0 ± 2.5

[1] Significant difference across eutrophication scenarios marked with an asterix*.

and $CaCO_3$ saturation state decreased with addition of RPMI for each OA scenario. However, no significant difference was found in calculated pCO_2 concentrations, pH, and $CaCO_3$ saturation state between eutrophication treatments in each OA scenario. Dissolved organic carbon and nutrient concentrations increased overall throughout incubations (Table 2).

3.3 Chemical bioerosion rates

In total, 72 chamber incubations were conducted (36 during the day and 36 at night) after one week exposure to treatments. Of all incubations, 13 were compromised due to technical complications. The results for the successful 59 incubations are presented here. For the present-day (PD) pCO_2 scenario, no data in treatment E2 during the day are available. As sponges experienced significant increase in pCO_2 concentrations throughout incubations, chemical rates were regressed against the average calculated pCO_2 obtained from A_T and DIC measurement at the start and end of each incubations. As a result, for each pCO_2 scenario, day and night pCO_2 levels differ from each other.

Chemical bioerosion rates of *C. caribbaea* increased significantly with pCO_2 and increased eutrophication levels but no interaction was found between the two effects

(Figure 3, Table 3 and 5).

In addition, day-time chemical bioerosion rates are shown to differ significantly from night-time rates, and an interaction between the effects of pCO_2 and day-night is revealed (Table 3 and 4). A post hoc pairwise comparison revealed that the significant differences in chemical bioerosion rates between day and night mostly occurred at low pCO_2 scenarios where day time rates were approximately 50 % higher than night-time rates. In high pCO_2 scenarios (RE and BU), average day-time and night-time rates were equal in E1 and average night-time rates surpassed day-time ones in E2 and E3 (Table 3). The increase in pCO_2 concentration during incubations at day and night was not significantly different between PD, RS and BU. This indicates that the switch from greater rates during the day at low pCO_2 scenarios (BA and PR) to equal/higher rates in RE and BU is not primarily linked to the difference in day and night pCO_2.

Average day and night chemical bioerosion rates increased significantly from E1 to E3 for each of the pCO_2 scenarios, however, increases in rates from E1 to E2

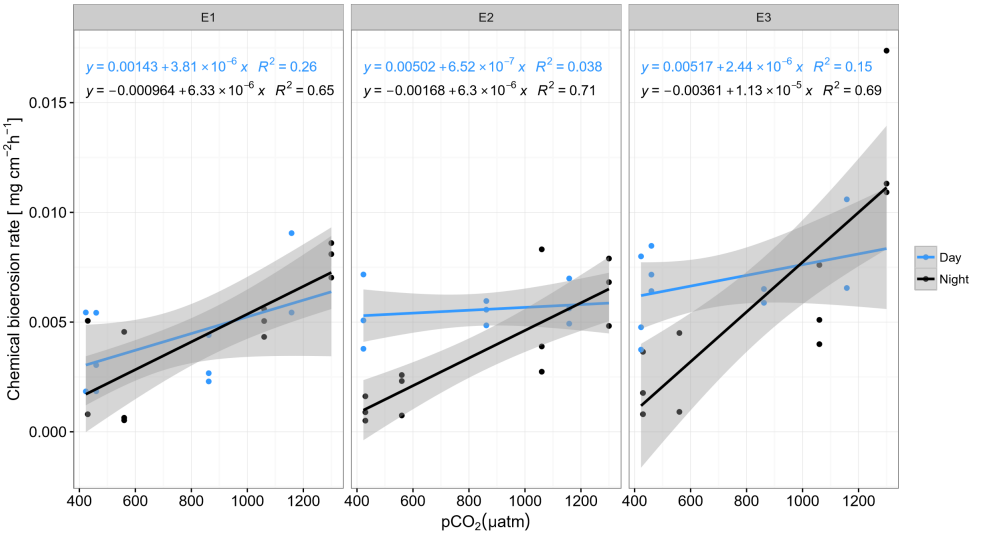

Figure 3: Chemical bioerosion rates in mg cm^{-2} h^{-1} as a function of pCO_2 for day and night and each eutrophication treatment. Linear regressions illustrate positive correlation between pCO_2 and dissolution rates. Slopes are significantly different between day (blue) and night (black) but not between eutrophication scenarios (E1-E3). Alkalinity titrations for incubations in Present scenario (PD) and E2 treatment during the day were of questionable quality due to equipment failure and therefore not represented here (n=59).

Table 3: Averages (± standard deviation) of chemical bioerosion rates in mg cm^{-2} h^{-1}, as calculated from change in A_T during incubations. Values are provided for in each OA scenario, eutrophication treatment and light regime. In BA and PR scenarios, day-time rates are generally more than ∼50% higher than night-time rates. In RE scenario, day-time and night-time rates are roughly similar, while in BU night-time rates surpass day-time rates in the in all eutrophication treatments.

pCO_2	Light	E1	E2	E3
BA	Day	0.004 ± 0.003	0.005 ± 0.002	0.006 ± 0.002
	Night	0.003 ± 0.003	0.001 ± 0.001	0.002 ± 0.001
PR	Day	0.004 ± 0.002	X	0.007 ± 0.001
	Night	0.002 ± 0.002	0.002± 0.001	0.003 ± 0.003
RE	Day	0.004 ± 0.002	0.005± 0.001	0.006 ± 0.001
	Night	0.005 ± 0.001	0.005 ± 0.003	0.006 ± 0.002
BU	Day	0.007 ± 0.003	0.006 ± 0.001	0.009 ± 0.003
	Night	0.008 ± 0.001	0.007 ± 0.002	0.010 ± 0.004

were minute and even negative at night. (Table 3). Daily chemical rates (mg cm^{-2} d^{-1}) in BA, PR, RE and BU increased by 80%, 83%, 20% and 53% from E1 to E3, respectively (Table 4). Rates in E1 and E3 increased by 150% and 109% respectively from current pCO_2 levels to the BU scenario (no PD, E2 chemical rate available). In these calculations, abiotic dissolution was assumed negligible as aragonite saturation states always remained above 1. Possible bioerosion by other organisms living in the cores is not accounted for in our calculations but is considered minimal throughout the incubation period due to very low A_T changes in control core incubations.

3.4 Mechanical and total bioerosion rates

Mechanical bioerosion estimated from chip collection was not significantly different between pCO_2 scenarios and eutrophication treatments and no interaction was found between effects (Table 4 & 5). The average hourly mechanical erosion rate for all pCO_2 scenarios and eutrophication treatments during day and night equaled 0.02 ± 0.01 mg cm^{-2} h^{-1}. The average daily rate estimated from the addition of night and day rates equaled to 0.40 ± 0.11 mg cm^{-2} d^{-1}.

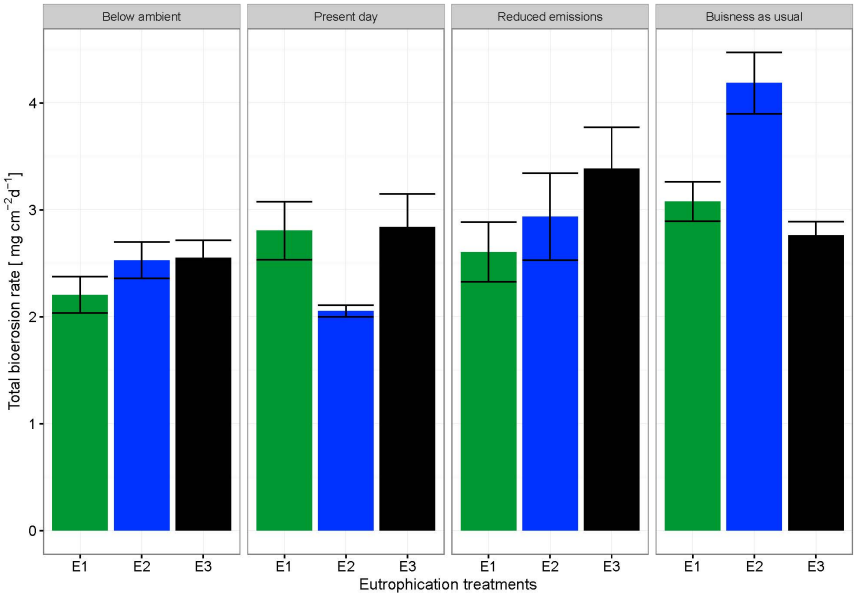

Figure 4: Total bioerosion rates of *C. caribbaea* in mg cm^{-2} d^{-1} estimated from buoyant weight measurements ± SEM for each pCO_2 and eutrophication scenario. Estimates for buoyant weighing are based on all individual measurements (n=59).

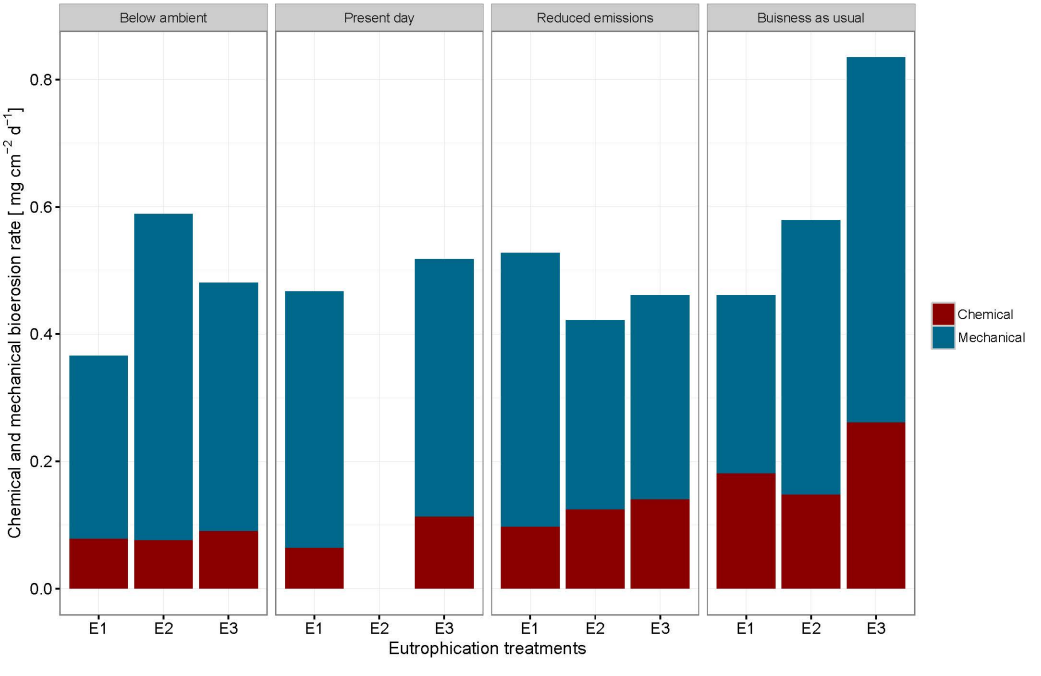

Figure 5: Sum of chemical and mechanical bioerosion in mg cm^{-2} d^{-1} for each pCO_2 and eutrophication scenario. Mechanical bioerosion rates were estimated using the weight of chips collected during 6 hour incubations. Chips were only collected for table A and B during the day and night (n=44).Chemical bioerosion rates were calculated from ΔA_T in incubations (n=59). Day (24h) rates were calculated by multiplying day and night mechanical and chemical hourly rates by 12 and adding them together for each pCO_2 and eutrophication scenario.

The change in buoyant weight yielded average net bioerosion rates of 2.47 ± 0.16, 2.63 ± 0.25, 2.96 ± 0.33 and 3.34 ± 0.26 mg cm^{-2} d^{-1} for BA, PD, RE and BU, respectively and increased significantly with pCO_2 (p = 0.009) (Figure 4, Table 5). Although in most pCO_2 scenarios, treatment E2 and E3 yielded higher total bioerosion rates than in E1, rates were not found to increase significantly with eutrophication (Figure 4, Table 5). Net bioerosion rates calculated from buoyant weight measurements were approximately 4-5 times higher than the sum of the measured chemical and mechanical (chips) bioerosion rates at day and night (Figures 4 & 5, Table 4).

Table 4: Daily averages (∼ standard deviation) of total, mechanical and chemical bioerosion rates in mg cm^{-2} d^{-1}. Values are provided for each OA scenario and eutrophication treatment. Daily total bioerosion rates are calculated using buoyant weight measurements. Daily mechanical and chemical bioerosion rates are the sum of hourly day and night rates, each multiplied by 12.

pCO_2	Type	E1	E2	E3
BA	Total BW	2.21 ± 0.61	2.53 ± 0.61	2.55 ± 0.59
	Mechanical	0.23 ± 0.03	0.51 ± 0.15	0.38 ± 0.08
	Chemical	0.05 ± 0.02	0.08 ± 0.01	0.09 ± 0.04
PR	Total BW	2.81 ± 0.98	2.05 ± 0.20	2.84 ± 1.12
	Mechanical	0.4 ± 0.09	0.31 ± 0.07	0.39 ± 0.13
	Chemical	0.06 ± 0.02	x	0.11 ± 0.04
RS	Total BW	2.61 ± 1.01	2.94 ± 1.47	3.39 ± 1.4
	Mechanical	0.5 ± 0.17	0.33 ± 0.09	0.40 ± 0.13
	Chemical	0.10 ± 0.02	0.13 ± 0.03	0.12 ± 0.05
BU	Total BW	3.08 ± 0.66	4.19 ± 1.04	2.76 ± 0.45
	Mechanical	0.23 ± 0.07	0.43 ± 0.18	0.59 ± 0.22
	Chemical	0.15 ± 0.06	0.15 ± 0.02	0.23 ± 0.08

3.5 Net Respiration and photosynthetic rates

Net holobiont (sponge + symbionts) respiration showed antagonistic behavior between day and night as pCO_2 increased. Net respiration during the day decreased with high pCO_2 while net respiration at night increased (Figure 6). Rates were found to vary significantly between day and night (p <0.001) but not between pCO_2 scenarios and eutrophication treatments. An interaction between factors day/night and pCO_2 lev-

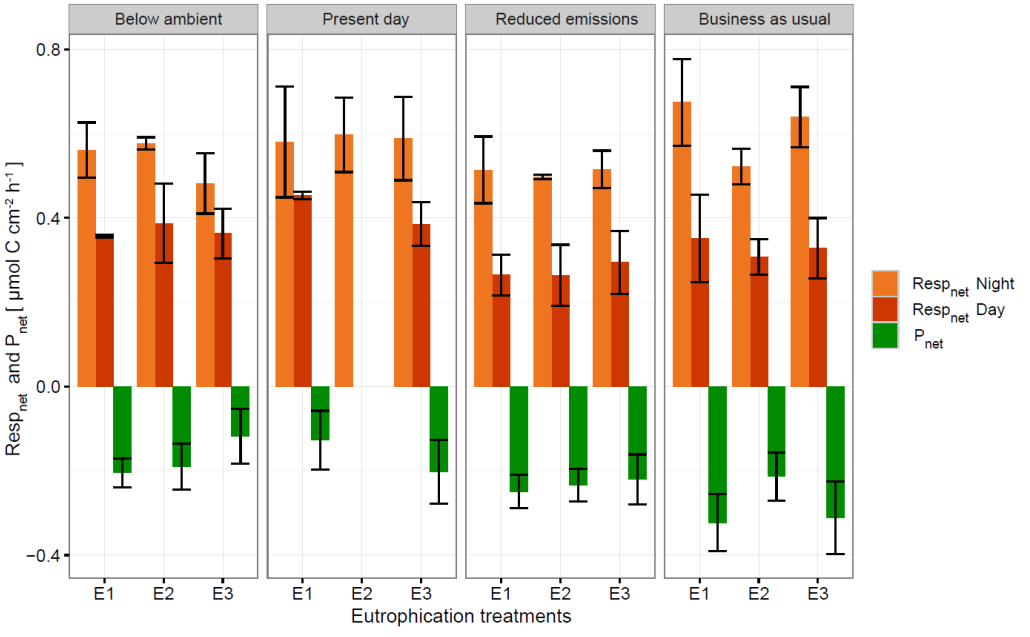

Figure 6: Net respiration rates (Resp_{net}) and net photosynthetic rates (P_{net}) of the holobiont (sponge + symbionts) during the day and night ± SEM for each $p\text{CO}_2$ and eutrophication scenario.

els was revealed (Table 5). Accordingly, photosynthetic rates, estimated from the difference between net respiration rates at day and night, increased significantly with increasing $p\text{CO}_2$ ($p = 0.004$) (Figure 6, Table 5). Although no significant difference was found between eutrophication scenarios, photosynthetic activity appeared to decrease with increasing eutrophication in most $p\text{CO}_2$ scenarios.

4 Discussion

Total bioerosion rates by the common coral excavating sponge *Cliona caribbaea* are experimentally shown to increase with rising $p\text{CO}_2$ (Figure 4), while the corresponding chemical bioerosion component increased significantly with both $p\text{CO}_2$ and eutrophication (Figure 3). Mechanical bioerosion exceeded chemical bioerosion by 3 to 6 times irrespective of $p\text{CO}_2$ and eutrophication. Contribution of eutrophication to higher chemical bioerosion rates was additive to $p\text{CO}_2$ effects (i.e. not synergetic). Differences between day-time and night-time chemical bioerosion rates at below-ambient and present $p\text{CO}_2$ levels suggests that photosynthetic activity by symbionts promotes

Table 5: Three-way ANCOVAs, with bioerosion rates (chemical: A_T change, mechanical: chip production and total: buoyant weight) and net respiration rates as dependent factors, eutrophication and day/night as independent categorical factors and pCO_2 as a continuous covariable. Total bioerosion rates and net photosynthesis rates were analyzed using two-way ANOVAs with two categorical factors (pCO_2, eutrophication).

	Variables	df	SS	MS	Fvalue	Pvalue
Chemical rates	pCO_2	2	2.1e-04	2.1e-04	31.19	**<0.001**
	Eutro	2	6.0e-05	3.0e-05	3.32	**0.04**
	day/night	1	8.9e-06	8.9e-06	0.91	0.34
	pCO_2:Eutro	2	1.4e-05	7.2e-05	1.77	0.18
	pCO_2:day/night	1	5.1e-05	5.1e-05	12.63	**<0.001**
	Eutro:day/night	2	1.0e-05	5.0e-06	1.24	0.30
	pCO_2:Eutro:day/night	2	1.1e-05	5.3e-06	1.31	0.28
	Residuals	51	2.1e-04	4.1e-06		
Mechanical rates	pCO_2	1	2.5e-05	2.5e-05	0.47	0.50
	Eutro	2	1.3 e-05	6.4e-06	0.12	0.89
	day/night	1	1.9e-06	1.9e-06	0.36	0.55
	pCO_2:Eutro	2	1.2e-04	6.3e-05	1.18	0.33
	pCO_2:day/night	1	1.4e-04	1.4e-04	2.65	0.12
	Eutro:day/night	2	8.6e-05	4.3e-05	0.81	0.46
	pCO_2:Eutro:day/night	2	2.1e-04	1.1e-04	1.99	0.16
	Residuals	19	1.0e-03	5.3e-5		
Total rates	pCO_2	1	0.01	0.01	7.63	**0.009**
	Eutro	2	0.002	0.001	0.52	0.6
	pCO_2:Eutro	2	0.01	0.003	2.34	0.11
	Residuals	48	0.07	0.001		
Net resp rates	pCO_2	1	0.03	0.03	1.73	0.19
	Eutro	2	0.04	0.02	1.15	0.33
	day/night	1	0.50	0.50	28.13	**<0.001**
	pCO_2:Eutro	2	0.001	0.001	0.04	0.96
	pCO_2:day/night	1	0.08	0.08	4.23	**0.04**
	Eutro: day/night	2	0.03	0.01	0.72	0.49
	pCO_2:Eutro:day/night	2	0.02	0.01	0.43	0.66
	Residuals	48	0.84	0.02		
Net photo rates	pCO_2	1	0.03	0.003	14.75	**0.004**
	Eutro	2	0.0004	0.0002	0.04	0.96
	pCO_2:Eutro	2	0.01	0.003	2.03	0.523
	Residuals	3	0.01	0.002		

the dissolution process. While under rising pCO_2, the symbiotic relationship appears to become negligible to the bioerosion activity as night-time rates equal/surpass day-time rates.

4.1 Effects of pCO_2 and eutrophication on bioerosion

Results regarding higher rates at increased pCO_2 are comparable to previous studies on other clionaid species (*C. orientalis* and *C. celata*) (Wisshak et al., 2012; Fang et al., 2013; Wisshak et al., 2013,0). Sponges and other borers are assumed to benefit from eutrophication (Holmes, 2000; Carballo et al., 2008). Many sponges on reefs harbor photosynthetic symbionts and in some cases they produce >50% of the energy requirements of the host (Erwin and Thacker, 2008). They rely nevertheless also on organic matter for food and their feeding strategy may be flexible depending on the type of symbionts or the environmental conditions. To maintain a positive energy budget, *C. caribbaea* likely relies mainly on autotrophic products (Weisz et al. 2010; Fang et al., 2014) and thus depends on the supply of N and P for maintenance and growth either as inorganic or organic matter taken up by the sponge, mineralized and transferred as inorganic nutrients to the symbiont. Considering the low phosphate concentrations in E1 ($\sim$ 0.01 µmol l^{-1}), primary production may have been limited by phosphate. However, the addition of RPMI and hence higher phosphate concentrations did not enhance photosynthetic activity from E1 to E3.

On the contrary, in most pCO_2 scenarios, net photosynthetic rate estimates decreased slightly (non-significant) from E1 to E3, while sponge chemical bioerosion rates were enhanced. Under increased organic matter and nutrient levels, the sponges are apparently less dependent on autotrophic products. However, as the increase in chemical bioerosion rates from E1 to E3 was more pronounced during the day (at low and ambient pCO_2 levels), it is likely that the autotrophic/heterotrophic ratio of energy supply only shifts slightly towards heterotrophy and the sponges still rely partly on autotrophic products.

Chemical bioerosion rates at night-time increase also (at a lesser degree) with higher eutrophication, indicating that chemical bioerosion does indeed benefit from a higher energy supply via heterotrophic feeding. This implies that increased eutrophication did not impact the productivity of the symbionts. Sponges can exercise control on symbiont growth and abundance by inhibiting division or ingesting them to avoid symbionts taking over. The observed increase of nitrate, nitrite, ammonium, phosphate and dissolved inorganic carbon (Table 2) was likely caused by the confinement of sponges in the incubation chambers. Depletion of the dissolved food and bacteria from the incubated water may have resulted in sponges re-filtering depleted water continuously which subsequently caused such increases in DOC and nutrients.

However, relative differences in bioerosional processes between treatments were still observed.

Total bioerosion rates calculated using buoyant weight measurements were experimentally shown to increase significantly with pCO_2 but not with eutrophication. These results are unexpected considering the significant impact eutrophication has on chemical bioerosion. However, the relatively short term experiment coupled with the smaller effect of eutrophication on chemical rates compared to the pCO_2 impact may have resulted in a loss of signal.

Buoyant weight rate estimates resulted in approximately 5 times higher rates than those based on the sum of chip production and the change in A_T (Figure 4 and 5). This is comparable to results from Fang et al. (2013) and may be explained by an underestimation of the chip removal capacity of the sponge. Rates calculated using buoyant weight measurements are based on a longer period of bioerosion (1 week), whereas the chip removal is based on their collection at the end of a relatively short incubation period (6 hours). Sponges might expel chips irregularly or they may temporarily reduce chip removal during incubations possibly due to stress caused by reduced food supply or build-up of waste products, both of which may become important towards the end of the 6 hour-incubation period. Therefore, the sum of chemical and mechanical bioerosion should be considered as being conservative. Here, total bioerosion rates yielded from buoyant weight measurements are regarded as more reliable and are comparable to results estimated from previous studies (Fang et al., 2013; Wisshak et al., 2013).

Rates of chip production did not differ significantly between pCO_2 scenarios, day/night and eutrophication treatments. Although the underlying method by which sponges expel chips is largely unknown, it appears that chips are expelled from the sponge body through excurrent canals (Ruetzler and Rieger, 1973). It is likely that chip removal processes utilize products from the dissolution to contract their tissue and move the chip up from the boring pit into an excurrent canal. Work on phototrophic cyanobacteria showed that microbial excavation was achieved by transcellular Ca^{2+} transport (Garcia-Pichel, 2006; Garcia-Pichel et al., 2010; Guida and Garcia-Pichel, 2016). We tentatively suggest that the excess in Ca^{2+} derived from the dissolution in $CaCO_2^-$ may be used by sponges to contract a conductive pathway, similarly to how muscle cell contract when triggered by an increase in intracellular Ca^{2+} (Sommerville and Hartshorne, 1986).

4.2 Treatment effect on symbiont photosynthesis and holobiont net respiration and resulting impact on bioerosion activity

Changes in chemical bioerosion activity can be associated with three processes within the holobiont using up or producing dissolved inorganic carbon (DIC): photosynthesis/respiration by the symbionts, respiration by the sponge and chemical bioerosion.

Photosynthesis promotes chemical bioerosion rates during the day at low pCO_2 levels (BA and PD) (Figure 3, Table 3). Differences in rates between day and night are comparable to results from previous studies where *C. orientalis* and *C. varians* (both symbiont bearing species) excavated with higher rates in day light compared to the dark or shade at ambient pCO_2 (Hill, 1996; Schönberg, 2006; Fang et al., 2016). Recent work by Fang et al. (2016) on the ecophysiology of *C. orientalis* showed that bioerosion rates in this sponge during day-time were approximately 40 % higher than in the dark. *C. celata* on the other hand, an azooxanthellate sponge, displayed no diurnal variability in bioerosion pattern (Schönberg, 2008). Based on these findings, presence of *Symbiodinium* spp. was assumed to be associated with higher bioerosion rates (Hill, 1996; Fang et al., 2016). This is a geochemical paradox because the autotrophic symbionts would tend to increase pH and enhance carbonate precipitation rather than its antagonistic process (Garcia-Pichel, 2010).

However, local acidification due to sponge respiration may balance out the alkalinization associated with photosynthesis. As symbionts do not produce a favorable environment for carbonate dissolution, photosynthesis must therefore support a high fraction of the energetic costs of the bioerosion process. Higher rates during the day at low and ambient pCO_2 indicate that the benefit of acquired energy from photosynthetic activity exceeds the benefit of increased pCO_2 levels at night due to respiration.

Due to the sponge's energetic dependence to the products of photosynthesis for greater bioerosion activity, the capacity of phototrophic sponges to excavate may be particularly sensitive to environmental changes impacting photosynthesis. Our results suggest that photosynthesis is enhanced with increased pCO_2 (Figure 6), possibly due to a switch from HCO_3^- to CO_2 as a source of DIC. Fang et al. (2014) describes a greater supply of photosynthetic products from symbionts in the "reduced emissions" scenario (pCO_2 = 645 µatm, temperature = 28.4°C) to meet higher metabolic demands. Photosynthetic products by symbionts may be used for biosynthesis and respiration within the zooxanthellae or transferred to the associated sponge where it is used for metabolic maintenance via respiration or growth (Fang et al., 2014).

Despite enhanced photosynthetic rates with rising pCO_2, day-time chemical rates did not seem to benefit from this boost in energy supply as they were found to be com-

parable and even lower than night-time rates. The relationship between the sponge and its symbionts regarding bioerosional processes seems to shift at higher pCO_2. We hypothesize that the increase in local alkalinization associated with enhanced photosynthesis may be too great to be balanced out by local respiration acidification. In other words, the increased photosynthetic activity may have an antagonistic effect with respect to acidification during day-time due to higher uptake of CO_2 by the symbionts. Borges and Gypens (2010) argued that the effect of enhanced primary production on carbon cycling can counter the effect of ocean acidification. In addition, increased respiration would stimulate primary production by increased translocation of CO_2 of the sponge to the symbionts. Although day and night net respiration rates showed antagonistic behaviors with rising pCO_2, decreased net respiration during the day at high pCO_2 is attributed to enhanced photosynthesis resulting in greater uptake of CO_2 by symbionts.

4.3 Comparison and extrapolation of bioerosion rates

Estimates of chemical and mechanical bioerosion for *C. caribbaea* were in a comparable range as those calculated for *C. orientalis* under a range of CO_2 concentrations (Fang et al., 2013a; Wisshak et al., 2013; Wisshak et al., 2014b). This is consistent with the membership of *C. caribbaea* to the *Cliona viridis*-complex (Schönberg, 2002). Our chemical rates ranged from 0.06 to 0.15 mg cm^{-2} d^{-1} from present day to business as usual pCO_2 levels. Estimates by Fang et al. (2013a) ranged from 0.08 to 0.3 mg cm^{-2} d^{-1} while the rates by Wisshak et al. (2014b) ranged from 0.02 to 0.26 mg cm^{-2} d^{-1}. Mechanical rates from Fang ranged from 0.12 to 0.16 mg cm^{-2} d^{-1} whilst our results ranged from 0.23 to 0.5 mg cm^{-2} d^{-1} (in E1). Total bioerosion rates from this study were nearly three times higher than Fang et al. (2013a) and Wisshak et al. (2014b). Discrepancies between results can be attributed to differences in the methodology and calculations within these experiment. For instance, Wisshak et al. (2014) carried out only dark incubations which would explain the lower rates at ambient pCO_2. These inconsistencies in the methodology between experiments are making comparison between results difficult. There is a need for method standardization regarding sponge bioerosion rates experiments. In addition, incubation methods are affecting sponges and are preventing accurate determination of rates. Up to now, closed incubations have been sufficient to observe relative variation between pCO_2, temperature and eutrophication treatments. This sheds light on how boring sponges may react to future environmental changes. However, if we are to quantify such reaction, it is essential that rates are more accurately measured. Using semi enclosed incubation chambers may increase greatly accuracy of chemical rates. Mechanical bioerosion rates are regarded as untrustworthy and therefore may be more reliable if

collection of chips was applied to a longer stretch in time.

When extrapolating chemical bioerosion rates from our experiment to yearly estimates, rates in the present-day (PD) pCO_2 scenario and in the business as usual (BU) scenario ranged from 0.22 to 0.55 kg m^{-2} y^{-1} in E1 and from 0.40 to 0.84 kg m^{-2} y^{-1} in E3. This corresponds to a doubling of rates by the end of this century. In a slightly more optimistic scenario, where CO2 emissions are reduced, chemical bioerosion rates would still increase by 50 % compared to present rates. However, combined effects of pCO_2 and eutrophication, result in rates ranging from 0.22 kg m^{-2} y^{-1} in PD: E1 to 0.84 kg m^{-2} y^{-1} in BU: E3 which nearly corresponds to a quadrupling in chemical bioerosion rates. These extrapolations should however be treated with caution as it is an enormous jump to go from 6 hour incubations to yearly estimates (McElhany, 2017).

Conclusions

Considering ongoing ocean acidification, combined with increasing coastal eutrophication around Caribbean islands, these finding suggests that sponge bioerosion will increase in the next century. The combined effect of OA and eutrophication on bioerosional activity was not synergetic but additive. Enhanced bioerosion in future oceans together with reduced calcifying potential of corals will inevitably tip the balance between reef accretion and bioerosion processes towards net loss of carbonate structure.

Results from our incubation experiments shed light in understanding the effect of symbionts on bioerosional activity. Greater chemical bioerosion during the day at low and ambient pCO_2 suggest that CO_2 diffusion is not the acting parameter of aragonite dissolution by sponges. We hypothesize that the energy gained by photosynthetic activity is fueling a high fraction of the metabolic cost at the site of erosion which may include ATP usage or proton motive force generation. At higher pCO_2, enhanced photosynthesis appears to have an antagonistic effect with respect to acidification due to higher uptake of CO_2 by the symbionts.

Acknowledgements

We thank the Caribbean Netherlands Science Institute (CNSI) for hosting the experiment and especially Johan Staple for his support. We also thank Masru Spanner for the nutrient analyses and Santiago Gonzalez for the dissolved organic carbon analyses. This project was funded by the Royal Netherlands Institute for Sea Research (NIOZ) and the Netherlands Organization for Scientific Research (NWO grants 858.14.021

and 858.14.022). Thank you to Bob Koster for the design and development of the pCO_2 set-up and to the NIOZ workshop whose help and work was crucial for the construction of the experimental set-up.

Supplements

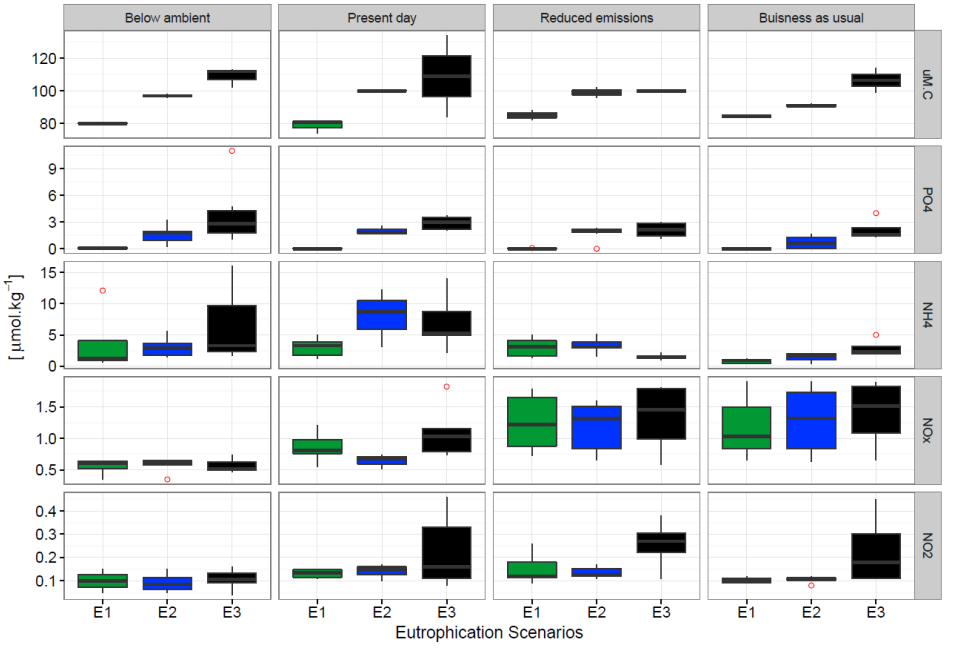

Figure S 1: Boxplot of initial nutrient and dissolved organic carbon (uM.C) concentrations for each pCO_2 scenario (top) and eutrophication treatments (E1, E2, E3) (n=59).

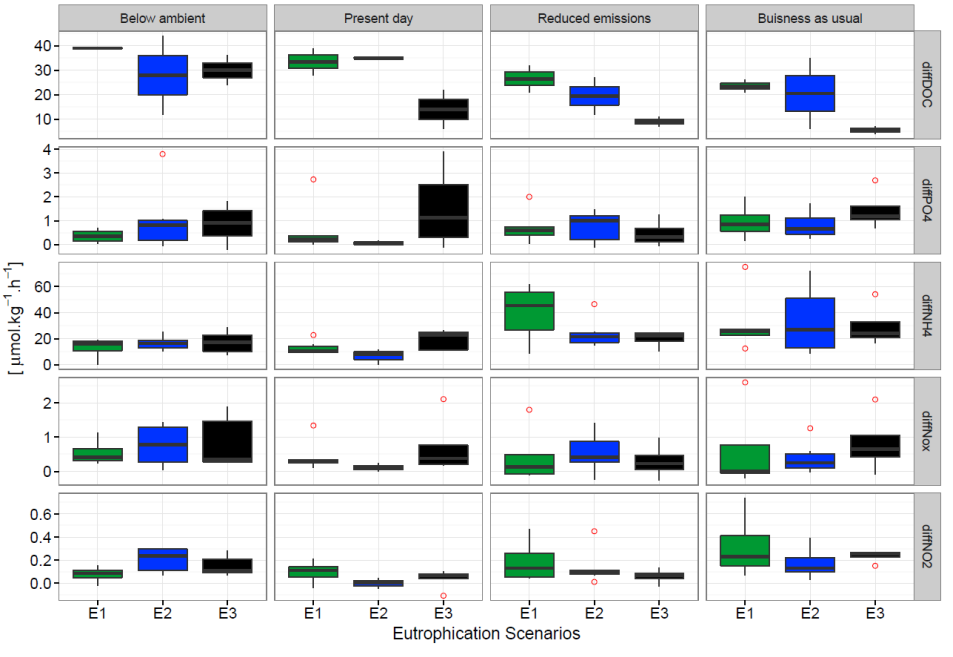

Figure S 2: Boxplot of nutrient and dissolved organic carbon concentration changes per hour in incubations for each pCO_2 scenario (top) and eutrophication treatments (E1, E2, E3) (n=59).

Table S 1: Daily averages ($\sim$ standard deviation) of total, mechanical and chemical bioerosion rates in mg cm^{-2} d^{-1}. Values are provided for each OA scenario and eutrophication treatment. Daily total bioerosion rates are calculated using buoyant weight measurements. Daily mechanical and chemical bioerosion rates are the sum of hourly day and night rates, each multiplied by 12.

pCO_2	Bioerosion	E1	E2	E3
BA	Total BW	-0.004 ± 0.001	-0.008 ± 0.002	-0.005 ± 0.002
	Mechanical	0	0	0
	Chemical	0.0002 ± 0.0002	0.0003 ± 0.0002	0.0002 ± 0.0001
PR	Total BW	-0.011 ± 0.005	-0.007 ± 0.002	-0.009 ± 0.002
	Mechanical	0	0	0
	Chemical	-0.0001 ± 0.0001	0.0003 ± 0.0002	0.0004 ± 0.0002
RS	Total BW	-0.008 ± 0.003	-0.009 ± 0.003	-0.001 ± 0.001
	Mechanical	0	0	0
	Chemical	0.001 ± 0.001	0.001 ± 0.001	0.001 ± 0.001
BU	Total BW	-0.009 ± 0.004	-0.016 ± 0.004	-0.007 ± 0.002
	Mechanical	0	0	0
	Chemical	0.001 ± 0.0004	0.001 ± 0.001	0.001 ±0.001

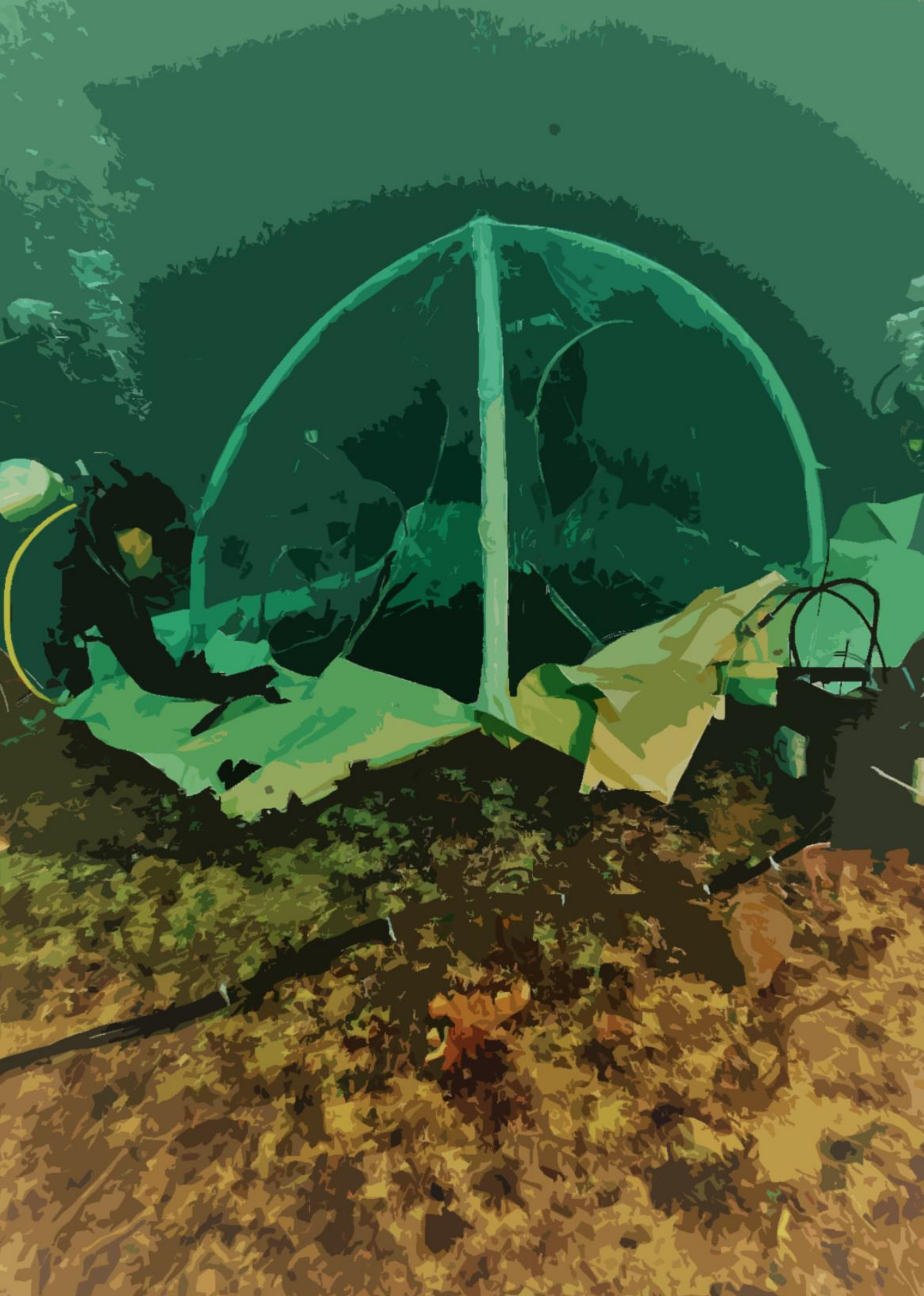

Chapter 5

In-situ Incubation of a Coral Patch for Community-scale Assessment of Metabolic and Chemical Processes on a Reef Slope

Steven M.A.C. van Heuven[+], Alice E. Webb[+], Didier M. de Bakker, Erik H. Meesters, Fleur C. van Duyl, Gert-Jan Reichart, Lennart J. de Nooijer

Van Heuven et al. 2018, PeerJ 6:e5966

[+]These authors contributed equally to this work.

Abstract

Anthropogenic pressures threaten the health of coral reefs globally. Some of these pressures directly affect coral functioning, while others are indirect, for example by promoting the capacity of bioeroders to dissolve coral aragonite. To assess the coral reef status, it is necessary to validate community-scale measurements of metabolic and geochemical processes in the field, by determining fluxes from enclosed coral reef patches. Here, we investigate diurnal trends of carbonate chemistry, dissolved organic carbon, oxygen and nutrients on a 20 meter deep coral reef patch offshore from the island of Saba, Dutch Caribbean by means of tent incubations. The obtained trends are related to benthic carbon fluxes by quantifying net community calcification (NCC) and net community production (NCP). The relatively strong currents and swell-induced near-bottom surge at this location caused minor seawater exchange between the incubated reef and ambient water. Employing a compensating interpretive model, the exchange is used to our advantage as it maintains reasonably ventilated conditions, which conceivably prevents metabolic arrest during incubation periods of multiple hours. No diurnal trends in carbonate chemistry were detected and all net diurnal rates of production were strongly skewed towards respiration suggesting net heterotrophy in all incubations. The NCC inferred from our incubations ranges from -0.2 to 1.4 mmol $CaCO_3$ m^{-2} h^{-1} (-0.2 to 1.2 kg $CaCO_3$ m^{-2} yr^{-1}) and NCP varies from -9 mmol m^{-2} yr^{-1} to -21.7 mmol m^{-2} yr^{-1} (net respiration). When comparing to the consensus-based ReefBudget approach, the estimated net community calcification rate for the incubated full planar area (0.36 kg $CaCO_3$ m^{-2} yr^{-1}) was lower, but still within range of the different NCC inferred from our incubations. Field trials indicate that the tent-based incubation as presented here, coupled with an appropriate interpretive model, is an effective tool to investigate, in-situ, the state of coral reef patches even when located in a relatively hydrodynamic environment.

1 Introduction

The functionality of many reef systems is intrinsically linked to their structural habitat complexity (Newman et al., 2006; Graham and Nash, 2013; Kennedy et al., 2013). On tropical coral reefs, the three-dimensional habitat relies primarily on the ability of corals to deposit large quantities of calcium carbonate. Over recent decades, corals reefs have been under threat at a global scale by a large number of anthropogenic impacts such as ocean warming, overfishing, eutrophication, and ocean acidification (Hoegh-Guldberg, 1999; Gardner et al., 2003; Hoegh-Guldberg et al., 2007; Anthony et al., 2008; Baker et al., 2008; De'ath et al., 2012).

The consequential decline in coral cover and the reduction in historically dominant framework building coral species has already resulted in a substantial loss of 3D complexity on many tropical reefs (Edinger and Risk, 2000; Alvarez-Filip et al., 2011; Perry et al., 2015; De Bakker et al., 2016; Hughes et al., 2007).

The impact of individual aspects of environmental change on coral reef health has been assessed in a number of laboratory experiments (Gilmour, 1999; Burkepile and Hay, 2009). However, in situ community-scale measurements of metabolic and geochemical processes would enable characterization of total reef metabolism. Net community calcification (NCC) is considered to reflect the overall response of the community to environmental change and is therefore monitored as a proxy for coral reefs' status (Gattuso et al., 1993; Kleypas et al., 1999; Edinger and Risk, 2000). Field validation of coral accretion/decline is required to test whether observed experimental responses can be translated to whole ecosystems and in situ conditions. Coral reef decline or community compositional change can be estimated qualitatively from visual inspection of the same site over time (Aronson and Precht, 1997), or by digital comparison of photographs taken at intervals (Porter and Meier, 1992; Coles and Brown, 2007; De Bakker et al., 2016).

The disadvantage of such visual assessments, however, is that results are confined to areas that have been visited previously and are not quantified with respect to NCC. Still,the latter may be estimated from visual inspections using typical, species-specific calcification rates (Perry et al., 2008). And although demonstrated to have fair accuracy (Porter and Meier, 1992; Alevizon and Porter, 2015; Chow et al., 2016), "carbonate budgeting" estimates do not allow estimating seasonal variability of NCC (Courtney et al., 2016), and are inherently insensitive to rapid environmental change. The same goes for elevation-change analyses using coral cores as alone do not relate alteration in sea floor structure to cause (Hubbard, Miller & Scaturo, 1990; Yates et al., 2017). Furthermore, the integrated effects due to organismal interactions cannot be assessed with such an approach. For example, ocean acidification may reduce coral NCC (Andersson and Gledhill, 2013) and at the same time increase erosion rates by sponges (Fang et al., 2013; Webb et al., 2017). Census approach has yet to include the role of several bioeroders (excavating sponges) (Murphy et al., 2016),which have been observed to become increasingly dominant on Caribbean reefs (Chaves-Fonnegra et al., 2007). Moreover, ongoing ocean acidification appears to promote the contribution of chemical $CaCO_3$ dissolution to total bioerosion by sponges even further (Duckworth and Peterson, 2013; Wisshak et al., 2013). Lastly, Silbiger and Donahue (2015) suggest that, under future climate conditions of increased pCO_2 and ongoing warming, dissolution of existing reef carbonates is likely to be more affected than the growing of new reefs as such. Together this implies that there is an urgent need for

in-situ determination of NCC at the ecosystem level.

Direct approaches to accurately quantify NCC generally rely on determining the flux of alkalinity between water column and reef (Smith et al., 1975). For reefs in environments characterized by a relatively linear flow of water over the reef, the upstream/downstream method (Odum and Hoskin, 1958; Gattuso et al., 1996) can be employed to determine NCC (e.g., Shaw et al., 2014; Koweek et al., 2015; Albright et al., 2016). For less unidirectional flow regimes, estimates based on overall residence time and knowledge of offshore conditions is needed (e.g., Courtney et al., 2016). In environments where low turbulence allows buildup of appreciable chemical vertical gradients, these gradients have been used to calculate net fluxes (e.g. McGillis et al., 2011; Takeshita et al., 2016). For fully exposed reefs, where no measurable accumulation may occur even in the boundary layer, the use of incubators is necessary. Several such incubation methods have been designed and applied. Most incubators cover a limited area (Patterson et al., 1991; Haas et al., 2013; Camp et al., 2015), allowing single-species incubations. In most cases, numerous incubations are necessary to accurately capture variability between different locations on a reef in accretion/erosion and thus accurately estimate whole ecosystem NCC. When employing small-volume incubators, care must also be taken to maintain representative hydrodynamic conditions for the incubation species. Moreover, incubations must be terminated before NCC becomes depressed (for example by depletion of oxygen). Larger incubation structures (e.g. Yates and Halley, 2003) better capture variability on a community scale and convey environmental hydrodynamic conditions (surge) which, on the other hand, may cause inadvertent leakage of enclosed water. This potential exchange between ambient and enclosed water complicates the interpretation of observed chemical changes, particularly for signals that take relatively long to manifest themselves (e.g., alkalinity). The latter limitation restricts this method into hydrodynamically favorable (i.e. calm) conditions (e.g. McGillis et al., 2011). Additionally, due to obvious logistical challenges, most or all in-situ incubations have been carried out on the reef flat. Here we aim to assess diurnal coral reef metabolic rates by investigating the in situ inorganic carbonate system over a reef slope coral reef patch offshore from the island of Saba, Dutch Caribbean. We use a tent-based incubation system in an environment with relatively strong currents and swell-induced near-bottom surge that caused modest exchange between the incubated reef and ambient water. Exchange between the enclosed and surrounding seawater is used to our advantage as this maintains oxygenated conditions during the incubation, thus allowing for increased incubation periods. Precise monitoring of temperature and salinity, both inside and outside the tent, allows for accurate determination of the amount of exchange across the enclosure. Explicitly accounting for the role of ambient variability, the benthic fluxes

originating within the tent are inferred with high accuracy. Comprehensive monitoring of CO_2 system parameters (DIC, total alkalinity), dissolved oxygen and nutrients (phosphate, nitrate, nitrite and ammonium) allows for subsequent quantification of integrated whole ecosystem coral reef metabolic processes (NCC and net community production, NCP) in a highly hydrodynamic environment.

2 Materials and methods

2.1 Site and substrate

Reef incubations were performed west of the island of Saba in Ladder Bay at the Ladder Labyrinth mooring site of the Saba National Marine Park (17.6261°N, 63.2602°W) (Field permit: RWS-2015/ 38370), between October 26th and 29th 2015, at a depth of 21 m (Figure 1). The reef in this area has a distinct spur-and-groove morphology, and is located on a steep incline from the heights of Saba towards the ∼500 m deep stretch between the island and the Saba Bank carbonate platform. Coral reefs around Saba harbour a relatively rich diversity of marine species in the context of the wider Caribbean (Etnoyer et al., 2010). The location at which the tent was placed, was chosen such that a patch of coral reef with a community representative of the wider area was fully enclosed (Figure 2). Within the 2x2 m enclosure, one larger and several smaller carbonate structures were present, acting as main substratum for benthic biota, together resulting in a in a total hard surface area ∼ 4.4 m^2 and a 14% surface enlargement (rugosity). Abiotic components (sand and bare rock) accounted for 61% of the total surface area within the enclosure. Algae (algal turf, *Lobophora* spp., *Dictyota* spp.) covered 22%, sponges (among others *Agelas* spp. and *Callyspongia plicifera*) covered 7% and calcifying species such as corals (including *Orbicella faviolata*, *Meadrina meandrites* and *Diploria clivosa*) and crustose coralline algae covered 4.2, and 6.6% of the total surface area, respectively (Figure 2). No macro-bioeroding organisms were visible. A small number of heterotrophic animals, including small fish, crustaceans and nudibranch, were present during the time of the incubation.

2.2 Enclosure

The incubation enclosure is a custom-made, semi-hemispherical, bottomless, transparent dome tent with a square, 4 m^2 footprint and ∼3.2 m^2 volume. The tent walls consist of transparent polyvinylchloride of 0.8 mm thickness, with nontransparent reinforcements along the edges. The tent was inflated (on sandy sediment) by pumping water into the ribs of the dome, after which the rigid tent was carefully moved in place over the coral mound. Flaps extended ∼50 cm outward from each of the tent's four

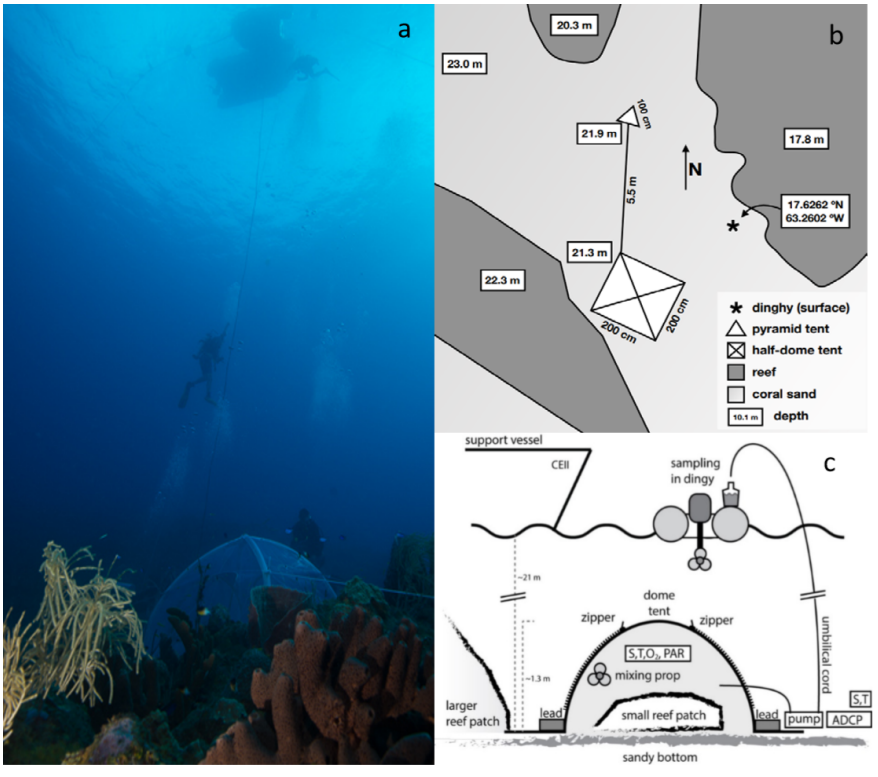

Figure 1: (a) Photograph depicting tent, umbilical cord, support divers and the dingy used for sample collection. (b) Schematic layout of the tent and surroundings. The Island of Saba is located to the east of this location. (c) Schematic side view of the employed setup for enclosure of a small patch of coral reef. The central structure is a rigid, inflatable dome tent, held securely in place by lead bricks and guy-lines (not shown). Inside the tent are located a battery powered mixing propeller for maintaining water circulation, and analyzers for salinity (S), temperature (T), oxygen (O_2) and PAR. External to the enclosure are located another S/T analyzer, a current profiler and a pump (powered intermittently from the surface) which through an umbilical cord delivers enclosure interior water to the sea surface for sampling. Sampling of exterior water was performed either by this pump (with SCUBA divers temporarily disconnecting the connection to the tent interior) or by divers using large volume syringes. Zippers allow for opening of tent windows for re-equilibrating interior and exterior conditions between incubations.

sides, allowing for proper sealing of the tent to the substrate by placing weights on the flaps. All four sides of the tent contained an opening of $\sim$0.3 m^2 to allow flushing of the enclosed volume between incubations: during each incubation this opening was

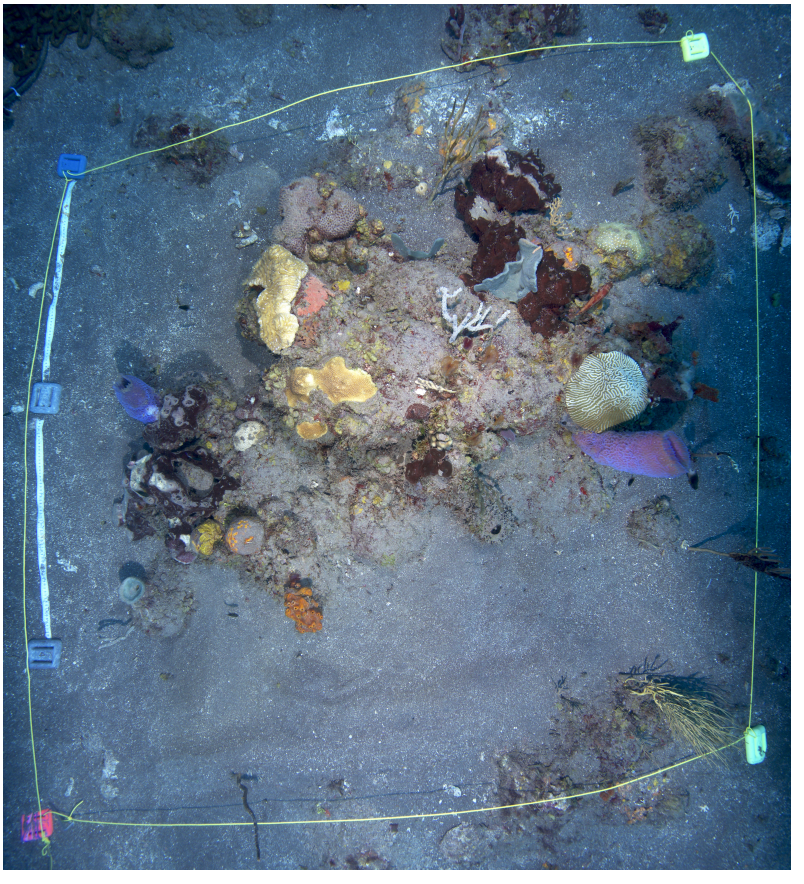

Figure 2: Overview of the enclosed coral reef patch, after termination of the tent incubation. Yellow lines mark the extent of the tent (approximately 2x2 m).

sealed. Water enclosed in the incubation tent was homogenized by a continuously running propeller pump (model PP20, Jebao Ltd, China). This pump was positioned close to one of the tent arches, at half the height of the tent, and generated a slight circulating turbulence, while minimizing stirring up of sediment. Effectiveness of the stirring was demonstrated by rapid and even dispersal of a small dose of injected fluorescein. Time required for initial deployment of the tent was approximately 4 hours. In total, five incubations were carried out on this location, three during the day (incubations 1, 3 & 5) and two at night (incubations 2 & 4) (Table 1).
On the sandy substrate, adjacent to the main tent, a small secondary incubator was deployed. Its design is tetrahedron-shaped, and features transparent PVC-walled, rigid edges of 1 m, with 0.5 m long flaps extending from bottom edge. It covers a

0.43 m^2 planar surface, and encloses a 118 l volume, resembling the cBIT described by Haas et al. (2013). Due to equipment constraints, only limited monitoring of this 'sediment blank' incubator was performed by determining the total alkalinity (A_T), total dissolved inorganic carbon (C_T), and nutrient concentrations.

Table 1: Incubation starting and end times, duration and light.

Incubation	1	2	3	4	5
Latitude	717.6261°N				
Longitude	763.2602°W				
Depth(m)	21				
Start(local time)	27/10, 09:17	27/10, 17:10	28/10, 08:33	28/10, 17:15	29/10, 08:10
End(local time)	27/10, 14:59	27/10, 22:13	28/10, 14:47	28/10, 23:20	29/10, 16:10
Duration(min)	342	303	374	365	480
Light mean(PAR)	65	3	58	3	91
Std	23	1	14	1	15
Minimum	22	2	11	2	5
Maximum	120	8	75	8	161

[1] The listed PAR values are in µmol quanta m^{-2} s^{-1}.

2.3 In-situ measurements

Measurement of salinity (S), temperature (T), dissolved oxygen (O_2), photosynthetically active radiation (PAR) and water current conditions within the large dome-shaped tent were performed throughout the duration of the incubations (four hours). S, T and O_2 were measured at 1-minute interval using an actively pumped SBE37 MicroCAT equiped with an SBE63 optical dissolved oxygen sensor (SeaBird Scientific Inc., Bellevue WA, USA). Drift of the involved sensors over the duration of our experiment was negligible, while precision ($\pm 1 \bullet 10^{-5}$, $\pm 1 \bullet 10^{-4}$ °C, ± 0.2 µmol kg^{-1}, respectively) is orders of magnitude better than the changes in S, T, and O_2 observed during incubations. PAR was assessed by an Odyssey light logger (Dataflow Systems PTY Ltd., Christchurch, NZ), calibrated in air against a superior instrument (Walz ULM500, Walz GmbH, Effeltrich, Germany). The MicroCAT and light logger were suspended from the apex of the enclosure at approximately half the tent's height. A second CTD unit (model CastAway, YSI Inc, Yellow Springs OH, USA) was deployed outside the tent to register ambient S and T during 2 out of the 5 incubations, due to logistical constraints.

2.4 Discrete Sampling

During incubations, discrete samples were collected every two hours for analysis of A_T, C_T, total organic carbon (TOC) and nutrients by pumping seawater from the tent interior (and, alternatingly, the exterior) up to the support vessel through a 50 m long 1/4" Dekabon gas-impermeable 'umbilical cord' (Figure 1). The total volume pumped upwards was ∼2 L per sampling event, after appropriate flushing (∼2 L) of the umbilical (internal volume ∼0.5 L). Most analyses for A_T were performed onboard (Caribbean Explorer II) using spectrophotometrically guided single-step acid titration (Liu et al., 2015). Additional samples for A_T and C_T were poisoned with $HgCl_2$ immediately after collection (Dickson et al., 2007) for post-cruise analysis on a VINDTA 3C instrument (Mintrop et al., 2000). Accuracy of both instruments was set using certified reference material (CRM; batch 144) supplied by Scripps Institute of Oceanography (Dickson et al., 2007). No appreciable bias in A_T was apparent between the two instruments. On the VINDTA, a total of ∼125 samples were analyzed for C_T and A_T. Precision of replicates from the same sample bottle was 1.5 µmol kg^{-1} for C_T and 1.0 µmol kg^{-1} for A_T (for both instruments). However, precision for field replicates (i.e., replicates from separate bottles; n=23) was 3.5 µmol kg^{-1} for C_T and 5.0 µmol kg^{-1} for A_T, possibly reflecting suboptimal sampling conditions and/or procedures (e.g., insufficient pre-flushing of umbilical before commencing filling of 1st replicate sample).

Samples for TOC determination were stored in pre-combusted 60 mL EPA vials and acidified and preserved with 8M HCl prior to shore-based analysis on a Shimadzu TOC-VCPN. Analytical precision for TOC (defined as standard deviation of differences between replicates) was ±9.9 µmol kg^{-1} (n=8).

Samples for dissolved inorganic macronutrients (NO_2+NO_3, NO_2, PO_4 and NH_4) were prepared by dispensing sampled water through 0.8/0.2 µm Acrodisk filters into 5 mL 'pony vials', and subsequently stored at -80°C for later analysis at NIOZ on a QuAAtro continuous flow analyser (SEAL Analytical, GmbH, Norderstedt, Germany) following GO-SHIP protocol (Hydes et al., 2010). Uncertainty of nutrient determinations (±0.1 µmol kg^{-1}, ±0.01 µmol kg^{-1}, ±0.005 µmol kg^{-1} and ±0.005 µmol kg^{-1}, respectively) was substantially smaller than the differences observed between samples taken over the incubation period.

Release of nutrients during respiration decreases A_T (or increases A_T for release of NH_4^+), confounding the interpretation of changes in A_T to represent $CaCO_3$ dissolution only. Following common protocol, we correct calculated A_T for nutrient release as follows:

$$A_T{}^{obsNC} = A_T{}^{obs} + PO_4 + NO_3 - NH_4$$

Throughout the remainder of the manuscript, A_T equals ${A_T}^{obsNC}$ as defined above.

2.5 Outline of data processing

After data collection, a 6-step approach was taken to infer fluxes from the measurements. Numbered steps are discussed in more detail in the following sections. Briefly, (1) the leak rate of the enclosure is inferred from measurements of S and T performed simultaneously inside and outside the tent during 2 of the 5 incubations. (2) Assuming the inferred leak rate to be valid throughout the experiment (i.e. for the other 3 incubations as well), time series of exterior S and T are inferred for all incubations from tent interior S and T. (3) Time series of ambient concentrations of C_T, A_T and O_2 are predicted from linear relationships with salinity. (4) We calculate, accounting for leakage at a known and assumed constant rate, the time rate of substance input into the tent interior that best reproduce the observations made inside the enclosure. (5) We apportion the input of C_T and A_T into the contributions by the processes of $CaCO_3$ dissolution and respiration. Lastly (6), all substance input rates are converted to fluxes.

(1) Rate of water exchange

The rate of water exchange across the enclosure f (in units of min^{-1}) was estimated from the dampened response of measured in-tent salinity (S) to the variability of measured ambient (i.e. outside the tent) salinity over the duration of an incubation. This was performed by iterative minimization (based on least squares) of the residuals q in equation 1.

$$ {S_{in}}^{calc}{}_{t+1} + q = ((1\text{-}f)\bullet {S_{in}}^{calc}{}_{t} + f\bullet {S_{ambient}}^{meas}{}_{t}) - {S_{in}}^{meas} \quad (1) $$

where, ${S_{in}}^{calc}{}_{t+1}$ is the calculated salinity inside the tent at time t+1, ${S_{in}}^{calc}{}_{t}$ the calculated salinity inside the tent at time t and ${S_{ambient}}^{meas}{}_{t}$ the measured salinity outside the tent at time t.

(2) Ambient hydrography

With the estimated leak rate estimate f, an approximation of ambient salinity ${S_{ambient}}^{calc}$ may be obtained from ${S_{in}}^{meas}$, which is available for all 5 incubations.

(3) Ambient chemistry

In order to know, at high temporal resolution, the concentrations of O_2, C_T and A_T outside the enclosure, we regress measurements of these parameters against ${S_{ambient}}^{calc}$. We use data collected (i) locally at the enclosure, supplemented by data obtained (i) by vertical profiling down to ∼75 m in the vicinity of the incubator and (ii) during expedition PE414 of the Dutch RV Pelagia in Aug/Sep 2016 close to Saba (hydrographic station #49, <5km from enclosure location; De Nooijer and Van Heuven 2017). The use of data collected nearly a year later might be considered inappropriate. However, comparison between (i) Pelagia and (ii) tent ambient A_T and C_T data (and near tent profiles) is rather favourable.

(4) Time rate of substance input R

Having inferred (i) the (assumed constant) rate of exchange of water between tent and environment and (ii) the time history of ambient concentrations Cout of the parameter of interest (i.e., A_T, C_T, etc.) next we subsequently determined the constant time rate of substance input R (in µmol kg^{-1} hr^{-1}) that best explains the observed changes of concentration C_{in} inside the enclosure while accounting for constant exchange with the environment. This is performed through iterative minimization of the residuals q in Equation (2).

$$ {C_{in}}^{t} + q = {C_{in}}^{t-1} \bullet (1\text{-}f) + {C_{ambient}}^{t-1} \bullet f + R \quad (2) $$

The inferred input rate R is somewhat sensitive to the choice of the initial interior concentration (${C_{in}}^{t=0}$). Using the measurement collected at the start of the incubation may affect the result due to stochastic measurement error. Therefore we used an initial $_{in}$ through careful observation of initial measurements performed in the enclosure and of the measured (and predicted) ambient conditions. The dictated initial interior concentrations were identical for all 5 incubations, supported by the observation of comparable ambient salinity at the start of each incubation. An estimate of the robustness of the input rates of O_2, C_T and A_T is obtained using a Monte Carlo approach (Figure S1). A thousand curve fits were performed as above, but after randomly perturbing (i) each of the measured values of C_T and A_T (both by samples from a normal distribution of width's' of 4 µmol kg^{-1}, representing the measurement precision), (ii) the times of collection of the samples (s=5 minutes) and the leak rate of the tent (s=0.1% min^{-1}). If the standard deviation of the 1000 obtained input rates was smaller than the calculated nominal input rate, this nominal rate is considered to be significantly different from zero.

(5) $CaCO_3$ dissolution and respiration rates

As outlined above, measurements of A_T haven been adjusted for the effect of nutrient release by respiration. Subsequently, the individual contributions of $CaCO_3$ dissolution and respiration to the observed concentrations (or fluxes) of A_T and C_T were calculated:

$\Delta A_T{}^{diss} = \Delta A_T{}^{obscNC}$ ..... change in A_T due to dissolution
$\Delta A_T{}^{resp} = 0$ ..... change in A_T due to respiration
$\Delta C_T{}^{diss} = \Delta A_T{}^{obscNC}/2$ ..... change in C_T due to dissolution
$\Delta C_T{}^{resp} = \Delta C_T{}^{obsc} - \Delta C_T{}^{diss}$ ..... change in C_T due to respiration

(6) Conversion to fluxes

The input rates R (again, in µmol kg^{-1} hr^{-1}) in the tent are converted to fluxes (µmol m^{-2} hr^{-1}), assuming an enclosed mass of water of 3000±150 kg (approximately 3200 litres enclosed; substrate volume is ∼250 L; seawater density ∼1022 kg m^{-3}) and an incubated planar surface of 4.4 m^2. Lastly, we compare our results with NCC estimates based on observed community composition and data published for the fluxes of various classes and species of reef organisms, following the *ReefBudget* approach of Perry et al. (2008). To measure the species specific cover within the incubated area, we took multiple photos from different angles and then used ImageJ v1.51j8 to quantify the precise cover of each functional benthic group. Rugosity was measured from 4 crossed transects through the incubated patch (see supplementary Table S1, S2 and S3).

3 Results

Application of Equation (1) to data collected during incubations 4 and 5 yields a leak rate of the enclosure f of ∼0.007 min^{-1}. This indicates that ∼25 kg of seawater (i.e., 0.007 × 3000 kg) is exchanged every minute between the incubation enclosure and the environment. Although f∼0.007 accurately relates interior and ambient salinity observations made during incubations 4 and 5, we have no direct means of ascertaining that it also applies to preceding incubations. However, given the sparse ambient salinity data, we assume this water exchange rate to be constant throughout all incubations. Because the sealing of the tent to the substrate remained unchanged from the second incubation onwards, the time history of ambient salinity Soutcalc was derived under the assumption of f being ∼0.007. During incubations the error between

$S_{out}{}^{meas}$ and $S_{out}{}^{calc}$ was -0.023±0.19 (range: 34.7-36.0). The good match indicates validity of this simple adjective exchange model.

The ambient hydrographic conditions reflect variable admixture of a deeper, colder and more saline component into the warmer, and fresher waterbody that is more commonly encountered at the incubation site (see Figure 3a).

In these ambient waters, C_T and A_T increase with S as is expected. Oxygen, too, is observed to increase with increasing S, due to the higher solubility in the more saline and - crucially - colder water. Regressions between S and $O_2/C_T/A_T$ are presented in Figure 3, panels b, d and f. The time histories of these properties, derived using $S_{ambient}{}^{calc}$, are presented in Figure 3, panels c, e and g. For nutrients, no regressions were performed since ambient concentrations were essentially invariant at zero compared to the in-tent changes during incubations (Figure S2).

Figure 4 illustrates the results of our approach for incubation 4. For an overview of all results from all incubations, please refer to supplementary Table S4 and/or Figure S3. The model employed fits the measurements for C_T and A_T relatively well: the rmse of the fit of C_T is 3.5 µmol kg^{-1} – identical to the measurement uncertainty of C_T itself. For A_T the fit (5.3 µmol kg^{-1}) is slightly worse than instrument precision (3.5 µmol kg^{-1}).

For the five incubations, consumption of oxygen from the incubated seawater ranged from -10 to -30 µmol $kgSW^{-1}$ $hour^{-1}$ (Table S4).

Concomitant increase of C_T, PO_4 and NO_{2+3} strongly suggests respiration to be the dominant process throughout these incubations. Respiration should decrease A_T slightly due to the release of nutrients, but an even larger decrease is inferred by the full model suggesting a significant role for net calcification during incubation 2, 3 and 4. For the incubation 1 and 5 on the other hand, slight $CaCO_3$ dissolution is inferred. Prior to inferring rates, values of A_T were adjusted to account for the release of nutrients during respiration according to equation (3). Therefore, by definition the respiration A_T rate is zero for all incubations (Table 2).

Results obtained from incubations using the smaller, secondary tent suggests at most a very limited role for sedimentary processes (see Supplementary Figure S4): although exterior concentrations of A_T and C_T increased by as much as 60 µmol kg^{-1} in the 2nd half of the incubation, interior A_T and C_T during those 4 hours did not increase at rates higher than 2.5 µmol kg^{-1} hr^{-1}. This limited response suggests a leak rate between 0.2 and 1 % min^{-1}. Appreciable accumulation may therefore be expected if fluxes are present, also because of the small tent's favorable volume-to-surface ratio (275 L m^{-2}, vs 750 L m^{-2} for the dome tent). Over the first 165 minutes of the incubation, however, interior A_T and C_T increase only by 1 and 2 µmol kg^{-1} compared to initial conditions (commensurate flux: ∼0.3 and 0.6 mmol

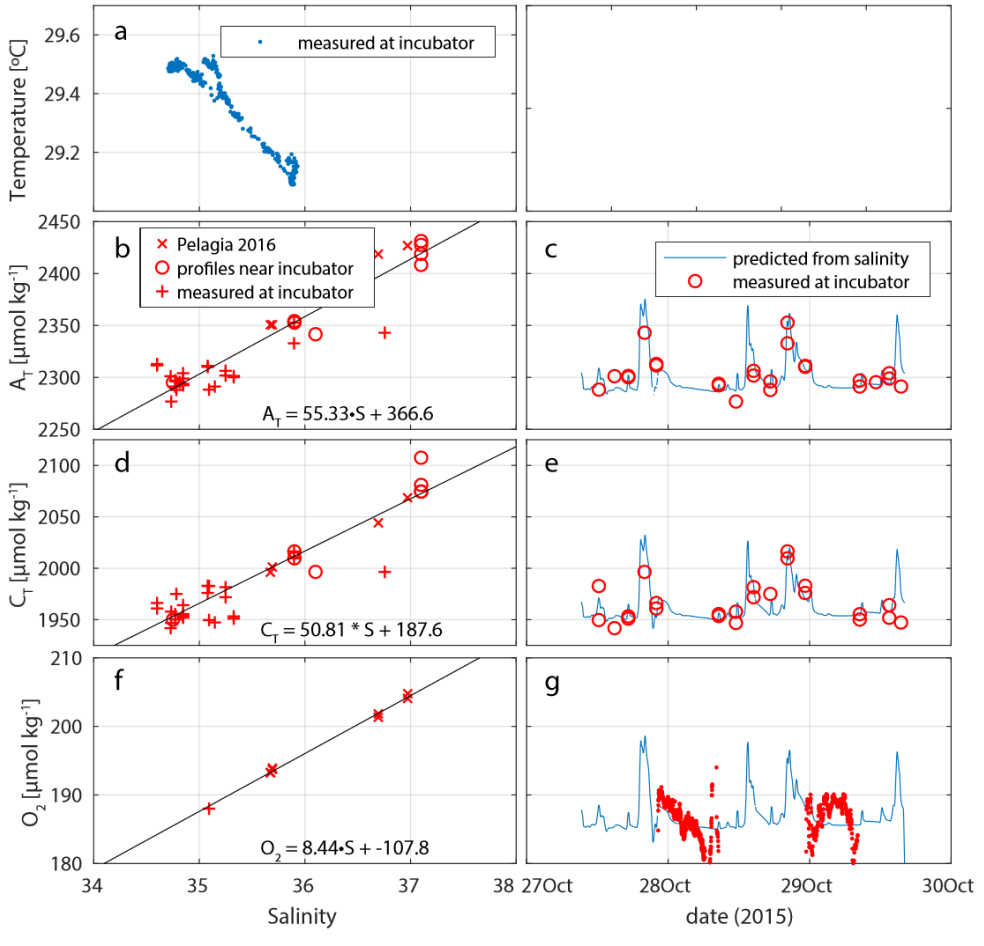

Figure 3: (a) Salinity and temperature recorded outside the enclosure show occasional mixing of a cool, saline deep water body into the warmer, fresher surface water component that is most commonly observed at the depth of the enclosure (as indicated by the high density of data points at S∼34.8). (b, d, f) Regression against salinity of, respectively, A_T, C_T and O_2. Samples in these regressions originate from three sources (two for O_2). (c, e, g) Measured values of, respectively A_T, C_T and O_2, plotted together with time trace of these values, generated from the regressions against salinity.

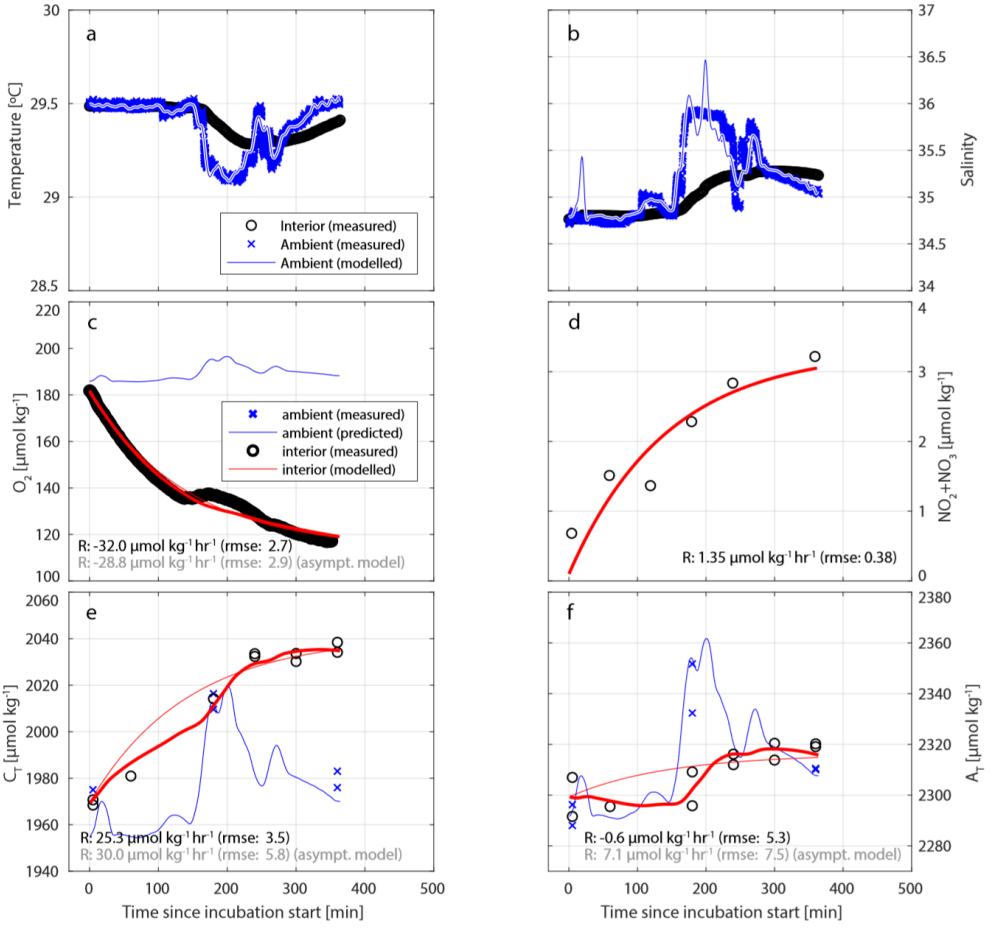

Figure 4: Illustrative results of the model (bold red line) employed to infer the substance input rates from observations, here for incubation 4. (a) A water exchange rate of 0.007 min^{-1} between enclosure and environment optimally relates ambient and interior measurements of salinity. Back-calculating ambient salinity from interior salinity is shown here to be feasible. (b) Ambient temperature co-varies with S. From T, the exchange rate is inferred to be 0.012 min^{-1} (higher than from S due to additional conductive equilibration). Additionally, in (c-f), we present results of a simplistic asymptotic curve fitting (thin red line) to show how the two methods may diverge appreciably, here mostly evidently for A_T. (Note that the uncertainty of the asymptotic fit is worse than that of the model used in this study).

Table 2: Summary of fluxes inferred from observed concentration changes in the enclosure during each of five incubation periods.

Incubation	1	2	3	4	5
PO_4	0.015 ± 0.004	0.009 ± 0.005	0.016 ± 0.005	0.031 ± 0.009	0.037 ± 0.007
NO_2+NO_3	0.49 ± 0.14	0.55 ± 0.21	0.83 ± 0.09	0.91 ± 0.18	0.81 ± 0.20
NH_4	0.21 ± 1.06	0.26 ± 0.48	0.18 ± 0.05	0.23 ± 0.04	0.17 ± 0.19
NO_2	0.02 ± 0.01	0.01 ± 0.01	0.02 ± 0.00	0.02 ± 0.00	0.01 ± 0.01
SIL	0.44 ± 0.10	0.00 ± 0.18	0.19 ± 0.10	-0.07 ± 0.20	-0.02 ± 0.15
DOC	1.4 ± 4.3	-1.1 ± 4.2	-0.9 ± 4.8	-1.9 ± 2.8	-0.1 ± 5.4
O_2	-9.0 ± 0.7	-13.5 ± 1.1	-13.6 ± 1.3	-21.7 ± 1.9	-17.0 ± 1.6
C_T	5.0 ± 0.8	11.1 ± 1.1	13.0 ± 1.0	17.1 ± 1.6	10.6 ± 1.1
A_T	0.4 ± 0.6	-2.5 ± 0.9	-2.8 ± 0.6	-0.4 ± 0.7	0.4 ± 0.5
C_{Tresp}	4.8 ± 0.8	12.3 ± 1.1	14.4 ± 1.0	17.3 ± 1.6	10.4 ± 1.1
A_{Tresp}	0.0 ± 0.0	0.0 ± 0.0	0.0 ± 0.0	0.0 ± 0.0	0.0 ± 0.0
C_{Tdiss}	0.2 ± 0.3	-1.2 ± 0.4	-1.4 ± 0.3	-0.2 ± 0.4	0.2 ± 0.2
A_{Tdiss}	0.4 ± 0.6	-2.5 ± 0.9	-2.8 ± 0.6	-0.4 ± 0.7	0.4 ± 0.5

See text for methods for derivation of rates and uncertainties.
All fluxes in mmol hour^{-1} m^{-2} (planar incubated surface area).
Negative dissolution fluxes are described (instead of positive calcification) to maintain co-directionality of the fluxes of respiration and dissolution.

m^{-2} hr^{-1}, i.e, one or two orders of magnitude lower than in the main tent; note that appreciable errors apply both to measurements and conversion to flux). These increases may be linked to exchange with ambient waters. No changes in pyramid tent nutrient concentrations were observed, suggesting low rates of productivity or respiratory processes. For subsequent calculations, we consider the contribution by sedimentary processes to be negligible.

Subsequently, the concentration changes in oxygen, inorganic carbon, etc. in the dome-tent were used to calculate the fluxes during each of the five main incubations (Table 2). No trends were observed in TOC concentrations within the tent during incubations, despite clear trends being observed for C_T. Deviations of the tent leak rate from the nominal 0.7 % min^{-1} (or 'breach events') are observed during all incubations. These deviations from our assumption may negatively affect the inferred rates of change in O_2 concentrations, as evident from the differing slopes of trace and fit near the starts of incubations. Considering only the first 30 minutes of the oxygen traces (preceding tentative breach events in all incubations), appreciably higher oxygen consumption is inferred than when considering the full traces (Table S5). At constant ambient S, O_2, C_T and A_T, leakage at a rate higher than the 0.7% min^{-1}

that we assume would result in underestimation of the true fluxes of O_T, C_T and A_T. No change would be observed in the O-flux/C-flux ratio that we infer. Conversely, at times of sudden high ambient S, O_T, C_T and A_T, leakage at a rate higher than the 0.7% min^{-1} that we assume would result in overestimation of C_T and A_T fluxes, and underestimation of O_2 fluxes. This would change the O-flux/C-flux ratio that we infer. However, as we do not know if the O_2 trace is asymptotic, or that the tent did indeed leak at higher or lower rates than 0.7% min^{-1}, results are likely still valid (i.e., when no breach events occurred, and O_2 deviations resulted from sensor artefacts or true biological activity). We therefore maintained the conceivably affected incubations in the paper.

The NCC inferred from our incubations ranges from -0.2 kg $CaCO_3$ m^{-2} yr^{-1} to 1.2 kg $CaCO_3$ m^{-2} yr^{-1} which is on average higher but still in range than the NCC estimated from the ReefBudget method (0.36 kg $CaCO_3$ m^{-2} yr^{-1}, Table 3).

Table 3: Net community calcification estimates from flux_based method and *ReefBudget method*.

Incubation	1	2	3	4	5
NCC_{flux}(kg $CaCO_3$ $m^{-2}year^{-1}$)	-0.2±0.3	+1.1±0.4	+1.2±0.3	+0.2±0.4	-0.2±0.2
NCC_{RB}(kg $CaCO_3$ $m^{-2}year^{-1}$)	0.36	0.36	0.36	0.36	0.36
NCC_{flux}(mmol $CaCO_3$ $m^{-2}h^{-1}$)	-0.2±0.3	+1.2±0.4	+1.4±0.3	+0.2±0.4	-0.2±0.2
NCC_{RB}(mmol $CaCO_3$ $m^{-2}h^{-1}$)	0.41	0.41	0.41	0.41	0.41

NCC of the planar total area inside the incubation calculated from fluxes and the *ReefBuget method*.

4 Discussion

Our results indicate that the tent incubation is an effective tool for in-situ quantification of reef fluxes in reef-overlaying water. Quantification of fluxes was achieved despite strong variability in ambient conditions and in the presence of appreciable swell induced seawater exchange. To this end we applied a comprehensive conceptual framework for the interpretation of the measured concentration differences. This method allows for a volume exchange between the environment and the incubation thereby replenishing the latter and keeping the O_2 levels within the tent near ambient conditions resulting in minimised unrepresentative reef community metabolism. By continuously monitoring the inside environment and assuming constant exchange rate, fluxes within our incubation can be treated as if acquired by a flow through system. Nonetheless, future application of this or similar incubation methods could be further improved by continuous monitoring of the exchange rate, rather than assum-

ing it to be constant throughout the incubation. This could be obtained for instance by running a second thermosalinograph outside the tent. The application of a conceptually simpler 'asymptotic' model yields different and less well-constrained results. Particularly, the direction of the $CaCO_3$ dissolution flux may be seen to be reversed in the simpler method (see also Figure 4). In all incubations, for both A_T and C_T, the uncertainty in measured concentration differences and the variability between results may be greater for the simpler model (Supplementary Table S4; supplementary Figure S3). In the case of A_T (Figure 4f), the assumed-to-be-constant input of A_T inferred by the model applied here is of opposite sign to the simpler asymptotic model result (-0.6 vs +7.1 µmol kg^{-1} hr^{-1}). This reversal of sign of the A_T rates observed between the two models (asymptotic and full) is caused by the inability of the asymptotic model to account for occasional intrusion of high-A_T ambient water into the tent during sudden changes in ambient hydrography. The asymptotic model (panels c & d) shows a relatively good fit of the observations of O_2 and NO_{2+3} around the fitted curve, which is due to the invariant ambient concentrations of these parameters.

In contrast with previous studies carried out at shallower depths using either Lagrangian drifts or incubations, all net diurnal rates from this study are strongly skewed towards respiration suggesting net heterotrophy in all incubations. Studies performed at shallower depths shift between net autrotophy and net heterotrophy over the course of a day (Yates et al., 2003, Albright et al., 2013; 2015). However, previously reported average net respiration rates occurring at night on shallower reefs are comparable to results from this study (14.5 to 35.5 mmol C m^{-2} h^{-1}). Results are also comparable to previously reported values at depth. For example, Middelburg et al. (2005) compiled a global mean coral reef respiration rate of 131±46 mol C m^{-2} yr^{-1}. Specifically for their categories 'outer reef slopes' and 'high activity areas' they report values of 140±70 and 413±187 mol C m^{-2} yr^{-1}, respectively. This range compares well to the rates reported here (105-298 mol C m^{-2} yr^{-1} for the full planar surface). A stoichiometric comparison of the inferred fluxes of C_T, oxygen and nutrients is combined with (i) the canonical 'Redfield ratio' (Redfield, 1963) of the elemental composition of open ocean phytoplankton and (ii) the median elemental composition of benthic macroalga (Atkinson and Smith, 1983), likely resembling the composition of the labile fraction of the locally present organic carbon (Table 4). This shows that the community incubated in this experiment respires carbon and nutrients in a ratio that resembles the composition of benthic macroalgae (Atkinson and Smith, 1983) which indicates that the observed signal is indeed originating from the sedimentary, benthic, macrofaunal, and/or bacterial constituents of the enclosed community.

A strong correlation between NCC and net community productivity in reef en-

Table 4: Stoichiometry of rates observed during 5 incubations.

Incubation	P	N	O	C	O/C
1	1	32.8 ± 12.2	337.5 ± 99.7	-608.7 ± 157.5	-1.80 ± 0.33
2	1	61.2 ± 42.1	1222.4 ± 714.9	-1485.3 ± 867.5	-1.22 ± 0.14
3	1	51.5 ± 17.9	805.8 ± 275.4	-842.9 ± 289.4	-1.05 ± 0.13
4	1	29.7 ± 10.7	557.9 ± 175.1	-706.6 ± 223.6	-1.27 ± 0.14
5	1	21.7 ± 6.5	313.3 ± 60.8	-455.2 ± 91.6	-1.45 ± 0.18
All	1	33.2 ± 5.6	535.6 ± 73.3	-691.7 ± 94.9	-1.29 ± 0.07
R_{1963}	1	16	106	-150	1.22
$A\&S_{1983}$	1	30	550	-610	NA

Values in column "avg." are calculated as the ratio of the sums of incubations 2-5.
[2] Uncertainties are calculated by error propagation.
[3] Rightmost two columns show literature values from (i) Redfield et al (1963) and (ii) Atkinson and Smith (1983), representing the elemental compositions of (i) marine phytoplankton and (ii) benthic macroalgae.
[4] Our incubation results most closely resemble the latter.

vironments is well documented (Gattuso et al., 1996; Shaw et al., 2012, Shaw et al., 2015; McMahon et al., 2013; Albright et al., 2015) however, no correlation was found in our incubations. The NCC inferred from our incubations ranged from -0.2 to 1.2 kg $CaCO_3$ m^{-2} yr^{-1} which is on average higher than the mean recorded rate of 0.2 kg $CaCO_3$ m^{-2} yr^{-1} associated with a Floridian reef patch (10% coral cover) in shallower waters (Yates, 2003) using a similar method.

Applying the *ReefBudget* approach to our benthic census data for comparison, we obtain a NCC for the full incubated substrate surface (i.e., sand and hard substrate) of ∼0.36 kg $CaCO_3$ m^{-2} yr^{-1} (see Table 3). This estimate is lower (but still within error) than the average NCC inferred from our incubations (∼0.88±1 kg $CaCO_3$ m^{-2} yr^{-1}, Table 3). The range of NCC estimates inferred from our results indicates how sensitive metabolic and chemical processes on coral reefs are to their environment. The chemical flux-based method as presented here is appreciably sensitive to the effects of the surrounding hydrological conditions on the substrate and this may be the source for a slight discrepancy compared to the *ReefBudget* approach. NCC rates acquired by Perry et al. (2013) associated with a coral cover ranging between 4-5% and at similar depth (17-20 meters) in the Bahamas are all negative (ranging from -0.01 kg $CaCO_3$ m^{-2} yr^{-1} to -0.23 kg $CaCO_3$ m^{-2} yr^{-1}). This may be explained by varying community composition such as the absence of macro-bioeroders within our tent. Furthermore, the flux-based method does not assess the mechanical component of bioerosion (caused by parrot fish or sponges for instance) which is important to the process of reef accretion.

The *ReefBudget* method offers a fast and convenient tool for estimating reef biogenic carbonate production states both on a remarkable temporal and spatial scale. Although the incubated flux-based approach, may be more sensitive to unstable and varying reef states, it cannot offer such a large spectrum of study. However, it provides an assessment of the full community without having to determine calcification/dissolution rates as a function of surface area. This can be very useful to assess the effect of endolithic species or determine the impact that some understudied organism may have on the chemical conditions. For instance, benthic cyanobacterial mats have been shown to proliferate around the islands of Curaçao and Bonaire since 2003 (De Bakker et al. 2017) and are described to effect pH on a local scale (Hallock, 2005; Paerl and Paul, 2012). However, close to no records on how these mats may alter reef chemical conditions and subsequently impact the calcifying/bioeroding community are available. Currently, the *ReefBudget* approach relies on various assumptions regarding the calculation of each biological component. As such, the flux-based approach described here should not be regarded as a substitute for survey methods such as the *ReefBudget*, but rather as a complementary tool. Using the flux-based approach, it will become easier to determine missing components and variations in chemical dissolution/calcification on a spatial (e.g. depth) and also smaller temporal scale (i.e. diurnal cycle, seasonality), therewith improving survey based carbonate budget assessments.

To determine if the respiration signal might be an artefact of the incubation treatment, we identify potential causes that may perturb the signal. The estimated contribution by macrofauna such as fish, crustaceans and nudibranchs to the observed respiration signal is deemed to be negligible: considering a fish mass-specific O_2 consumption rate of $\sim$100 mgO_2 h^{-1} kg^{-1} (Roche et al., 2013), and assuming 100 grams of fish to be present in the tent (which is likely a strong overestimate as only very few small fish were observed during incubations), we calculate a contribution to C_T in the incubation of $\sim$0.1 µmol kg^{-1} h^{-1}, which is two orders of magnitude smaller than the observed respiration rates of 10-30 µmol kg^{-1}. Additionally, we rule out that 'free floating' TOC (e.g., coral exudates) is the material that is respired. While clear fluxes are inferred for C_T, no trends were observed in TOC concentrations within the tent during incubations. Alternatively, no significant depression was observed of average interior TOC values (84$\pm$9 µmol kg^{-1}, n=39) relative to exterior TOC (86$\pm$7 µmol kg^{-1}, n=8). Although the tentative drop in TOC resembles the small drop observed in dedicated DOC depletion experiments (e.g., De Goeij and Van Duyl 2007), the lack of volume flow through the tent means TOC cannot be more than a very minor source of respirable carbon. Absence of depletion of suspended labile TOC notwithstanding, TOC may still play a role in the form of mucus if that is adhered to substrate or

incubator, out of reach of sampling but available for bacterial respiration. However, the respiring biomass required for the observed C_T increases is unlikely to be present in the form of bacteria, especially shortly after incubation start. Indeed, Wild et al. (2004) show from small-scale incubations that the bacterial degradation of coral mucus, introduced into their incubators (containing only sediment and water column) at high concentrations, occurs at rates of 0.7-2.1 mmol m^{-2} hr^{-1}. That compares to rates around 60-175 mmol m^{-2} hr^{-1} observed in our experiment, suggesting remineralization of adhered mucus plays at best a minor role in our incubations, further suggesting the observed fluxes to originate from the macroscopic biotic substrate.

In that category, sponges are the most likely organisms respiring, having appreciable biomass and containing ample energy stores to maintain respiration during the incubation periods, in which only limited amounts of organic carbon are available for filter feeding. Hadas et al. (2008) report (Red Sea) sponge basal oxygen consumption to be ∼50% of consumption featured during full water pumping activity, which means that sponge respiration largely continues even when filter feeding ceases. These authors report a rate of 2.4 µmol O_2 hr^{-1} g^{-1} (wet weight). Similarly, (Ludeman et al., 2017) report sponge oxygen consumption (standardized to sponge volume) ranging from 0.3-3 µmol h^{-1} ml^{-1}, with strong species dependence. Assuming the higher end of this range applies to the sponges incubated in our experiment (mostly *Agelas* sp., *Callyspongia plicifera*), and assuming as much as 5 kg wet weight of sponge to have been present in the enclosure, we account for ∼5 µmol kg^{-1} hr^{-1} of the observed rates of ∼30 µmol kg^{-1} hr^{-1}. Maintained respiration by sponges throughout the series of incubations could be fuelled by filter feeding during the ∼50% of the time in which the incubator was open to the ambient water. Recent research by McMurray et al. (2018) showed that species hosting abundant symbiotic microbes (i.e. high microbial abundance or HMA) primarily consumed dissolved organic carbon (DOC), while the diet of species with low microbial abundances (LMA) primarily consisted of detritus and picoplankton. They further pointed out that it remained unknown if DOC released by LMA species could be a source of food for HMA species. The main sponges incubated in our experiment are *Agelas* sp. and *Callyspongia plicifera* and represent respectively a HMA and a LMA sponge. We tentatively infer that this may explain partly the observed high respiration rate. Nevertheless, we cannot infer if sponges are able to maintain metabolic balance throughout the incubation period, or that they deplete their stores. Further analyses such as bacterial counts would be needed to answer such questions. From Table 2 we conclude oxygen consumption rate during daytime (incubations 2 and 4) to be lower by ∼5 µmol kg^{-1} hr^{-1} than night time rates (incubations 3 and 5), hinting at a role of primary producers (corals, CCA, macro and microalgae).

The lack of accumulation of C_T in the secondary, small incubation places our sediment at the very low end of literature values regarding respiration. For example, Middelburg et al. (2005) report a global mean sediment respiration value of ∼8.5±7 mmol C m^{-2} h^{-1} (as approximated from their Figure 11.3). Our observed low values may be reasonable considering the highly hydrodynamic nature of the incubation environment which likely hampers settlement of substantial amounts of organic matter onto and into the sediment. In addition, the volcanic sandy composition of the sediment around Saba may be less prone to dissolution than coralline sediment and could explain the insignificant increase in A_T in the small tent. However, Eyre et al. (2018) shows similar results for sediment around Cook Islands which is mostly composed of calcareous fragments (Wood, 1967). Eyre et al. (2018) shows that dissolution in reef sediment across different locations around the world is negatively correlated with the aragonite saturation state (Ωar). Average Ωar of ambient water around the tent incubation throughout the experiment is calculated to be 3.85 which is more comparable to islands (Bermuda and Tetiaroa) showing accretion in reef sediment. The combined effects of hydrodynamics and sand composition are likely to explain why our results present neither accretion nor dissolution in our tent's sediment.

Conclusions

Flux-based carbonate budget studies, as presented here, provide quantitative data on the functional state of reefs in terms of biologically driven carbonate production which is particularly sensitive to ambient environmental conditions. As such, they can be particularly useful for temporal studies, especially to reveal not only diurnal and seasonal patterns but also to capture shifts in functionality of reef systems. We incubated a coral reef patch situated in a high-energy environment which caused a limited amount of seawater exchange. Monitoring of conditions within and outside the tent allowed for determination of the exchange rate and thereby allowed for correcting the respiration and calcification rates. Application of this procedure shows that this reef patch is characterized by NCC inside the tent at a rate within range but on average higher than fluxes reported in previous studies for shallower reef systems indicating coherence in our results. However, the range of NCC estimates inferred from our results accounts for the sensitivity of this reef patch to the surrounding environment. Furthermore, the net heterotrophy reported here both during the day and the night differs from studies performed at shallower depths where shifts between net autotrophy and net heterotrophy are observed. Future research may include various types of substrates and comparison between regions with varying water quality.

Acknowledgements

The authors are particularly grateful to the captain and crew of *Caribbean Explorer II*, who have been outstandingly helpful and accommodating. We also would like to thank the institutional support of Saba Marine Parks, Caribbean Netherlands Science Institute (CNSI) and Wageningen Marine Research (WMR). Additional gratitude is reserved for Janine Nauw, Johan Stapel, Steve Piontek, and volunteer divers Oscar Bos, Dahlia Hassell, Jarno Knijff, Ewan Tregarot, Lodewijk van Walraven and Bas Westerhof.

Supplements

Table S 1: Total calcification using the *ReefBudget* method. *ReefBudget* method applied to the 4.4 m^2 full planar surface of the tent.

Species	**Area [cm^2]**	**Specific calc. rate**[a)b)]	**Cover**[c)]	**Rugosity**[d)]	**Calc. rate**
Meandrina meandrites	496	2.19	1.12	1.36	0.033
Orbicella faveolata	276	9.07	0.62	1.36	0.077
Siderastrea siderea	85	8.53	0.19	1.36	0.022
Diploria clivosa	756	4.99	1.71	1.36	0.116
Montastraea cavernosa	101	9.07	0.23	1.36	0.028
Millipora spp.	107	28.10	0.24	1.36	0.092
Madracis decactis	26 34	.36	0.06	1.36	0.027
Total Coral Calc.					0.396
Total CCA Calc.	2940	0.18	17.00	1.36	0.042
Total Microbioerosion	9397	0.27	21.22	1.36	0.078
[kg $CaCO_3$ m^{-2} yr^{-1} planar incubation surface]					0.360
[mmol m^{-2} h^{-1} planar incubation area]					0.411

[1] [kg $CaCO_3$ m^{-2} organism yr^{-1}].
[2] The specific calcification rates are from Perry's *ReefBudget* website, the 5-10 meter deep sheet; http://geography.exeter.ac.uk/media/universityofexeter/schoolofgeography/reefbudget/documents/Benthic_Data_Entry_Template_5-10m_depth.xls
[3] [% of full planar 4.4 m^2].
[4] [kg $CaCO_3$ m^{-2} yr^{-1} planar incubation surface].

Table S 2: Surface area of substrate classes

Substrate classification	**Area [cm^2]**	**%of Total**	**%of Hard**	**Source / comments**
Total Quadrat	44284			(photo survey; planar surface)
Total Sand	26990	60.9		(difference Total-Hard; planar surface)
Total Hard Substrate	17294	39.1		(photo survey; planar surface)
of which...				
Coral	1846	4.2	10.7	(photo survey; planar surface)
Sponge	3111	7	18	(photo survey; planar surface)
CCA	2940	6.6	17	(photo survey; planar surface)
Available for bioerosion	9397	21.2	54.3	(difference Hard Subst. - Coral - Sponge - CCA)

Table S 3: Rugosity, planar area and 3D.

Substrate	**Planar area[cm^2]**	**Rugosity[cm^2]**	**3D area[cm^2]**
Hard	17294	1.36	23468
Sand	26991	1.00	26991
Total	44284	1.14	50458

[1] Planar areas were determined from photogrammetry, based on photographs collected after incubator removal at end of the experiment.
[2] Rugosity of 1.36 was determined in the field after removal.
[3] Rugosity of the sandy part of the patch was assumed to be approximately 1.00.
[4] Average rugosity of the patch is calculated.

Table S 4: Calculated rates within the enclosure.

PO_4	0.022±0.005 (rmse=0.009)	0.013±0.008 (rmse=0.011)	0.024±0.008 (rmse=0.014)	0.045±0.014 (rmse=0.020)	0.055±0.010 (rmse=0.020)
NO_2+NO_3	0.72±0.20 (rmse=0.33)	0.82±0.31 (rmse=0.42)	1.23±0.13 (rmse=0.22)	1.35±0.26 (rmse=0.38)	1.20±0.29 (rmse=0.56)
NH_4	0.32±1.57 (rmse=2.56)	0.38±0.70 (rmse=0.98)	0.26±0.07 (rmse=0.11)	0.34±0.07 (rmse=0.10)	0.24±0.28 (rmse=0.57)
NO_2	0.02±0.02 (rmse=0.03)	0.02±0.02 (rmse=0.03)	0.02±0.01 (rmse=0.01)	0.03±0.01 (rmse=0.01)	0.02±0.01 (rmse=0.02)
SIL	0.64±0.15 (rmse=0.21)	0.00±0.26 (rmse=0.37)	0.28±0.15 (rmse=0.30)	-0.10±0.30 (rmse=0.46)	-0.03±0.22 (rmse=0.45)
DOC	2.1±6.4 (rmse=17.8)	-1.6±6.2 (rmse=7.4)	-1.3±7.1 (rmse=13.0)	-2.8±4.1 (rmse=7.0)	-0.1±7.9 (rmse=15.4)
O_2	-13.4±NaN (rmse=3.1)	-19.9±NaN (rmse=3.3)	-20.0±NaN (rmse=2.2)	-32.0±NaN (rmse=2.7)	-25.2±NaN (rmse=1.2)
C_T	7.4±1.1 (rmse=6.0)	16.4±1.4 (rmse=8.3)	19.2±1.7 (rmse=6.0)	25.3±2.4 (rmse=3.5)	17.3±1.8 (rmse=3.6)
A_T	0.7±0.9 (rmse=4.3)	-3.6±1.3 (rmse=7.1)	-4.2±0.9 (rmse=5.4)	-0.6±1.2 (rmse=5.3)	0.6±0.7 (rmse=2.4)
$C_T$resp	7.1	18.2	21.2	25.6	17.0
$A_T$resp	0.0	0.0	0.0	0.0	0.0
$C_T$diss	0.3	-1.8	-2.1	-0.3	0.3
$A_T$diss	0.7	-3.6	-4.2	-0.6	0.6
$O_{2\,-const.env.}$	-11.3±0.2 (rmse=3.1)	-15.7±0.3 (rmse=3.7)	-17.4±0.2 (rmse=2.4)	-28.8±0.2 (rmse=2.9)	-23.9±0.1 (rmse=1.8)
$C_{T\,-const.env.}$	7.1±2.4 (rmse=6.4)	26.8±5.4 (rmse=10.1)	23.8±5.0 (rmse=11.4)	30.0±2.4 (rmse=5.8)	20.5±2.0 (rmse=5.5)
$A_{T\,-const.env.}$	3.7±1.5 (rmse=4.3)	5.8±5.6 (rmse=12.0)	-6.4±3.3 (rmse=8.3)	7.1±2.9 (rmse=7.5)	2.4±1.7 (rmse=5.1)

[1] Rates in µmol $kgSW^{-1}$ $hour^{-1}$; the s.e. of the fit; and the rmses of the fits.

Table S 5: O_2 change rates.

Incubation	Time.of.day	Full.incubation	First.30.minutes
1	day	-11.3±0.4	-14.2±0.2
2	night	-15.7±0.6	-28.4±0.5
3	day	-17.4±0.3	-23.1±0.5
4	night	-28.8±0.4	-31.5±0.6
5	day	-23.9±0.2	-26.2±0.4

[1] Comparison of rates of change in O_2 concentrations inferred from either the full O_2 concentration history (third column) or from only the first 30 minutes of each incubation (rightmost column).
[2] The latter method provides a more consistent separation between day and night time incubations (especially when ignoring incubation 1).
[3] The daytime average O_2 consumption is ∼20% below the night time rate.

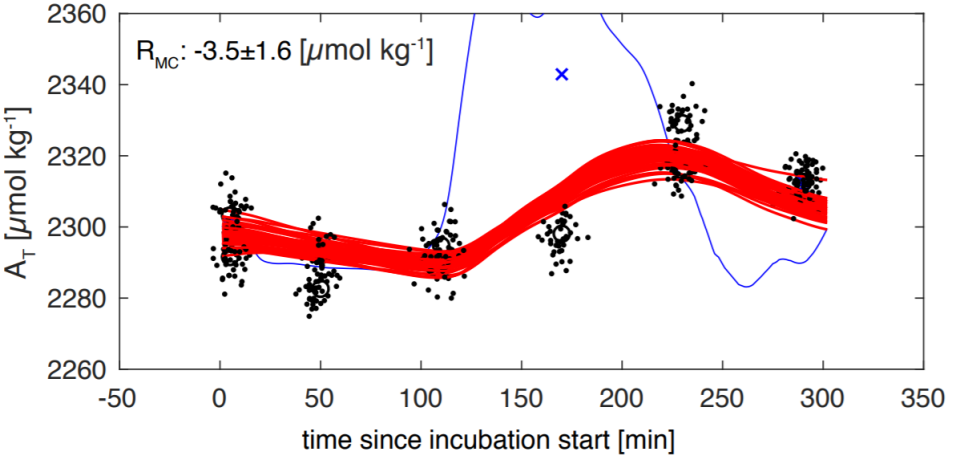

Figure S 1: Method to assess robutstness of the inferred rates. Example of results of the Monte Carlo method used to assess robustness of inferred time rates of change of concentrations during incubation. Here, we measured values of A_T and the leak rate are varied slightly (∼4 µmol kg^{-1} for A_T, ±0.1% min^{-1} for leak rate), and curves are repeatedly fit. The average and standard deviation of one throusand such fits are presented. In this example, the rate average is slightly larger than the associated uncertainty, and the rate is thus assumed to be significantly different of zero.

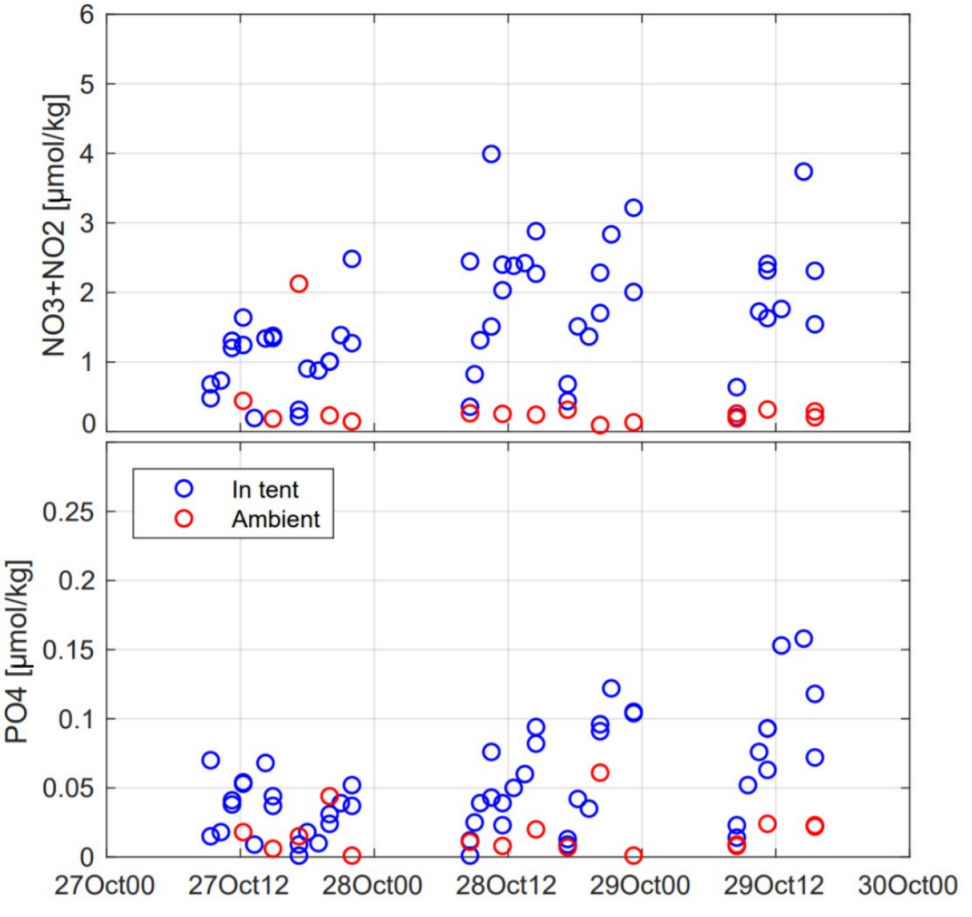

Figure S 2: In-tent and ambient nutrients. Interior and ambient nutrient concentrations.

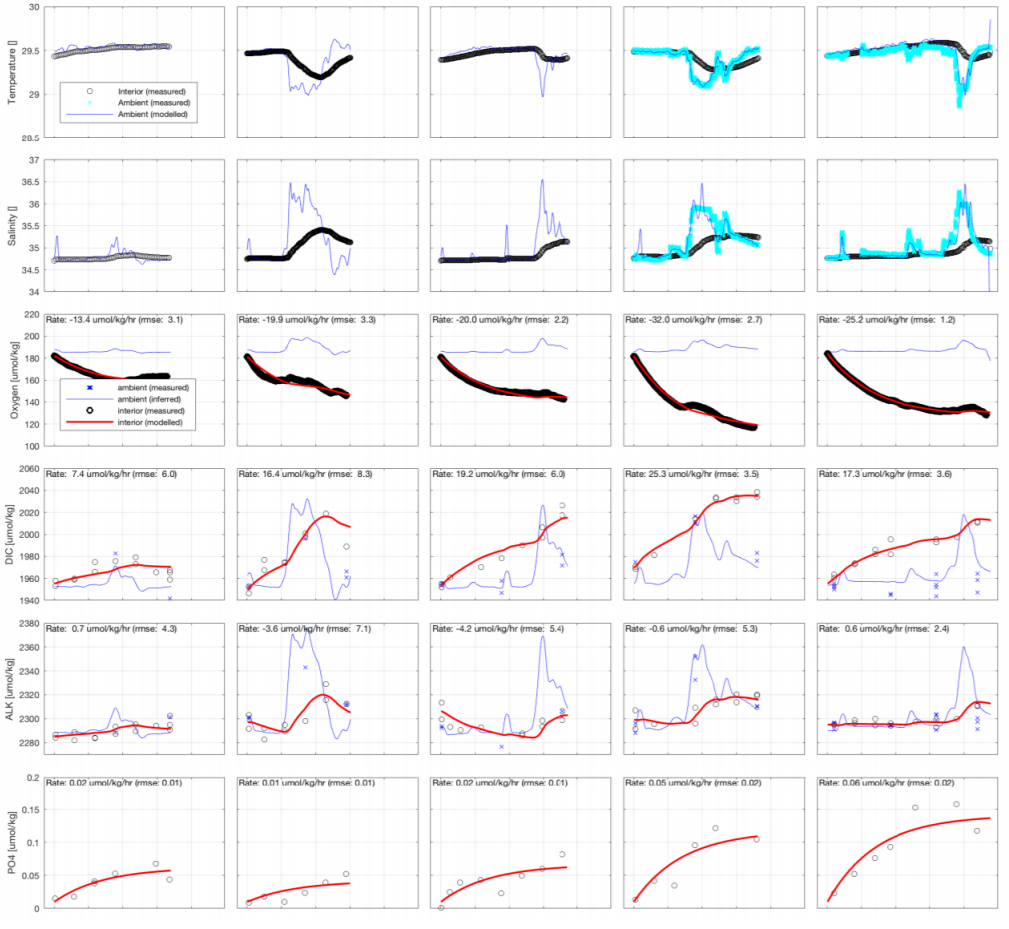

Figure S 3: (1^{st} part) Data from secondary 'pyramid' incubator, placed on bare sediment. In-tent measurements and model fits of all five incubation periods. Second and fourth incubations were during nighttime. The legend presented in the third row of panels applies to all subsequent rows (except PAR, which was measured).

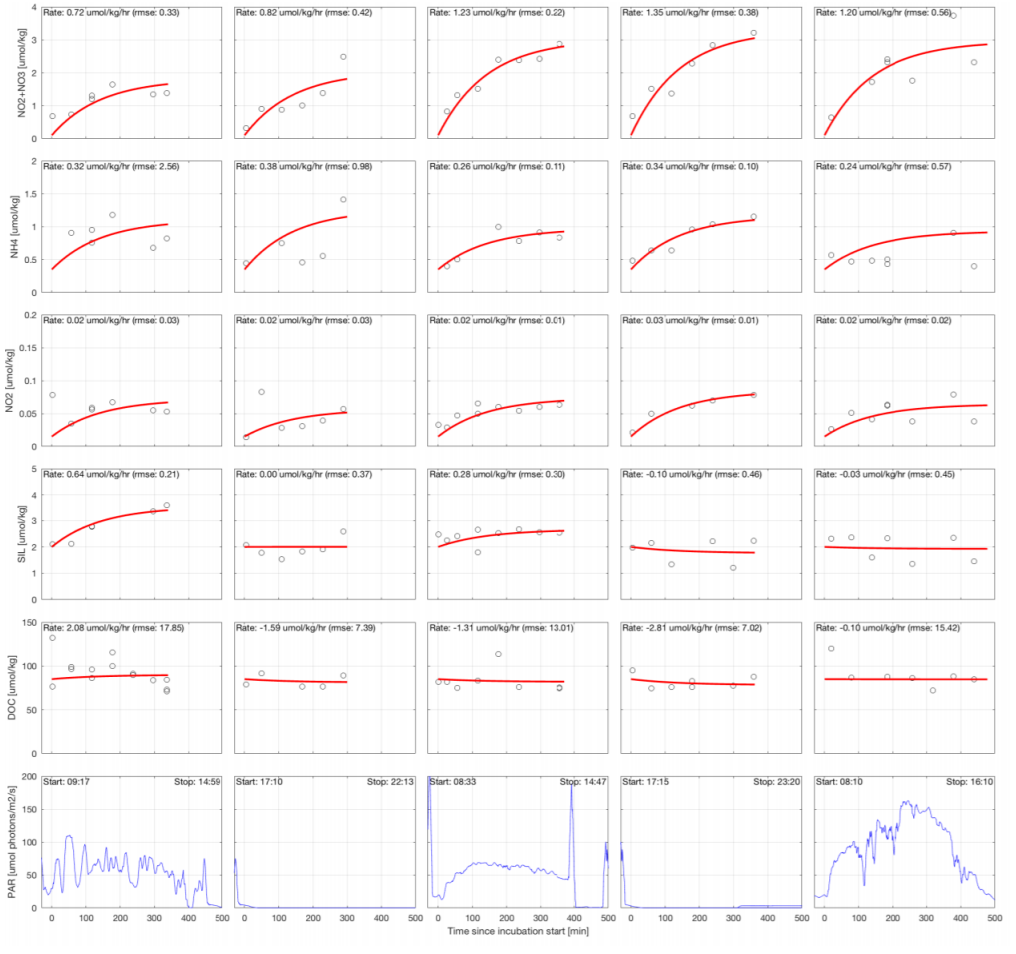

Figure S 3: (2^{nd} part) Data from secondary 'pyramid' incubator, placed on bare sediment. In-tent measurements and model fits of all five incubation periods. Second and fourth incubations were during nighttime. The legend presented in the third row of panels applies to all subsequent rows (except PAR, which was measured).

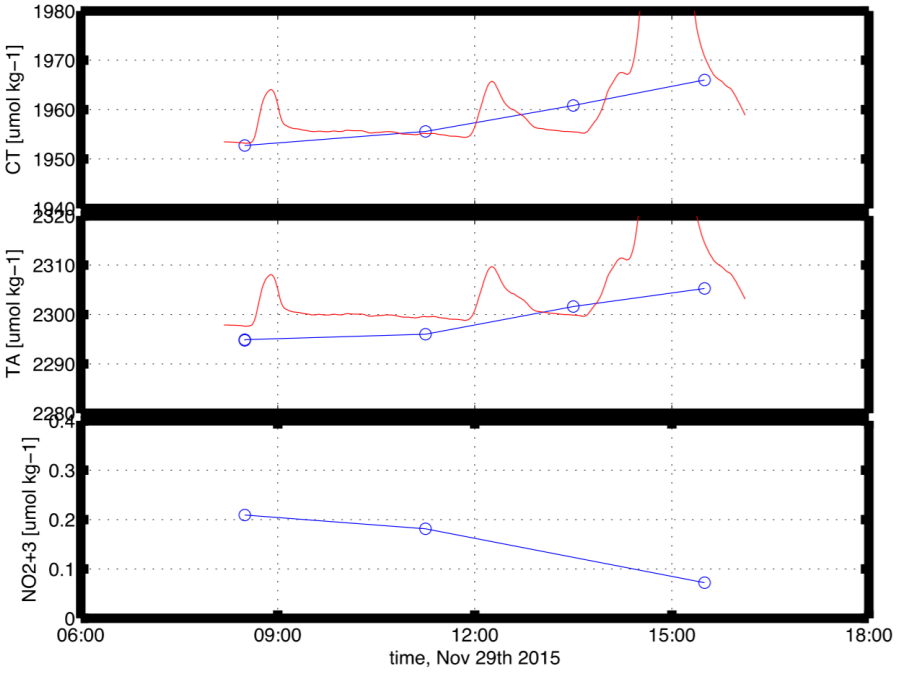

Figure S 4: Example of results of the 'Monte Carlo' method used to assess robustness of inferred time rates of change of concentrations during incubation. Data from secondary 'pyramid' incubator, placed on bare sediment. The observed trends are the result of the (unknown) balance between (i) exchange with the environment and (ii) sedimentary processes. Irrespective of dominant process, sedimentary fluxes are inferred to be negligibly low compared to those observed in the primary incubator (see main text).


SCIENTIFIC RESEARCH
IN PROGRESS
PLEASE DO
NOT DISTURB

Chapter 6

Carbonate Dissolution Mediated by Key Benthic Communities on a Degrading Coral Reef

Alice E. Webb, Didier M. de Bakker, Tamara da Costa, Steven M.A.C. van Heuven, Fleur C. van Duyl, Gert-Jan Reichart, Lennart J. de Nooijer

Abstract

The decline in living coral cover since the 1970s has inherently slowed down reef construction on a global scale. This is especially relevant for the Caribbean region and Gulf of Mexico with an estimated decrease in scleractinian coral cover up to 80% on many reefs. Present Caribbean reefs bear very little resemblance in configuration with reefs pre-1980s, in terms of benthic composition, coral cover and structural complexity. Areas covered by sand, rubble, cyanobacteria, excavating sponges, turf and macroalgae have increased at the expense of coral. Developing robust relationships between the coral reef metabolism and the benthic composition aim to facilitate meaningful predictions of how reef calcification will change in the face of ocean acidification and ocean warming. Here, benthic metabolic rates (i.e. net community calcification (NCC) and production (NCP)) are quantified in situ across five different benthic assemblages that currently characterized shallow Caribbean reef substrate. To do this, a custom made tent incubation is placed over communities dominated either by turf and macroalgae, sand, bioeroding sponges, benthic cyanobacteria mats or coral in order to determine chemical fluxes between water column and reef during day and night. Incubations yielded negative NCC rates when integrated over 24 hours for three out of the five community types tested here, indicating net dissolution. Only coral dominated substrate (∼14-35% coral cover) contributed to reef accretion but NCC rates were still found to be relatively low compared to those reported for reef flats worldwide. Integrating the NCP values over 24 hours only yielded rates skewed towards net respiration, indicating that the study site was net heterotrophic over the study period. Present results suggest that reef calcification is barely able to compensate the $CaCO_3$ losses due to dissolution from other opportunistic benthic residents.

1 Introduction

Survival and sustainability of carbonate systems, such as coral reefs, depend on the delicate balance between constructive (biomineralisation and cementation) and destructive processes (physical erosion, chemical dissolution, and bioerosion) (Hoegh-Guldberg et al., 2007; Kennedy et al., 2013). The calcium carbonate ($CaCO_3$) framework of coral reefs is produced by biogenic calcification from a range of calcifying organisms and provides numerous ecosystem services such as coastal protection and habitat provision for a large diversity of organisms (Moberg and Rönnbäck, 2003). Erosion and dissolution of the carbonate structure are achieved by abiotic forces such as waves, as well as through bioerosion by grazing fish, micro- and macroboring organisms such as endolithic bacteria and excavating sponges (Schönberg, 2008;

Guida and Garcia-Pichel, 2016). For coral reefs to persist, the rate of $CaCO_3$ production must be sufficiently greater than the rate of erosion to enable positive growth (Hoegh-Guldberg et al., 2007). However, this fine balance is ever more under pressure by global change (ocean acidification and climate change) and local stressors alike (eutrophication, overfishing) (Koop et al., 2001; Langdon and Atkinson, 2005; Andersson and Gledhill, 2013). In recent decades, the functioning of coral reefs worldwide changed drastically owing to shifts in community structure with declines in coral cover and increases in turf and fleshy macroalgae (De'ath et al., 2012; Chen et al., 2015). This is especially relevant for the Caribbean region and Gulf of Mexico with an estimated decrease in scleractinian coral cover up to 80% on many reefs (Gardner et al., 2003; Jackson et al., 2014). Present Caribbean reefs bear very little resemblance in configuration with reefs pre-1980s, in terms of benthic composition, coral cover and structural complexity (Alvarez-Filip et al., 2009; De Bakker et al., 2016; De Bakker et al., 2017). Areas covered by sand, rubble, cyanobacteria, excavating sponges, turf and macroalgae have increased at the expense of coral. Shifts from calcifying to opportunistic non-calcifying organisms on reefs, increase in substrates available for colonization by excavating euendolithic organisms and boring sponges, as well as the recognised impacts of ongoing ocean acidification and eutrophication on calcification and bioerosion processes (Webb et al., 2017; Schönberg et al., 2017; Webb et al., 2019), might tip the balance from a growing reef to a reef in a state of net loss. In-situ benthic metabolic rate measurements, i.e. net community calcification (NCC) and net community production (NCP), are used as important indicators of reef status (Koweek et al., 2015). Understanding how the integrated coral reef metabolism will change in response to changes in the composition of the benthos, as well as ocean warming and acidification is critical because it relates to a reef's ability to accrete $CaCO_3$.

Field-based studies relating community metabolism and chemical fluxes to benthic community composition and environmental conditions (e.g. temperature, light, hydrodynamics and nutrients) are necessary to predict the response of calcification and production on reefs to ongoing climate change. Direct approaches to accurately quantify reef metabolic processes are based on determining chemical fluxes between water column and reef (Smith et al., 1975). For reefs in environments characterized by a relatively linear flow of water over the reef, the upstream/ downstream method can be employed (Shaw et al., 2014; Koweek et al., 2015; Albright et al., 2016). For less unidirectional flow regimes, estimates based on overall residence time and quantification of offshore biochemical and hydrological conditions is necessary (Courtney et al., 2016). In environments where low turbulence allows buildup of appreciable chemical vertical gradients, net fluxes (of e.g. nutrients) can be calculated (McGillis

et al., 2011; Takeshita et al., 2016). For fully exposed reefs, where no detectable accumulation may occur even in the boundary layer, incubation of communities is the only way to quantify the fluxes of compounds into and out of the overlying water.

In the present study, benthic metabolic rates are quantified in situ across five different benthic assemblages that currently characterized shallow Caribbean reef substrate. To do this, a custom made tent incubator is placed over communities dominated either by turf and macroalgae, sand, bioeroding sponges, benthic cyanobacteria mats or coral in order to determine chemical fluxes between water column and reef during day and night. Incubations were carried out on the leeward side of Curaçao close to the entrance to Piscadera Bay (12°07'16.3"N 68°58'13.2"W). The water within this basin is characterised by being very turbid and eutrophied due to terrestrial runoffs including those of an ineffective waste water treatment plant. Sediment plumes transporting high concentrations of nitrate, ammonium and phosphate near the shore fringing reef at the outlet of Piscadera Bay are commonly encountered after a period of heavy rainfall (Den Haan et al., 2016). The shallow reef flat nearby the entrance of this bay is characterised by rubble and patchy distribution of small coral heads making this location particularly suitable for the deployment of tent incubations.

2 Materials and methods

2.1 Study Site

Reef incubations were carried out on the leeward side of Curaçao (Piscadera bay; 12°07'16.3"N 68°58'13.2"W) between February 12th and March 22th 2018, at depths ranging from 5 to 7 meters.

2.2 Tent Incubations

The incubation enclosure consists of custom made, tetrahedron-shaped "tent" (figure 1). It has transparent, vinyl-and-butanyl walls with rigid edges of 1 m, resembling the cBIT described by Haas et al. (2013). It also includes 0.5 m long flaps extending outward from each of the tent's three sides, allowing for proper sealing of the tent to the substrate by placing weights on the flaps. It covers a 0.43 m^2 planar surface, and encloses a 118 L volume. All three sides of the tent contained an opening to allow flushing of the enclosed volume between incubations: during incubations this opening was sealed. Water enclosed in the incubation tent was homogenized during the experiment by means of a continuously running brushless submergible water pump (BLDC pump Co., Ltd.). This pump was attached to one of the tent poles, at half the height of the tent, generating a vertical circulating turbulence, while minimizing

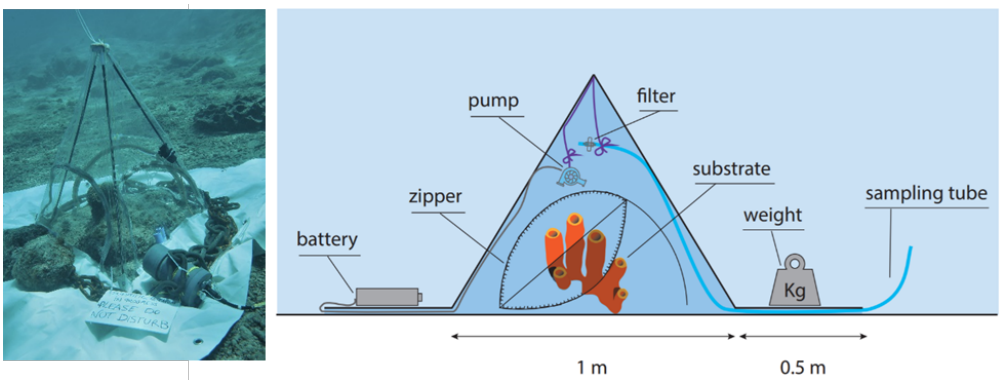

Figure 1: Illustration of the tent incubation setup used. (Left) Photograph depicting the tent incubation during the experiments. (Right) Schematic cross section of the employed setup for enclosing a small patch of coral reef. A battery powered mixing propeller for maintaining water circulation, and analyzers for salinity (S), temperature (T), oxygen (O_2), and light (PAR) are located inside the tent. External to the enclosure another S/T and PAR analyzer are located, as well as the battery for the pump. Sampling of exterior and interior water (though sampling tube) was performed by divers using large volume syringes. Zippers allow for opening of tent windows for re-equilibrating the interior to the exterior conditions between incubations.

stirring up of sediment. Effectiveness of the stirring was demonstrated by rapid and even dispersal of a small dose of injected fluorescein prior to the incubation. Surge movement was retained due to the non-rigid texture of the tent walls. Five different types of substrate dominated either by turf and macroalgae, sand, bioeroding sponges, benthic cyanobacteria mats or coral (figure 2) were incubated both during daytime (in triplicates) and at nighttime (in duplicates) for 4 hours each.

2.3 Substrate composition

Substrates dominated by either, turf and macroalgae (TMA), sand, cyanobacteria mats (BCM), bioeroding sponges (BES), or coral were incubated (Figure 2). Three reef patches of each reef assemblage were chosen depending on their dominant benthic component. Incubated substrate included hard substrate (except for sand incubations) surrounded by sand for better enclosure deployment. For substrates dominated by coral, coral cover of the hard substrate incubated ranged from 14 to 35%. Turf and macroalgae cover was between 79 to 94%, bioeroding sponge cover varied from 49 to 55%, and cyanobacterial mats cover ranged from 81 to 90% (see detailed substrate composition in supplements table S1).

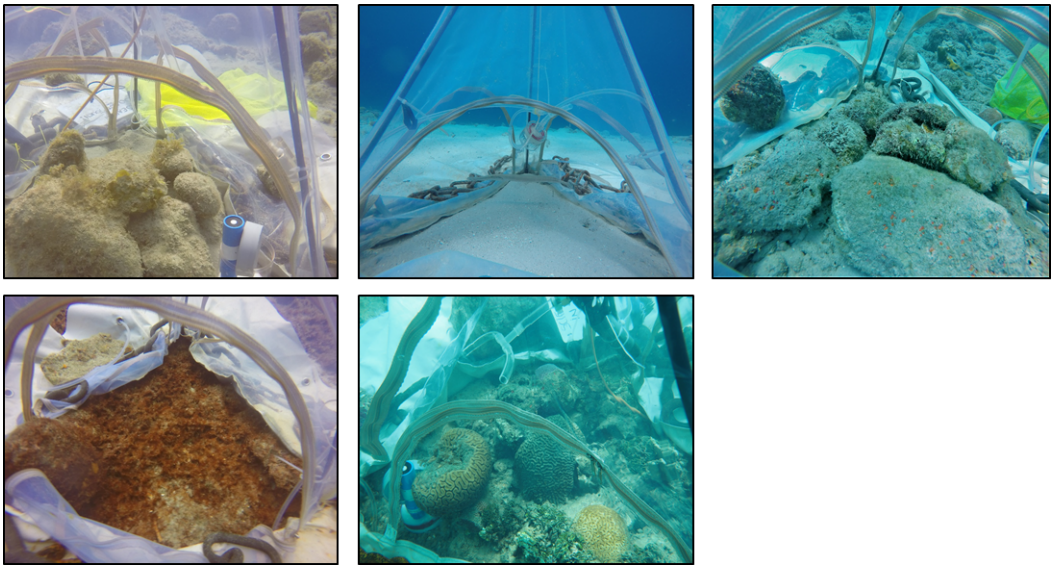

Figure 2: Photographs depicting one of the replicates for each of the targeted substrate types. From left to right, TMA, SAND, BES, BCM and CORAL.

2.4 In situ measurements

Measurements of salinity (S), temperature (T), dissolved oxygen (O_2) and photosynthetically active radiation (PAR) within the tent were recorded at 1 min intervals throughout the duration of the incubations. S and T were measured using a Star-Oddi DST CTD, O_2 was recorded using a HOBO U26 dissolved oxygen data logger and PAR was assessed by an Odyssey light logger (Dataflow Systems PTY Ltd., Christchurch, NZ), calibrated in air against Walz instrument (Walz ULM500, Walz GmbH, Effeltrich, Germany). In addition, S, T and PAR were measured for the duration of the incubations outside the tent using the same sampling frenquency. All instruments within the tent were attached to the 3 ridges except the Odyssey logger which was placed on the substrate facing upwards (covering approximately 150 cm^2 of the substrate).

2.5 Discrete sampling

During each incubation, discrete samples both inside and outside the tent were collected at T_0, T_2 and T_4 by scuba diving for the analyses of total alkalinity (A_T), total inorganic carbon (C_T) and nutrients. Sampling of the tent interior was carried out from the outside by drawing seawater through 150 ml plastic syringes connected

to a 1.5 m gas-impermeable tube (tygon). Syringes were flushed three times with the sampling water before collecting an actual sample. The tubing was fixed around a rigid edge of the tent in such way that the seawater was sampled from the center of the tent incubation. The tube end located inside the tent was equipped with a Whatman® filter (G/F 0.47 µm). Analyses for AT were performed within 2 hours upon sampling using spectrophotometrically guided single-step acid titration (Liu et al., 2015). Samples for dissolved inorganic macronutrients (NO_2+NO_3, NO_2, PO_4 and NH_4) were prepared by dispensing sampled water through 0.8/0.2 µm Acrodisk filters into 5 mL pony vials, and subsequently stored at -20˚C until analysis at NIOZ on a QuAAtro continuous flow analyser (SEAL Analytical, GmbH, Norderstedt, Germany) following GO-SHIP protocol (Hydes et al., 2010).

2.6 Rates of water exchange

After sampling water at T_0 for A_T, C_T and nutrients, 450 ml of water saturated in salt was injected into the tent. The rate at which the elevated interior salinity decreases towards ambient salinity during the incubation is used to estimate the rate of water exchange with the surrounding sea water for each incubation. Interior salinity at any given time is estimated to be as follow:

$$S(t) = b + (S_0\text{-}b) * e^{-f/t} \qquad (1)$$

Where b is the average background salinity and S0 is the max salinity inside the tent, i.e. the initial interior salinity, f the water exchange rate.
We perform an exponential fit through in-tent salinity measurements. This provides the decay rate f which is then converted to liters per minute by multiplying f with the volume of the tent.

2.7 Rate of variable input

Accordingly we calculating the rate of exchange of water f between the interior of the tent and the ambient environment for each tent. Subsequently we determined the constant time rate of substance input R (in µmol kg^{-1} hr^{-1}) that best explains the observed changes of concentration Cin inside the enclosure while accounting for constant exchange with the environment. This is performed through Equation (2).

$$C_{in}=R/(f\ )+C_{out}+(\ C_0\text{-}\ R/(f\ )\text{-}C_{out}\ )\ e^{-ft} \qquad (2)$$

Where C_{in} is the concentration inside the tent, C_{out} is the ambient concentration, C_0 is the initial in-tent input concentration f is the rate of exchange of water between the inside of the tent and the ambient environment and R, the variable input rate.

2.8 A_T and C_T correction

Release of nutrients during respiration decreases A_T (or increases A_T for release of NH_4^+), confounding the interpretation of changes in A_T to represent $CaCO_3$ dissolution only. Following common protocol, we correct measured A_T for nutrient release as follows:

$$A_T{}^{obsNC} = A_T{}^{obs} + PO_4 + NO_3 - NH_4. \quad (3)$$

Throughout the remainder of the manuscript, A_T equals $A_T{}^{obsNC}$ as defined above. Subsequently, the contributions of $CaCO_3$ dissolution or precipitation (net community calcification) and net respiration to the observed concentrations (or fluxes) of A_T and C_T were calculated:

$\Delta A_T{}^{diss} = \Delta A_T{}^{obscNC}$ ..... change in A_T due to diss. or calc.
$\Delta A_T{}^{resp} = 0$ ..... change in A_T due to resp. or photo.
$\Delta C_T{}^{diss} = \Delta A_T{}^{obscNC}/2$ ..... change in C_T due to diss. or calc.
$\Delta C_T{}^{resp} = \Delta C_T{}^{obsc} - \Delta C_T{}^{diss}$ ..... change in C_T due to resp. or photo.

2.9 Conversion to fluxes

The input rates R (in µmol kg^{-1} hr^{-1}) in the tent are converted to fluxes from the water-substrate interface (mmol m^{-2} hr^{-1}), assuming an enclosed mass of water of 108 $\sim$ 10 kg (tent encloses approximately 118 liters of volume; of which substrate volume is $\sim$10 L; seawater density $\sim$1022 kg m^{-3}) and an incubated planar surface of 0.43 m^2.

Net community calcification (NCC) rates were determined using $\Delta A_T{}^{diss}$. This technique captures only net calcification and/or dissolution and does not distinguish the relative contributions of gross calcification and dissolution to the integrated NCC rate. Net community production (NCP) was calculated from the change in C_T corrected for changes in alkalinity, i.e., from $\Delta C_T{}^{resp}$, as explained above.

3 Results

In-tent light and temperature were only slightly impacted by the tent enclosure compared to the exterior (Figure 3). Light was on average 17% lower inside the tent and changes in temperature were dampened within the tent. In-tent temperatures were 0.2°C higher on average than those outside the tent.

Application of Equation (1) to salinity data collected during all incubations yields leak rates of the enclosure f ranging between 0.004 and 0.045 min^{-1}. This indicates that 0.5 to 4.9 kg of seawater (i.e., $f \times 108$ kg) is exchanged every minute between the incubation enclosure and the environment. These rates correspond to the intensity of the water movement observed and recorded visually at the time of each incubation. Figure 4 shows the data used to estimate the rate of water exchange of a relatively

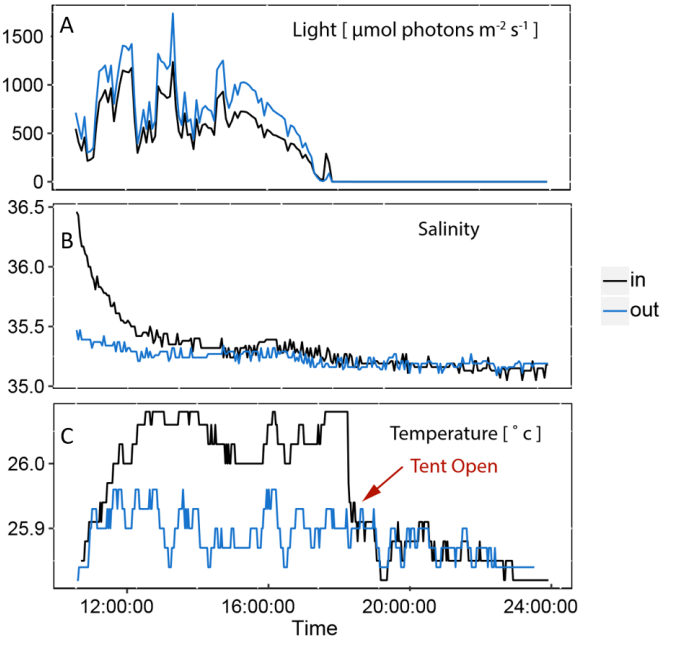

Figure 3: Exterior and interior light (µmol photons m^2 s^{-1}), salinity and temperature (°C) for 3 representative incubations performed throughout this study. (A) difference in light between the inside of the tent and the ambient environment. (B) injection of salt within the tent at the start of the incubation and its gradual return to ambient salinity. (C) temperature within the tent compared to exterior conditions, when the tent is opened at the end of the incubation, temperature immediately matches ambient conditions.

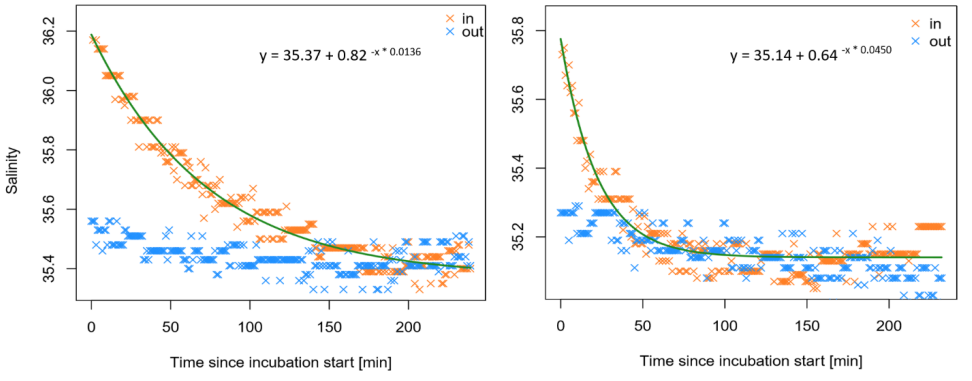

Figure 4: (A, B) Best fit explaining in-tent salinity at any given time (equation 1, green line). In-tent salinity measurements are in orange and ambient salinity measurements are in blue. A) illustrates an incubation that leaked relatively slowly with f = 0.0136 (0.0136 * 108 = 1.5 liters per minute), while B) depicts a more rapidly leaking tent with f = 0.0450 (0.0450 × 108 = 4.9 liters per minute).

slow leaking tent (A) and a fast leaking tent (B). In these examples, in-tent salinity returns to ambient concentrations after ∼1 and ∼2 hours respectively. The slopes f = 0.0136 and f = 0.0450 indicate that these particular tents leaked at a rate of 1.5 to 4.9 kg of seawater per minute.

Graphic results for the model employed (Equation) to infer average A_T, $C_T{}^{resp}$ and O_2 in-tent fluxes are presented in figures 5, 6 and 7 respectively. Values of A_T were adjusted to account for the release of nutrients during respiration according to equation (3). A clear diurnal signal resides in A_T fluxes for all substrates involved (Figure 5). The decrease in A_T for incubations with substrates dominated by coral, bioeroding sponges, BCMs and TMA during the day, indicates net $CaCO_3$ precipitation. At night, BES and BCMs dominated substrates, show clear net $CaCO_3$ dissolution. Slight A_T increases in incubations with sand and TMA incubations suggest modest net dissolution at night. The absence of A_T signal for coral dominated substrates during the night demonstrates that dissolution processes compensate calcification during these incubations. Substrates dominated by coral generated the fastest drop in A_T (net precipitation) during daytime yielding NCC rates ranging from 0.25 to 0.44 mmol $CaCO_3$ m^2 h^{-1}. Highest increase in A_T (net dissolution) was found at nighttime for incubations of substrate dominated by bioeroding sponges, ranging from -0.24 to -0.45 mmol $CaCO_3$ m^2 h^{-1}. These were closely followed by incubations of BCMs, also at night, ranging from -0.16 to -0.30 mmol $CaCO_3$ m^2 h^{-1}. All average fluxes and respective 95% confidence intervals are listed in table 1.

$C_T{}^{resp}$ fluxes also show a clear diurnal pattern (Figure 6). While all NCP values are modestly skewed towards net autotrophy during the day, the strongest signal is found for substrates dominated by BCMs ranging from -8.9 to 6.7 mmol m^{-2} h^{-1}. All night NCP values indicate net respiration ranging from an average of 2.4 mmol m^{-2} h^{-1} on substrates dominated by TMA to 22.3 mmol m^{-2} h^{-2} on substrates dominated by bioeroding sponges. Concomitant increases of C_T, PO_4 and NO_{2+3} during the night are in line with respiration dominating throughout all incubations (Table 1). The $C_T{}^{resp}$ fluxes correspond well with in-tent oxygen concentrations increasing only slightly during the day on all substrate type, except for substrate dominated by BCMs where a clear signal for O_2 production is recorded (9.9 to 11 mmol m^{-2} h^{-1}). During the night, all signals are skewed towards net respiration (Figure 6) ranging from -30.7 mmol m^{-2} h^{-1} (95% ci = -37.0; -24.4) on substrates dominated by bioeroding sponges to -5.78 mmol m^{-2} h^{-1} (95% ci = -6.3; -5.3) on sand substrates.

Nutrient measurements indicated net NO_x, NO_2, PO_4 and NH_4 release in most incubations (table 2) except in communities dominated by turf and macroalgae and sand where NO_x uptake was recorded during the day and the night. Communities dominated by BCM have the largest nutrient effluxes, especially at night and NH_4.

Table 1: Summary of average net community calcification, net respiration and net community production fluxes in benthic communities with respective 95% confidence interval inferred from observed concentration changes in the tent enclosure on every substrate and during all incubation periods.

Substrate	NCC			Net Respiration			NCP		
	mean	lowerCI	upperCI	mean	lowerCI	upperCI	mean	lowerCI	upperCI
TMA	0.10	0.08	0.12	-0.30	-0.51	-0.10	0.41	0.41	0.41
	-0.06	-0.09	-0.03	0.43	0.35	0.51	-0.85	-0.86	-0.84
SAND	-0.004	-0.009	0.001	-0.14	-0.26	-0.03	-0.04	-0.05	-0.04
	-0.02	-0.04	0.00	0.67	0.56	0.77	-0.82	-0.82	-0.82
BES	0.25	0.19	0.30	-0.14	-0.51	0.22	0.13	0.09	0.17
	-0.34	-0.44	-0.25	3.60	3.13	4.08	-5.71	-5.93	-5.49
BCM	0.14	0.13	0.16	-1.34	-1.60	-1.09	1.65	1.64	1.67
	-0.23	-0.29	-0.16	3.00	2.45	3.54	-3.20	-3.28	-3.13
CORAL	0.37	0.32	0.43	-0.61	-0.92	-0.30	0.31	0.30	0.33
	0.002	-0.005	0.009	1.34	1.14	1.54	-2.52	-2.52	-2.51

[1] White cells show day fluxes, while grey cells depict night fluxes.
[2] NCC values are in mmol $CaCO_3$ m^{-2} h^{-1}, Net Respiration values are in mmol $C_T{}^{resp}$ m^{-2} h^{-1}) and NCP values are in mmol O_2 m^{-2} h^{-1}.

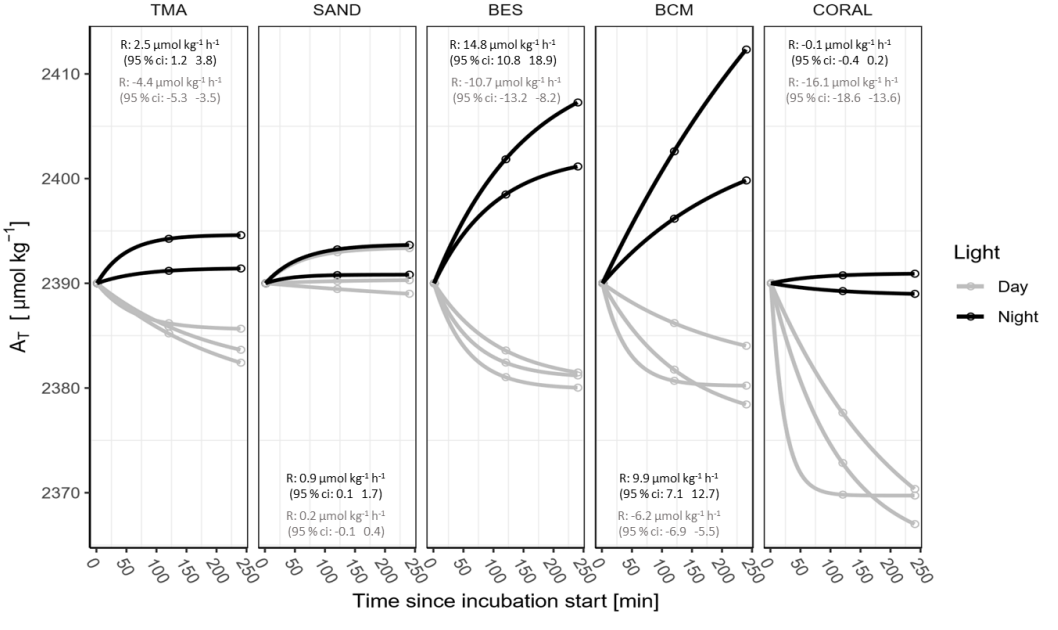

Figure 5: Results of the model employed (equation 3) to infer every A_T input rates (µmol kg^{-1} h^{-1}) from observations for each substrate recorded during the day (grey) and at night (black). Circles represent discrete A_T values measured at T_0, T_2 and T_4. Average rates and respective 95% confidence interval are depicted for each substrate and light.

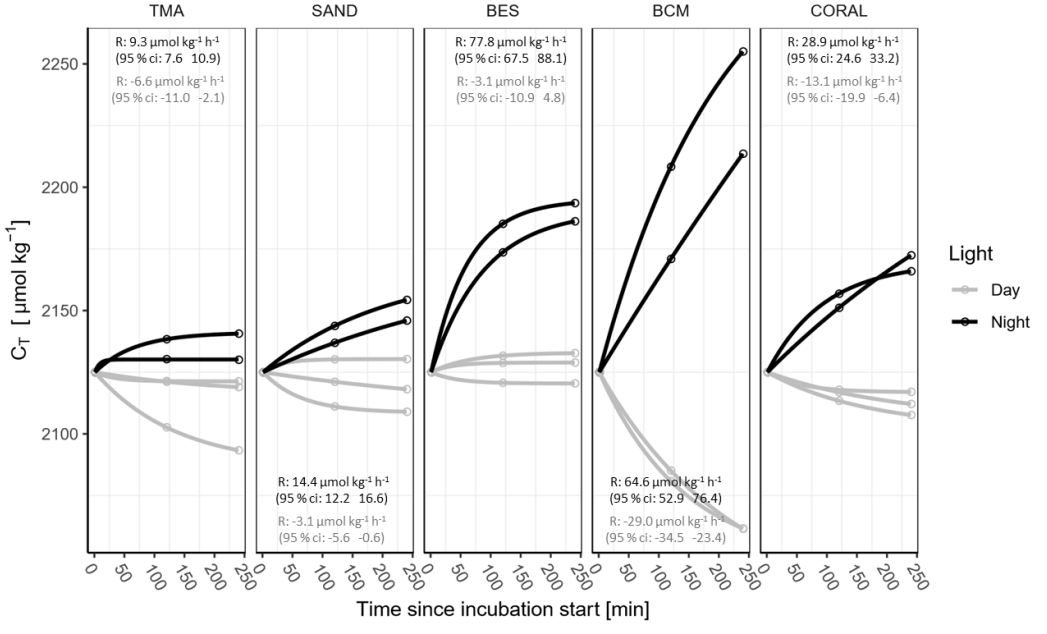

Figure 6: Results of the model employed (equation 3) to infer every $C_T{}^{resp}$ input rates (µmol kg^{-1} h^{-1}) from observations for each substrate recorded during the day (grey) and at night (black). Circles represent discrete $C_T{}^{resp}$ values measured at T_0, T_2 and T_4. Average rates and respective 95% confidence interval are depicted for each substrate and light.

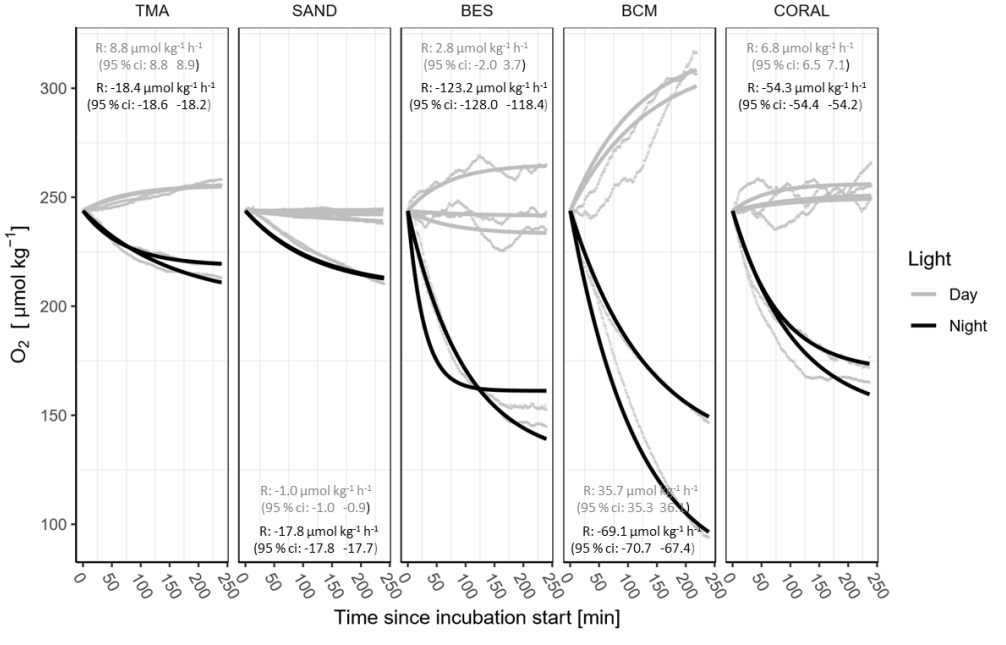

Figure 7: Results of the model employed (equation 3) to infer every O_2 input rates (µmol kg^{-1} h^{-1}) from observations for each substrate recorded during the day (grey) and at night (black). Small grey points represent continous O_2 values measured throughout each incubation. Average rates and respective 95% confidence interval are depicted for each substrate and light.

Table 2: Average nutrient fluxes in benthic communities with respective 95% confidence interval inferred from observed concentration changes in the tent enclosure on every substrate and during all incubation periods.

Substrate	PO_4			NO_2			NO_{3+2}			NH_4		
	mean	lowerCI	upperCI	mean	lowerCI	upperCI	mean	lowerCI	upperCI	mean	lowerCI	upperCI
TMA	0.000	0.000	0.000	0.002	-0.002	0.006	-0.002	-0.003	0.000	0.003	0.000	0.006
	0.000	0.000	0.000	0.000	0.000	0.001	-0.003	-0.004	-0.002	0.002	-0.004	0.008
SAND	0.001	0.001	0.001	-0.001	-0.001	0.000	-0.003	-0.003	-0.002	0.000	0.000	0.001
	0.002	0.001	0.002	0.000	0.000	0.000	-0.008	-0.013	-0.004	0.007	0.004	0.00
BES	0.001	0.001	0.002	0.002	0.001	0.002	0.009	0.005	0.012	0.008	0.004	0.011
	0.003	0.003	0.003	0.004	0.002	0.006	0.018	0.012	0.024	0.013	0.004	0.021
BCM	0.001	0.001	0.002	0.004	0.003	0.005	0.046	0.035	0.057	0.016	0.003	0.029
	0.003	0.001	0.005	0.006	0.004	0.008	0.067	0.042	0.092	0.084	0.022	0.145
CORAL	0.002	0.002	0.003	0.003	0.002	0.003	0.033	0.029	0.036	0.003	0.000	0.007
	0.004	0.001	0.006	0.004	0.003	0.005	0.044	0.017	0.071	0.011	0.006	0.016

[1] Positive values represent net release by the benthic community and negative values, net uptake.
[2] White cells show day fluxes, while grey cells depict night fluxes.
[3] All fluxes are in mmol m^{-2} h^{-1}.

4 Discussion

4.1 Net dissolution and calcification rates

At an NCC of 0, a reef is poised between net accretion and erosion (McMahon et al., 2013). The present incubations yielded negative NCC rates for three out of the five community types tested here, indicating net dissolution (integrating day and night dissolution rates; table 3). For two out of these three communities (bioeroding sponges and cyanobacterial mates), daytime NCC rates were positive, but not high enough to compensate for the $CaCO_3$ dissolution at night (table 1 and 3). It should be noted that NCC diurnal dynamics are more complex than assumed here (McMahon et al., 2013; Koweek et al., 2015; Shaw et al., 2015). Our approach does not allow for quantifying short-term fluctuations and although NCC values do not vary substantially during dark hours, a slight overestimation of daytime NCC in the present study might be expected as dawn and dusk NCC rates are expected to be depressed due to low light intensities. Substrates dominated by turf and macroalgae and coral are the only two community types that contribute to net accretion of the reef (considering their signal over 24 h) with average NCC rates of 0.3 mmol $CaCO_3$ m^{-2} $24h^{-1}$ (95% ci = -0.3; 0.9) and 4.1 mmol $CaCO_3$ m^{-2} $24h^{-1}$ (95% ci = 2.6; 5.7) respectively.

NCC rates for coral dominated substrates are lower than those reported for reef flats worldwide (ranging from 20 to 250 mmol $CaCO_3$ m^{-2} $24h^{-1}$, with an average of 130 mmol $CaCO_3$ m^{-2} $24h^{-1}$) (Atkinson, 2011). Incubations of Floridian and Hawaiian patch reefs (10-22% coral cover) yielded higher but comparable NCC averages (11.2 mmol CaCO3 m^{-2} $24h^{-1}$)(Yates and Halley, 2003) although the coral cover incubated was on average slightly higher in the present study (14-35%). Overall, most in-situ coral reefs' NCC values recorded elsewhere (Albright et al., 2015; Shaw et al., 2015; Silverman et al., 2007) are significantly higher, especially in the Indo-Pacific (Koweek et al., 2015; Takeshita et al., 2016).

The very few in situ flux-based experiments carried out on Caribbean reefs suggest they exhibit among the lowest NCC rates worldwide (Yates and Halley, 2003; Muehllehner et al., 2016; van Heuven et al., 2018). Cyronak et al. (2018) estimated semi-quantitatively the NCC potential of 23 coral reef locations worldwide and reported that events of net dissolution mainly occurred at night coinciding with net respiration, high CO_2 concentrations, and low rate of gross calcification. They also occurred on a seasonal basis during winter months on coral reefs in both Florida and Bermuda (Bates et al., 2010; Muehllehner et al., 2016). Relatively low NCC rates for communities dominated by coral in the present study may be due to the experiment being carried out in Caribbean winter months, although local reef conditions. (Lapointe and Mallin, 2011; Den Haan et al., 2016) are also likely to impact calcification.

This said, more pristine environments within the Caribbean are also characterized by relatively low NCC (van Heuven et al., 2018; Yates and Halley, 2003), indicating that Caribbean reefs in general are the slow growing counterparts of the Indo-Pacific reefs.

4.2 Diurnal metabolic variability

A strong correlation between NCC and net community productivity in reef environments is well documented with light and benthic composition being the primary drivers for the variability observed between metabolic rates (Silverman et al., 2007; Albright et al., 2015; Koweek et al., 2015; Shaw et al., 2015). Here, net community dissolution and negative NCP rates are tightly coupled, however, net productivity is less obviously coupled with net calcification (figure 5 and 7). During daytime, all substrates except the bare sand were characterized by net calcification (table 1). However, dissolution exceeded calcification during dark hours on most substrates except those dominated by coral and TMA. On assemblages dominated by bioeroding sponges, hard coral cover varied from 3.9 to 6.7% (Table S1) and appeared to be sufficient to compensate for net dissolution by sponges during the day. However, such low coral cover, which is on the lower end but still representative of shallow Caribbean reefs (Jackson et al., 2014; De Bakker et al., 2016), results in overall NCC rates skewed towards net dissolution when integrated over 24 hours.

Modest calcification signals are also recorded during the day for substrates where no major calcifiers were observed, i.e. for TMA and BCMs dominated communities. However, presence of coralline calcifying algae (CCA), as well as all kind of micro calcifyers such as foraminifera and juvenile shells residing in the rubble of each incubation cannot be excluded and may account for part of the observed calcification. This suggests that cementation/lithification processes carried out by CCA and benthic microbial community trapping and binding rubble and sediment may continue in cryptic habitats and within/on the rubble, even on such impacted coral reefs, counteracting some of the dissolution in these communities and stabilising coral rubble into a consolidated reef framework.

Average daytime NCP rates are characterised by low values for most community types (except BCMs) indicating that autotrophic processes are hardly dominating during the day. Integrating the NCP values over 24 hours (day + night) yielded rates skewed towards net respiration, indicating heterotrophy in all incubations. Differences between net respiration and O_2 consumption, mostly at night, suggest that respiration is not the only process taking up O_2 at night time (table 1). Re-oxidation of reduced compounds may be taking place during the night. For instance, efflux of nitrate from communities dominated by BCMs, BES and corals suggest that nitrification is occurring in these communities.

Although net community production of reef flats has been reported to vary greatly over the course of the day (Koweek et al., 2015), with values ranging from -220 to 310 mmol C m^{-2} $24h^{-1}$ (Atkinson, 2011), significant shifts between net autotrophy and net heterotrophy are usually recorded between day and night (Yates and Halley, 2003; Albright et al., 2013,0; Koweek et al., 2015). Integrating the NCP values over 24 hours yielded rates skewed towards net respiration, indicating that the study site was net heterotrophic over the study period. The net efflux of inorganic nutrients and respiration of communities with exception of sand attest to the dominance of heterotrophic processes during the day and the night on these reefs. This is in contrast with other studies, although tent incubations at greater water depth (20m) off the island Saba also recorded NCP rates skewed towards net respirations (van Heuven et al., 2018). Furthermore evidences of seasonal heterotrophy were recorded analogous to seasonal reef dissolution in Florida and Bermuda (Bates et al., 2010; Muehllehner et al., 2016). These results may suggest that most reefs in the Caribbean basin undergo seasonal heterotrophic events which has severe implications for the future of this system. This can potentially be ascribed to the combination of lower light intensities during winter (cloud cover) and overall increase in local pressures on the environment associated with the unprecedented expansion of the population locally. The total population of the Caribbean has more than double in the last 50 years (Guzman et al., 2006), causing a significant increase in terrestrial runoff especially due to untreated waste water. This is exacerbated by the basin-like morphological and hydrological features that promote retention of polluted and eutrophied water within the Caribbean basin (Roff and Mumby, 2012).

4.3 Comparison with census based data approach

As most NCC values already recorded in the Caribbean were largely estimated using the *ReefBudget* approach (Perry et al., 2012,0), this method was also applied to the benthic census data of the patches studied here. Obtained *ReefBudget* results yielded significantly different from ncc measurements yielded here. The yearly $NCC_{ReefBudget}$ estimates range from -1175.6 g $CaCO_3$ m^{-2} yr^{-1} (95% ci = -1445.5; -905.8) for substrates dominated by bioeroding sponges, to 1437.5 g $CaCO_3$ m^{-2} yr^{-1} (95% ci = 484.3; 2390.6) for coral dominated communities. The average yearly NCC_{Flux} values range from -38.4 (95% ci = -43.4; -33.5) g to 150.8 (95% ci = 95.3; 206.3) g $CaCO_3$ m^{-2} yr^{-1} for communities dominated by bioeroding sponges and coral respectively. It should be noted that the flux-based method, unlike the *Reefbudget* method, does not encompass the mechanical component of bioerosion (caused by sponges or parrot fish for instance), however this is unlikely to cover such discrepancies.

The *ReefBudget* approach is based on biotic abundance and coral calcification

Table 3: Average nutrient fluxes in benthic communities with respective 95% confidence interval inferred from observed concentration changes in the tent enclosure on every substrate and during all incubation periods.

Substrate	NCC [$_{flux}$ mmol $CaCO_3$ m^{-2} $24h^{-1}$]			NCC_{budget} [mmol $CaCO_3$ m^{-2} $24h^{-1}$]		
	mean	lowerCI	upperCI	mean	lowerCI	upperCI
TMA	0.3	-0.3	0.9	-4.9	-5.7	-4.0
SAND	-0.2	-0.6	0.2	0.0	0.0	0.0
BCM	-0.9	-1.9	0.0	-6.7	-6.9	-6.5
BES	-1.1	-1.2	-0.9	-32.2	-39.6	-24.8
CORAL	4.1	2.6	5.7	39.4	13.3	65.5
Substrate	NCC_{flux} [g $CaCO_3$ m^{-2} yr^{-1}]			NCC_{budget} [g $CaCO_3$ m^{-2} yr^{-1}]		
	mean	lowerCI	upperCI	mean	lowerCI	upperCI
TMA	10.1	-11.8	31.9	-178.2	-208.9	-147.5
SAND	-8.4	-22.9	6.1	0.0	0.0	0.0
BCM	-34.6	-68.6	-0.5	-244.9	-252.0	-237.8
BES	-38.4	-43.4	-33.5	-1175.6	-1445.3	-905.8
CORAL	150.8	95.3	206.3	1437.5	484.3	2390.6

rates obtained from literature (Perry et al., 2012). It offers a fast and convenient tool to estimate reef biogenic carbonate production states both on a large temporal and spatial scale but it does not capture the actual processes and hence the state of the various substrate assemblages. Significant short or long term variability in production or calcification may occur depending on the water condition or the season. Here, the studied reef suffers from the vicinity of numerous holiday houses and the proximity to the outlet of the inefficient waste water plant and the coral condition, including their ability to calcify, is likely to be impacted. As the flux-based method assesses the full community without having to determine calcification/dissolution rates as a function of surface area, it can be useful to estimate the effect of endolithic species (microbioerosion) or determine the impact that some understudied organism or substrate may have on the chemical conditions. Sand, for instance, has been shown to contribute to net community calcification. Recent studies have shown that dissolving calcium carbonate sands could greatly exacerbate reef loss associated with reduced calcification (Andersson, 2015; Fink et al., 2017; Eyre et al., 2018). This is because they act as the cement of the reef whereby accumulating in cracks and crevices and starting to glue together due to microbial activity which in turns forms substrate.

Benthic cyanobacterial mats, are shown here to impact the chemical conditions of the overlying water. As BCMs have been shown to proliferate around the islands

of Curaçao and Bonaire since 2003 (De Bakker et al., 2017), there is a necessity to account for these in carbonate budgets. At night, average NCC rates on substrates dominated by BCMs all exhibit net dissolution with rates comparable to fluxes associated to substrate dominated by bioeroding sponges. Dissolution is likely achieved by very local alteration of carbonate chemistry due to heavy respiration decreasing ΩAr below 1 and (Brocke et al., 2015a). Research on how BCMs alter the biogeochemical environment is sparse, although benthic primary producers can significantly alter key biogeochemical parameters in their surroundings via basic physiological processes. They appear to be facilitated by environmental conditions associated with anthropogenic impact such as eutrophication (Brocke et al., 2015b). BCMs, in turn, generate positive feedback for eutrophication as they release part of their photosynthetically fixed carbon as DOC into the water column at a higher rate than benthic algae (turf and macroalgae)(Mueller et al., 2014; Brocke et al., 2015b). Increased DOC release is reported at night, most likely as a result of anaerobic metabolism and degradation processes (Brocke et al., 2015a). Changes in their abundance can therefore significantly alter the quantity and chemical composition of organic materials supplied to the reef environment.

Conclusions

Community scale in-situ experiments using incubations, lagrangian drifts and boundary layer approaches, when local conditions allow it, provide valuable insight into benthic community metabolism. Unlike most previous cited research, the current study focuses on a system heavily influenced by human perturbation which has already undergone severe benthic composition shifts. Being able to integrate metabolic rates across different temporal and spatial scales is critical to understand how coral reefs as a whole respond to current and ongoing local and global environmental perturbations, such as pollution, climate change and OA. Still, additional field studies with co-located biogeochemical and ecological measurements, as well as mesocosm studies, are crucial to achieve this. These experiments will provide further insight into the competitive dynamics of coral reef ecology and significantly improve predictive capabilities for how coral reef ecosystems will respond to or potentially buffer forcing from global change. Present results indicate that reef calcification is barely able to compensate the $CaCO_3$ losses due to dissolution from other opportunistic benthic residents on this reef terrace. Considering the trajectories of change for dominant benthic groups on Curaçao and Bonaire in the past 40 years, and the ongoing global and local pressures, the delicate balance between $CaCO_3$ accretion and loss is likely to tip. The Caribbean reefs of today give an insight into tomorrow's reefs worldwide,

in which community assemblages have changed, structural complexity has lessened and waters are moving away from oligotrophy.

Acknowledgements

The authors are particularly grateful to the Carmabi research station as a whole and particularly Dr. Mark Vermeij for his support and facilitating the fieldwork on Curaçao. We also would like to thank Jasper de Goeij for lending us some equipment. We extend our sincere gratitude to Karel Bakker and Sharyn Ossebaar for analysing nutrient and DIC samples.

Supplements

Table S 1: Substrate dominant composition for each triplicate of every assemblage type.

replicates	substrate dominated by	% hard substrate	% available substrate	% coral cover	% bioeroding sponge cover	% BCM cover	% turf/ algae cover	% sand cover
1	CORAL	100	66.9	14	2.1	0	0	0
2	CORAL	89.1	82.9	17.1	0	0	2.5	10.9
3	CORAL	61.6	61.5	34.9	3.6	0	1.8	38.4
1	BES	96.7	44.8	6.7	48.5	0	1.3	3.31
2	BES	95.2	40.3	4.4	55.3	0	12.7	4.8
3	BES	94.8	30	3.9	51.6	0	15.9	5.2
1	BCM	91	100	0	0	90	0	9
2	BCM	95	100	0	0	88	0	5
3	BCM	84	100	0	0	81	0	6
1	TMA	60.6	100	0	0	0	81.3	39.4
2	TMA	71.3	100	0	0	0	79	28.7
3	TMA	62.5	100	0	0	0	93.8	37.5
1	SAND	0	0	0	0	0	0	100
2	SAND	0	0	0	0	0	0	100
3	SAND	0	0	0	0	0	0	100

[1] Hard substrate represents all substrate except sand.
[2] Available substrate represents substrate where micro-bioerosion may occur.
[3] Turf and cyanobacteria covered substrate is considered as available substrate.
[4] Percentage cover of the main dominant benthic components are a percentage of the cover of the hard substrate, not the total incubation.

Miscellaneous

References

Achlatis, M., Pernice, M., Green, K., Guagliardo, P., Kilburn, M. R., Hoegh-Guldberg, O., and Dove, S. (2018). Single-cell measurement of ammonium and bicarbonate uptake within a photosymbiotic bioeroding sponge. *ISME Journal*, 12(5):1308–1318.

Achlatis, M., Schönberg, C. H., van der Zande, R. M., LaJeunesse, T. C., Hoegh-Guldberg, O., and Dove, S. (2019). Photosynthesis by symbiotic sponges enhances their ability to erode calcium carbonate. *Journal of Experimental Marine Biology and Ecology*, 516:140–149.

Achlatis, M., Van Der Zande, R. M., Schönberg, C. H. L., Fang, J. K. H., Hoegh-Guldberg, O., and Dove, S. (2017). Sponge bioerosion on changing reefs: Ocean warming poses physiological constraints to the success of a photosymbiotic excavating sponge. *Scientific Reports*, 7(1):1–13.

Albright, R., Benthuysen, J., Cantin, N., Caldeira, K., and Anthony, K. (2015). Coral reef metabolism and carbon chemistry dynamics of a coral reef flat. *Geophysical Research Letters*, 42(10):3980–3988.

Albright, R., Caldeira, L., Hosfelt, J., Kwiatkowski, L., Maclaren, J. K., Mason, B. M., Nebuchina, Y., Ninokawa, A., Pongratz, J., Ricke, K. L., et al. (2016). Reversal of ocean acidification enhances net coral reef calcification. *Nature*, 531(7594):362.

Albright, R., Langdon, C., and Anthony, K. (2013). Dynamics of seawater carbonate chemistry, production, and calcification of a coral reef flat, central great barrier reef. *Biogeosciences*, 10(10):6747–6758.

Alevizon, W. S. and Porter, J. W. (2015). Coral loss and fish guild stability on a caribbean coral reef: 1974–2000. *Environmental Biology of Fishes*, 98(4):1035–1045.

Alvarez-Filip, L., Dulvy, N. K., Gill, J. A., Côté, I. M., and Watkinson, A. R. (2009). Flattening of Caribbean coral reefs: Region-wide declines in architectural complexity. *Proceedings of the Royal Society B: Biological Sciences*, 276(1669):3019–3025.

Alvarez-Filip, L., Gill, J. A., and Dulvy, N. K. (2011). Complex reef architecture supports more small-bodied fishes and longer food chains on caribbean reefs. *Ecosphere*, 2(10):1–17.

Andersson, A. J. (2015). A fundamental paradigm for coral reef carbonate sediment dissolution. *Frontiers in marine Science*, 2(July):1–8.

Andersson, A. J. and Gledhill, D. (2013). Ocean Acidification and Coral Reefs: Effects on Breakdown, Dissolution, and Net Ecosystem Calcification. *Annual Review of Marine Science*, 5(1):321–348.

Anthony, K. R., Kline, D. I., Diaz-Pulido, G., Dove, S., and Hoegh-Guldberg, O. (2008). Ocean acidification causes bleaching and productivity loss in coral reef builders. *Proceedings of the National Academy of Sciences*, 105(45):17442–17446.

Aronson, R. B. and Precht, W. F. (1997). Stasis, biological disturbance, and community structure of a holocene coral reef. *Paleobiology*, 23(3):326–346.

Atkinson, M. and Smith, S. (1983). C: N: P ratios of benthic marine plants 1. *Limnology and Oceanography*, 28(3):568–574.

Bagby, R. M. (1966). The fine structure of myocytes in the sponges Microciona prolifera (Ellis and Solander) and Tedania ignis (Duchassaing and Michelotti). *Journal of morphology*, 118(2):167–181.

Baker, A. C., Glynn, P. W., and Riegl, B. (2008). Climate change and coral reef bleaching: An ecological assessment of long-term impacts, recovery trends and future outlook. *Estuarine, coastal and shelf science*, 80(4):435–471.

Bates, N. R., Amat, A., and Andersson, A. J. (2010). Feedbacks and responses of coral calcification on the Bermuda reef system to seasonal changes in biological processes and ocean acidification. *Biogeosciences*, 2:2509–2530.

Björk, M., Weil, A., Semesi, S., and Beer, S. (1997). Photosynthetic utilisation of inorganic carbon by seagrasses from zanzibar, east africa. *Marine Biology*, 129(2):363–366.

Borges, A. V. and Gypens, N. (2010). Carbonate chemistry in the coastal zone responds more strongly to eutrophication than ocean acidification. *Limnology and Oceanography*, 55(1):346–353.

Brocke, H. J., Polerecky, L., De Beer, D., Weber, M., Claudet, J., and Nugues, M. M. (2015a). Organic matter degradation drives benthic cyanobacterial mat abundance on caribbean coral reefs. *PLoS One*, 10(5):e0125445.

Brocke, H. J., Wenzhoefer, F., de Beer, D., Mueller, B., van Duyl, F. C., and Nugues, M. M. (2015b). High dissolved organic carbon release by benthic cyanobacterial mats in a Caribbean reef ecosystem. *Scientific Reports*, 5(1):8852.

Bruno, J. F., Sweatman, H., Precht, W. F., Selig, E. R., and Schutte, V. G. (2009). Assessing evidence of phase shifts from coral to macroalgal dominance on coral reefs. *Ecology*, 90(6):1478–1484.

Burkepile, D. E. and Hay, M. E. (2009). Nutrient versus herbivore control of macroalgal community development and coral growth on a caribbean reef. *Marine Ecology Progress Series*, 389:71–84.

Cai, W.-J., Hu, X., Huang, W.-J., Murrell, M. C., Lehrter, J. C., Lohrenz, S. E., Chou, W.-C., Zhai, W., Hollibaugh, J. T., Wang, Y., et al. (2011). Acidification of subsurface coastal waters enhanced by eutrophication. *Nature geoscience*, 4(11):766.

Camacho, F. G., Chileh, T., García, M. C., Mirón, A. S., Belarbi, E., Gómez, A. C., and Grima, E. M. (2006). Sustained growth of explants from mediterranean sponge crambe crambe cultured in vitro with enriched rpmi 1640. *Biotechnology progress*, 22(3):781–790.

Camp, E. F., Krause, S.-L., Santos, L. M., Naumann, M. S., Kikuchi, R. K., Smith, D. J., Wild, C., and Suggett, D. J. (2015). The "flexi-chamber": a novel cost-effective in situ respirometry chamber for coral physiological measurements. *PloS one*, 10(10):e0138800.

Canadell, J. G., Le Quéré, C., Raupach, M. R., Field, C. B., Buitenhuis, E. T., Ciais, P., Conway, T. J., Gillett, N. P., Houghton, R., and Marland, G. (2007). Contributions to accelerating atmospheric co2 growth from economic activity, carbon intensity, and efficiency of natural sinks. *Proceedings of the national academy of sciences*, 104(47):18866–18870.

Carballo, J. L., Bautista-Guerrero, E., and Leyte-Morales, G. E. (2008). Boring sponges and the modeling of coral reefs in the east pacific ocean. *Marine Ecology Progress Series*, 356:113–122.

Carballo, J. L., Ovalle-Beltrán, H., Yáñez, B., Bautista-Guerrero, E., and Nava-Bravo, H. (2017). Assessment of the distribution of sponge chips in the sediment of East Pacific Ocean reefs. *Marine Ecology*, 38(1):1–11.

Cesar, H., Burke, L., and Pet-Soede, L. (2003). The economics of worldwide coral reef degradation. Technical report, Cesar environmental economics consulting (CEEC).

Chaves-Fonnegra, A. and Zea, S. (2011). Coral colonization by the encrusting excavating Caribbean sponge Cliona delitrix. *Marine Ecology*, 32(2):162–173.

Chaves-Fonnegra, A., Zea, S., and Gómez, M. L. (2007). Abundance of the excavating sponge cliona delitrix in relation to sewage discharge at san andrés island, sw caribbean, colombia. *Boletín de Investigaciones Marinas y Costeras-INVEMAR*, 36(1):63–78.

Chen, P. Y., Chen, C. C., Chu, L. F., and McCarl, B. (2015). Evaluating the economic damage of climate change on global coral reefs. *Global Environmental Change*, 30:12–20.

Chen, X.-W. and Gao, K.-S. (2004). Roles of carbonic anhydrase in photosynthesis of Skeletonema costatum. *Zhi wu sheng li yu fen zi sheng wu xue xue bao = Journal of plant physiology and molecular biology*, 30(5):511–6.

Chisholm, J. R. M. and Gattuso, J.-P. (1991). Validation of the alkalinity anomaly technique for investigating calcification of photosynthesis in coral reef communities. *Limnology and Oceanography*, 36(6):1232–1239.

Chow, M., Tsang, R. H., Lam, E. K., and Ang Jr, P. (2016). Quantifying the degree of coral bleaching using digital photographic technique. *Journal of experimental marine biology and ecology*, 479:60–68.

Clayton, T. D. and Byrne, R. H. (1993). Spectrophotometric seawater ph measurements: total hydrogen ion concentration scale calibration of m-cresol purple and at-sea results. *Deep Sea Research Part I: Oceanographic Research Papers*, 40(10):2115–2129.

Coles, S. and Brown, E. (2007). Twenty-five years of change in coral coverage on a hurricane impacted reef in hawai 'i: the importance of recruitment. *Coral Reefs*, 26(3):705–717.

Connell, J. H. (1978). Diversity in tropical rain forests and coral reefs. *Science*, 199(4335):1302–1310.

Cotte, J. (1902). Note sur le mode de perforation des Cliones. *CR Séance Soc Biol Paris*, 54:636–637.

Courtney, T. A., Andersson, A. J., Bates, N. R., Collins, A., Cyronak, T., de Putron, S. J., Eyre, B. D., Garley, R., Hochberg, E. J., Johnson, R., et al. (2016). Comparing chemistry and census-based estimates of net ecosystem calcification on a rim reef in bermuda. *Frontiers in Marine Science*, 3:181.

Cyronak, T., Andersson, A. J., Langdon, C., Albright, R., Bates, R., Caldeira, K., Carlton, R., Corredor, J. E., Dunbar, R. B., Enochs, I., Erez, J., Eyre, B. D., Gattuso, J.-p., Lantz, C., Lazar, B., Manzello, D., Mcmahon, A., Mele, M., Page, H. N., Santos, I. R., Schulz, K. G., Shaw, E., and Silverman, J. (2018). Taking the metabolic pulse of the world ' s coral reefs. *PLoS ONE*, (Dic):1–17.

Cyronak, T., Santos, I. R., Erler, D. V., Maher, D. T., and Eyre, B. D. (2014). Drivers of pco2 variability in two contrasting coral reef lagoons: The influence of submarine groundwater discharge. *Global Biogeochemical Cycles*, 28(4):398–414.

De Bakker, D. M., Meesters, E. H., Bak, R. P. M., Nieuwland, G., and Van Duyl, F. C. (2016). Long-term Shifts in Coral Communities On Shallow to Deep Reef Slopes of Curaçao and Bonaire: Are There Any Winners? *Frontiers in Marine Science*, 3(November):1–14.

De Bakker, D. M., van Duyl, F. C., Bak, R. P. M., Nugues, M. M., Nieuwland, G., and Meesters, E. H. (2017). 40 Years of benthic community change on the Caribbean reefs of Curaçao and Bonaire: the rise of slimy cyanobacterial mats. *Coral Reefs*, 36(2):355–367.

De Bakker, D. M., Webb, A. E., van den Bogaart, L. A., Van Heuven, S. M., Meesters, E. H., and van Duyl, F. C. (2018). Quantification of chemical and mechanical bioerosion rates of six Caribbean excavating sponge species found on the coral reefs of Curaçao. *PLoS ONE*, 13(5):1–22.

De Ceccatty, M. P. (1966). Ultrastructures et rapports des cellules mésenchymateuses de type nerveux de l'Éponge Tethya lyncurium Lmk. *Ann. Sci. nat. Zool.*, 8:577–614.

De Ceccatty, M. P. (1971). Effects of drugs and ions on a primitive system of spontaneous contractions in a sponge (Euspongia officinalis). *Experientia*, 27(1):57–59.

De Ceccatty, M. P. (1974). Coordination in sponges. The foundations of integration. *American Zoologist*, 14(3):895–903.

De Goeij, J. M. and Van Duyl, F. C. (2007). Coral cavities are sinks of dissolved organic carbon (doc). *Limnology and Oceanography*, 52(6):2608–2617.

De'ath, G., Fabricius, K. E., Sweatman, H., and Puotinen, M. (2012). The 27 – year decline of coral cover on the Great Barrier Reef and its causes. *PNAS*.

Den Haan, J., Huisman, J., Brocke, H. J., Goehlich, H., Latijnhouwers, K. R., Van Heeringen, S., Honcoop, S. A., Bleyenberg, T. E., Schouten, S., Cerli, C., et al. (2016). Nitrogen and phosphorus uptake rates of different species from a coral reef community after a nutrient pulse. *Scientific reports*, 6:28821.

Dickson, A. and Millero, F. J. (1987). A comparison of the equilibrium constants for the dissociation of carbonic acid in seawater media. *Deep Sea Research Part A. Oceanographic Research Papers*, 34(10):1733–1743.

Dickson, A. G., Sabine, C. L., and Christian, J. R. (2007). *Guide to best practices for ocean CO2 measurements*. North Pacific Marine Science Organization.

Doney, S. C., Fabry, V. J., Feely, R. A., and Kleypas, J. A. (2009). Ocean acidification: the other co2 problem. *Annual review of marine science*, 1:169–192.

Dove, S. G. and Hoegh-Guldberg, O. (2006). The cell physiology of coral bleaching. *Coral Reefs and Climate Change: Science and Management, Coastal and Estuarine Studies (Eds J. Phinney, O. Hoegh-Guldberg, J. Kleypas, W. Skirving, A. Strong)*, 61:55.

Dove, S. G., Kline, D. I., Pantos, O., Angly, F. E., Tyson, G. W., and Hoegh-Guldberg, O. (2013). Future reef decalcification under a business-as-usual CO2 emission scenario. *Proceedings of the National Academy of Sciences*, 110(38):15342–15347.

Duchassaing De Fonbressin, P. and Michelotti, G. (1864). Spongiaires de la mer Caraïbe. Natuurkundige verhandelingen van de Hollandsche maatschappij der wetenschappen te Haarlem, 21 (2), 1–124. *IX-124*.

Duckworth, A. R. and Peterson, B. J. (2013). Effects of seawater temperature and pH on the boring rates of the sponge Cliona celata in scallop shells. *Marine Biology*, 160(1):27–35.

Dunham, P., Anderson, C., Rich, A. M., and Weissmann, G. (1983). Stimulus-response coupling in sponge cell aggregation: Evidence for calcium as an intracellular messenger. *Proceedings of the National Academy of Sciences*, 80(15):4756–4760.

Eakin, C. M., Morgan, J. A., Heron, S. F., Smith, T. B., Liu, G., Alvarez-Filip, L., Baca, B., Bartels, E., Bastidas, C., Bouchon, C., et al. (2010). Caribbean corals in crisis: record thermal stress, bleaching, and mortality in 2005. *PloS one*, 5(11):e13969.

Edinger, E. N. and Risk, M. J. (2000). Reef classification by coral morphology predicts coral reef conservation value. *Biological Conservation*, 92(1):1–13.

Enochs, I. C., Manzello, D. P., Carlton, R. D., Graham, D. M., Ruzicka, R., and Colella, M. A. (2015). Ocean acidification enhances the bioerosion of a common coral reef sponge: implications for the persistence of the florida reef tract. *Bulletin of Marine Science*, 91(2):271–290.

Erwin, P. M. and Thacker, R. W. (2008). Phototrophic nutrition and symbiont diversity of two caribbean sponge–cyanobacteria symbioses. *Marine Ecology Progress Series*, 362:139–147.

Etnoyer, P. J., Wirshing, H. H., and Sánchez, J. A. (2010). Rapid assessment of octocoral diversity and habitat on saba bank, netherlands antilles. *PLoS One*, 5(5):e10668.

Eyre, B. D., Cyronak, T., Drupp, P., De Carlo, E. H., Sachs, J. P., and Andersson, A. J. (2018). Coral reefs will transition to net dissolving before end of century. *Science*, 359(6378):908–911.

Fabricius, K. E. (2005). Effects of terrestrial runoff on the ecology of corals and coral reefs: review and synthesis. *Marine pollution bulletin*, 50(2):125–146.

Fang, J. K., Schönberg, C. H., Hoegh-Guldberg, O., and Dove, S. (2016). Day–night ecophysiology of the photosymbiotic bioeroding sponge cliona orientalis thiele, 1900. *Marine biology*, 163(5):100.

Fang, J. K. H., Mello-Athayde, M. A., Schönberg, C. H. L., Kline, D. I., Hoegh-Guldberg, O., and Dove, S. (2013). Sponge biomass and bioerosion rates increase under ocean warming and acidification. *Global change biology*, 19(12):3581–3591.

Fang, J. K. H., Schönberg, C. H. L., Mello-Athayde, M. A., Hoegh-Guldberg, O., and Dove, S. (2014). Effects of ocean warming and acidification on the energy budget of an excavating sponge. *Global change biology*, 20(4):1043–1054.

Fink, A., Haan, J. D., Chennu, A., Uthicke, S., Beer, D. D., and Fink, A. (2017). Ocean Acidification Changes Abiotic Processes but Not Biotic Processes in Coral Reef Sediments. *Frontiers in Marine Science*, 4(March):1–13.

Freeman, C. J. and Thacker, R. W. (2011). Complex interactions between marine sponges and their symbiotic microbial communities. *Limnology and Oceanography*, 56(5):1577–1586.

Furla, P., Galgani, I., Durand, I., and Allemand, D. (2000). Sources and mechanisms of inorganic carbon transport for coral calcification and photosynthesis. *The Journal of experimental biology*, 203(Pt 22):3445–57.

Garcia-Pichel, F. (2006). Plausible mechanisms for the boring on carbonates by microbial phototrophs. *Sedimentary Geology*, 185(3-4):205–213.

Garcia-Pichel, F., Ramírez-Reinat, E., and Gao, Q. (2010). Microbial excavation of solid carbonates powered by p-type atpase-mediated transcellular ca2+ transport. *Proceedings of the National Academy of Sciences*, 107(50):21749–21754.

Gardner, T. A., Côté, I. M., Gill, J. A., Grant, A., and Watkinson, A. R. (2003). Long-term Regional-wide declining in Caribbean corals. *Science*, 301(5635):958–960.

Gast, G., Jonkers, P., Van Duyl, F., and Bak, R. (1999). Bacteria, flagellates and nutrients in island fringing coral reef waters: influence of the ocean, the reef and eutrophication. *Bulletin of Marine Science*, 65(2):523–538.

Gattuso, J., Pichon, M., Delesalle, B., Canon, C., and Frankignoulle, M. (1996). Carbon fluxes in coral reefs. i. lagrangian measurement of community metabolism and resulting air-sea co2 disequilibrium. *Marine Ecology Progress Series*, 145:109–121.

Gattuso, J., Pichon, M., Delesalle, B., and Frankignoulle, M. (1993). Community metabolism and air-sea c [o. sub. 2] fluxes in a coral reef ecosystem (moorea french polynesia). *Mar. Ecol. Prog. Ser*, 96:259–267.

Gattuso, J.-P., Frankignoulle, M., and Wollast, R. (1998). Carbon and Carbonate Metabolism in Coastal Aquatic Ecosystems. *Annual Review of Ecology and Systematics*, 29(1):405–434.

Gattuso, J.-P. and Hansson, L. (2011). *Ocean acidification*. Oxford University Press.

Gilmour, J. (1999). Experimental investigation into the effects of suspended sediment on fertilisation, larval survival and settlement in a scleractinian coral. *Marine Biology*, 135(3):451–462.

Glynn, P. W. (1996). Coral reef bleaching: facts, hypotheses and implications. *Global change biology*, 2(6):495–509.

Glynn, P. W. and Manzello, D. P. (2015). Bioerosion and coral reef growth: a dynamic balance. In *Coral reefs in the Anthropocene*, pages 67–97. Springer.

Goiran, C., Al-Moghrabi, S., Allemand, D., and Jaubert, J. (1996). Inorganic carbon uptake for photosynthesis by the symbiotic coral/dinoflagellate association I. Photosynthetic performances of symbionts and dependence on sea water bicarbonate. *Journal of Experimental Marine Biology and Ecology*, 199(2):207–225.

Goreau, T. F. (1959). the Physiology of Skeleton Formation in Corals. I. a Method for Measuring the Rate of Calcium Deposition By Corals Under Different Conditions. *The Biological Bulletin*, 116(1):59–75.

Gorgula, S. K. and Connell, S. D. (2004). Expansive covers of turf-forming algae on human-dominated coast: the relative effects of increasing nutrient and sediment loads. *Marine Biology*, 145(3):613–619.

Govers, L. L., Lamers, L. P., Bouma, T. J., de Brouwer, J. H., and van Katwijk, M. M. (2014). Eutrophication threatens caribbean seagrasses–an example from curaçao and bonaire. *Marine pollution bulletin*, 89(1-2):481–486.

Graham, N. and Nash, K. (2013). The importance of structural complexity in coral reef ecosystems. *Coral Reefs*, 32(2):315–326.

Grant, R. E. (1826). *Notice of a New Zoophyte (Cliona Celata, Gr.) from the Frith of Forth.*

Grigg, R. W., Polovina, J. J., and Atkinson, M. J. (1984). Model of a coral reef ecosystem. *Coral Reefs*, 3(1):23–27.

Grottoli, A. G., Warner, M. E., Levas, S. J., Aschaffenburg, M. D., Schoepf, V., McGinley, M., Baumann, J., and Matsui, Y. (2014). The cumulative impact of annual coral bleaching can turn some coral species winners into losers. *Global Change Biology*, 20(12):3823–3833.

Guida, B. S. and Garcia-Pichel, F. (2016). Extreme cellular adaptations and cell differentiation required by a cyanobacterium for carbonate excavation. *Proceedings of the National Academy of Sciences*, 113(20):5712–5717.

Guinotte, J. M. and Fabry, V. J. (2008). Ocean acidification and its potential effects on marine ecosystems. *Annals of the New York Academy of Sciences*, 1134(1):320–342.

Guzman, J. M., Rodriguez, J., Martinez, J., Contreras, J. M., and Gonzalez, D. (2006). The Demography of Latin America and the Caribbean since 1950. *Population*, 61(5-6):519–620.

Haas, A. F., Nelson, C. E., Rohwer, F., Wegley-Kelly, L., Quistad, S. D., Carlson, C. A., Leichter, J. J., Hatay, M., and Smith, J. E. (2013). Influence of coral and algal exudates on microbially mediated reef metabolism. *PeerJ*, 1:e108.

Hadas, E., Ilan, M., and Shpigel, M. (2008). Oxygen consumption by a coral reef sponge. *Journal of Experimental Biology*, 211(13):2185–2190.

Hallock, P. (2005). Global change and modern coral reefs: new opportunities to understand shallow-water carbonate depositional processes. *Sedimentary Geology*, 175(1-4):19–33.

Hancock, A. (1849). XXXVI.—On the excavating powers of certain sponges belonging to the genus Cliona; with descriptions of several new species, and an allied generic form. *Annals and Magazine of Natural History*, 3(17):321–348.

Hatch, W. I. (1980). The implication of carbonic anhydrase in the physiological mechanism of penetration of carbonate substrata by the marine burrowing sponge Cliona celata (Demospongiae). *The Biological Bulletin*, 159(1):135–147.

Hendriks, I. E., Duarte, C. M., and Álvarez, M. (2010). Vulnerability of marine biodiversity to ocean acidification: a meta-analysis. *Estuarine, Coastal and Shelf Science*, 86(2):157–164.

Hill, M. S. (1996). Symbiotic zooxanthellae enhance boring and growth rates of the tropical sponge Anthosigmella varians forma varians. *Marine Biology*, 125(4):649–654.

Hoegh-Guldberg, O. (1999). Climate change, coral bleaching and the future of the world's coral reefs. *Marine and freshwater research*, 50(8):839–866.

Hoegh-Guldberg, O., Mumby, P. J., Hooten, A. J., Steneck, R. S., Greenfield, P., Gomez, E., Harvell, C. D., Sale, P. F., Edwards, A. J., Caldeira, K., Knowlton, N., Eakin, C. M., Iglesias-Prieto, R., Muthiga, N., Bradbury, R. H., Dubi, A., and Hatziolos, M. E. (2007). Coral reefs under rapid climate change and ocean acidification. *Science (New York, N.Y.)*, 318(5857):1737–1742.

Holmes, K. E., Edinger, E. N., Limmon, G. V., Risk, M. J., et al. (2000). Bioerosion of live massive corals and branching coral rubble on indonesian coral reefs. *Marine Pollution Bulletin*, 40(7):606–617.

Hughes, T. P. (1994). Catastrophes, phase shifts, and large-scale degradation of a caribbean coral reef. *Science*, 265(5178):1547–1551.

Hughes, T. P., Baird, A. H., Bellwood, D. R., Card, M., Connolly, S. R., Folke, C., Grosberg, R., Hoegh-Guldberg, O., Jackson, J. B., Kleypas, J., et al. (2003). Climate change, human impacts, and the resilience of coral reefs. *science*, 301(5635):929–933.

Hughes, T. P., Barnes, M. L., Bellwood, D. R., Cinner, J. E., Cumming, G. S., Jackson, J. B., Kleypas, J., Van De Leemput, I. A., Lough, J. M., Morrison, T. H., Palumbi, S. R., Van Nes, E. H., and Scheffer, M. (2017). Coral reefs in the Anthropocene. *Nature*, 546(7656):82–90.

Hughes, T. P., Rodrigues, M. J., Bellwood, D. R., Ceccarelli, D., Hoegh-guldberg, O., Mccook, L., Moltschaniwskyj, N., Pratchett, M. S., Steneck, R. S., and Willis, B. (2007). Report Phase Shifts , Herbivory , and the Resilience of Coral Reefs to Climate Change. *Current Biology*, pages 360–365.

Hydes, D. J., Aoyama, M., Aminot, A., Bakker, K., Becker, S., Coverly, S., Daniel, A., Dickson, A. G., Grosso, O., Kerouel, R., Van Ooijen, J., Sato, K., Tanhua, T., Woodward, M., and Zhang, J.-Z. (2010). Determination of dissolved nutrients (N, P, Si) in seawater with high precision and inter-comparability using gas-segmented continuous flow analysers. *The GO-SHIP Repeart Hydrography Manual: A Collection of Expert Reports and Guidelines*, pages 1–87.

Jackson, J., Donovan, M., Cramer, K., and Lam, V. (2014). Status and trends of caribbean coral reefs: 1970-2012. global coral reef monitoring network. *International Union for the Conservation of Nature Global Marine and Polar Program: Washington, DC*.

Jackson, J. B., Kirby, M. X., Berger, W. H., Bjorndal, K. A., Botsford, L. W., Bourque, B. J., Bradbury, R. H., Cooke, R., Erlandson, J., Estes, J. A., et al. (2001). Historical overfishing and the recent collapse of coastal ecosystems. *science*, 293(5530):629–637.

Jacques, T. and Pilson, M. (1980). Experimental ecology of the temperate scleractinian coral astrangia danae i. partition of respiration, photosynthesis and calcification between host and symbionts. *Marine Biology*, 60(2-3):167–178.

Johnson, K., Wills, K., Butler, D., Johnson, W., and Wong, C. (1993). Coulometric total carbon dioxide analysis for marine studies: maximizing the performance of an automated gas extraction system and coulometric detector. *Marine chemistry*, 44(2-4):167–187.

Kennedy, E. V., Perry, C. T., Halloran, P. R., Iglesias-Prieto, R., Schönberg, C. H. L., Wisshak, M., Form, A. U., Carricart-Ganivet, J. P., Fine, M., Eakin, C. M., and Mumby, P. J. (2013). Avoiding coral reef functional collapse requires local and global action. *Current Biology*, 23(10):912–918.

Kleypas, J. A., Buddemeier, R. W., Archer, D., Gattuso, J.-P., Langdon, C., and Opdyke, B. N. (1999). Geochemical consequences of increased atmospheric carbon dioxide on coral reefs. *science*, 284(5411):118–120.

Kleypas, J. A., Feely, R. A., Fabry, V. J., Langdon, C., Sabine, C. L., and Robbins, L. L. (2005). Impacts of ocean acidification on coral reefs and other marine calcifiers: a guide for future research. In *Report of a workshop held*, volume 18, page 20.

Kleypas, J. A. and Langdon, C. (2006). Coral reefs and changing seawater carbonate chemistry. *Coastal and Estuarine Studies: Coral Reefs and Climate Change Science and Management*, 61:73–110.

Kleypas, J. A. and Yates, K. K. (2009). Coral reefs and ocean acidification. *Oceanography*, 22(4):108–117.

Knowlton, N. and Jackson, J. B. (2008). Shifting baselines, local impacts, and global change on coral reefs. *PLoS biology*, 6(2):e54.

Koop, K., Booth, D., Broadbent, A., Brodie, J., Bucher, D., Capone, D., Coll, J., Dennison, W., Erdmann, M., Harrison, P., Hoegh-Guldberg, O., Hutchings, P., Jones, G. B., Larkum, A. W. D., O'Neil, J., Steven, A., Tentori, E., Ward, S., Williamson, J., and Yellowlees, D. (2001). ENCORE: The effect of nutrient enrichment on coral reefs. Synthesis of results and conclusions. *Marine Pollution Bulletin*, 42(2):91–120.

Koweek, D., Dunbar, R. B., Price, N., Mucciarone, D., and Teneva, L. (2015). Environmental and ecological controls of coral community metabolism on Palmyra Atoll. *Coral Reefs*, pages 339–351.

Kuffner, I. B. and Paul, V. J. (2001). Effects of nitrate, phosphate and iron on the growth of macroalgae and benthic cyanobacteria from cocos lagoon, guam. *Marine Ecology Progress Series*, 222:63–72.

Langdon, C. and Atkinson, M. J. (2005). Effect of elevated pCO2on photosynthesis and calcification of corals and interactions with seasonal change in temperature/ irradiance and nutrient enrichment. *Journal of Geophysical Research C: Oceans*, 110(9):1–16.

Langdon, C., Takahashi, T., Sweeney, C., Chipman, D., Goddard, J., Marubini, F., Aceves, H., Barnett, H., and Atkinson, M. J. (2000). Effect of calcium carbonate saturation state on the calcification rate of an experimental coral reef. *Global Biogeochemical Cycles*, 14(2):639–654.

Lapointe, B. E. and Mallin, M. (2011). Nutrient Enrichment and Eutrophication on Fringing Coral Reefs of Bonaire and Curaçao , Netherlands Antilles. *Report to the United Nations Environment Programme for the NACRI Coral Reef Monitoring Program, Harbor Branch Oceanographic Institute, Ft. Pierce Fl*, pages 0–42.

Le Quéré, C., Moriarty, R., Andrew, R., Canadell, J., Sitch, S., Korsbakken, J., Friedlingstein, P., Peters, G., Andres, R., Boden, T., et al. (2015). Global carbon budget 2015, earth syst. sci. data, 7, 349–396.

Leggat, W., Marendy, E. M., Baillie, B., Whitney, S. M., Ludwig, M., Badger, M. R., and Yellowlees, D. (2002). Dinoflagellate symbioses: strategies and adaptations for the acquisition and fixation of inorganic carbon.

Leys, S. P. (2015). Elements of a 'nervous system'in sponges. *Journal of Experimental Biology*, 218(4):581–591.

Liu, X., Byrne, R. H., Lindemuth, M., Easley, R., and Mathis, J. T. (2015). An automated procedure for laboratory and shipboard spectrophotometric measurements of seawater alkalinity: Continuously monitored single-step acid additions. *Marine Chemistry*, 174:141–146.

Liu, X., Patsavas, M. C., and Byrne, R. H. (2011). Purification and characterization of meta-cresol purple for spectrophotometric seawater ph measurements. *Environmental Science and Technology*, 45(11):4862–4868.

Lorenz, B., Bohnensack, R., Gamulin, V., Steffen, R., and Müller, W. E. G. (1996). Regulation of motility of cells from marine sponges by calcium ions. *Cellular signalling*, 8(7):517–524.

Ludeman, D. A., Reidenbach, M. A., and Leys, S. P. (2017). The energetic cost of filtration by demosponges and their behavioural response to ambient currents. *Journal of Experimental Biology*, 220(6):995–1007.

Macgeachy, J. K. and Stearn, C. W. (1976). Boring by macro-organisms in the coral montastrea annularis on barbados reefs. *Internationale Revue der Gesamten Hydrobiologie und Hydrographie*, 61(6):715–745.

Mcallister, D. E. (1991). What is the status of the world's coral reef fishes. *Sea Wind*, 5(1):14–18.

McElhany, P. (2017). Co2 sensitivity experiments are not sufficient to show an effect of ocean acidification. *ICES Journal of Marine Science*, 74(4):926–928.

McGillis, W. R., Langdon, C., Loose, B., Yates, K. K., and Corredor, J. (2011). Productivity of a coral reef using boundary layer and enclosure methods. *Geophysical Research Letters*, 38(3).

McMahon, A., Santos, I. R., Cyronak, T., and Eyre, B. D. (2013). Hysteresis between coral reef calcification and the seawater aragonite saturation state. *Geophysical Research Letters*, 40(17):4675–4679.

McMurray, S. E., Stubler, A. D., Erwin, P. M., Finelli, C. M., and Pawlik, J. R. (2018). A test of the sponge-loop hypothesis for emergent caribbean reef sponges. *Marine Ecology Progress Series*, 588:1–14.

Middelburg, J. J., Duarte, C. M., and Gattuso, J.-P. (2005). Respiration in coastal benthic communities. *Respiration in aquatic ecosystems*, pages 206–224.

Mintrop, L., Pérez, F. F., Dávila, M. G., Casiano, J. M. S., and Körtzinger, A. (2000). Alkalinity determination by potentiometry: Intercalibration using three different methods. *Ciencias Marinas*, 26(1):23–27.

Miyamoto, H., Miyashita, T., Okushima, M., Nakano, S., Morita, T., and Matsushiro, A. (2002). A carbonic anhydrase from the nacreous layer in oyster pearls. *Proceedings of the National Academy of Sciences*, 93(18):9657–9660.

Moberg, F. and Rönnbäck, P. (2003). Ecosystem services of the tropical seascape: Interactions, substitutions and restoration. *Ocean and Coastal Management*, 46(1-2):27–46.

Moroney, J. V., Husic, H. D., and Tolbert, N. E. (1985). Effect of Carbonic Anhydrase Inhibitors on Inorganic Carbon Accumulation by Chlamydomonas reinhardtii. *Plant Physiology*, 79(1):177–183.

Moya, A., Tambutté, S., Bertucci, A., Tambutté, E., Lotto, S., Vullo, D., Supuran, C. T., Allemand, D., and Zoccola, D. (2008). Carbonic Anhydrase in the Scleractinian Coral Stylophora pistillata . *Journal of Biological Chemistry*, 283(37):25475–25484.

Muehllehner, N., Langdon, C., Venti, A., and Kadko, D. (2016). Dynamics of carbonate chemistry, production, and calcification of the Florida Reef Tract (2009–2010): Evidence for seasonal dissolution. *Global Biogeochemical Cycles*, pages 661–688.

Mueller, B., Goeij, J. M. D., Vermeij, M. J. A., Mulders, Y., Ent, E. V. D., Ribes, M., and Duyl, F. C. V. (2014). Natural Diet of Coral-Excavating Sponges Consists Mainly of Dissolved Organic Carbon (DOC). *PLoS ONE*, 9(2).

Müller, W. E., Schröder, H. C., Schlossmacher, U., Grebenjuk, V. A., Ushijima, H., and Wang, X. (2013). Induction of carbonic anhydrase in saos-2 cells, exposed to bicarbonate and consequences for calcium phosphate crystal formation. *Biomaterials*, 34(34):8671–8680.

Murphy, G. N., Perry, C. T., Chin, P., and McCoy, C. (2016). New approaches to quantifying bioerosion by endolithic sponge populations: applications to the coral reefs of Grand Cayman. *Coral Reefs*, 35(3):1109–1121.

Nasonov, N. (1924). Sur l'éponge perforante Clione stationis Nason. et le procédé du creusement des galeries dans les valves des huîtres. *CR Acad Sci Russia*, 1924:113–115.

Nava, H. and Carballo, J. L. (2008). Chemical and mechanical bioerosion of boring sponges from Mexican Pacific coral reefs. *Journal of Experimental Biology*, 211(17):2827–2831.

Neumann, A. C. and Jan, N. (1966). Observations on Coastal Erosion in Bermuda and Measurements of the Boring Rate of the Sponge , Cliona lampa. *Limnology*, 11(1):92–108.

Newman, M. J., Paredes, G. A., Sala, E., and Jackson, J. B. (2006). Structure of caribbean coral reef communities across a large gradient of fish biomass. *Ecology letters*, 9(11):1216–1227.

Odum, H. and Hoskin, C. (1958). Comparative studies of the metabolism of texas bays. *Publications of the Institute of Marine Science, University of Texas*, 5:16–46.

Odum, H. T. and Odum, E. P. (1955). Trophic structure and productivity of a windward coral reef community on eniwetok atoll. *Ecological monographs*, 25(3):291–320.

Paerl, H. W. and Paul, V. J. (2012). Climate change: links to global expansion of harmful cyanobacteria. *Water research*, 46(5):1349–1363.

Pandolfi, J. M., Bradbury, R. H., Sala, E., Hughes, T. P., Bjorndal, K. A., Cooke, R. G., McArdle, D., McClenachan, L., Newman, M. J., Paredes, G., et al. (2003). Global trajectories of the long-term decline of coral reef ecosystems. *Science*, 301(5635):955–958.

Pandolfi, J. M., Connolly, S. R., Marshall, D. J., and Cohen, A. L. (2011). Projecting coral reef futures under global warming and ocean acidification. *Science*, 333(6041):418–422.

Patterson, M. R., Sebens, K. P., and Olson, R. R. (1991). In situ measurements of flow effects on primary production and dark respiration in reef corals. *Limnology and Oceanography*, 36(5):936–948.

Perry, C. T., Edinger, E. N., Kench, P. S., Murphy, G. N., Smithers, S. G., Steneck, R. S., and Mumby, P. J. (2012). Estimating rates of biologically driven coral reef framework production and erosion: A new census-based carbonate budget methodology and applications to the reefs of Bonaire. *Coral Reefs*, 31(3):853–868.

Perry, C. T., Murphy, G. N., Graham, N. A., Wilson, S. K., Januchowski-Hartley, F. A., and East, H. K. (2015). Remote coral reefs can sustain high growth potential and may match future sea-level trends. *Scientific Reports*, 5:18289.

Perry, C. T., Murphy, G. N., Kench, P. S., Edinger, E. N., Smithers, S. G., Steneck, R. S., and Mumby, P. J. (2014). Changing dynamics of Caribbean reef carbonate budgets: emergence of reef bioeroders as critical controls on present and future reef growth potential. *Proc. R. Soc. B*, 281(1796):20142018.

Perry, C. T., Murphy, G. N., Kench, P. S., Smithers, S. G., Edinger, E. N., Steneck, R. S., and Mumby, P. J. (2013). Caribbean-wide decline in carbonate production threatens coral reef growth. *Nature Communications*, 4:1402–1407.

Perry, C. T., Spencer, T., and Kench, P. S. (2008). Carbonate budgets and reef production states: A geomorphic perspective on the ecological phase-shift concept. *Coral Reefs*, 27(4):853–866.

Pomponi, S. A. (1977). Etching cells of boring sponges: an ultrastructural analysis. In *Proceedings of the Third International Coral Reef Symposium*, volume 2, pages 485–490.

Pomponi, S. A. (1980). Cytological mechanisms of calcium carbonate excavation by boring sponges. *International review of Cytology*, 65:301–319.

Porter, J. W. and Meier, O. W. (1992). Quantification of loss and change in floridian reef coral populations. *American Zoologist*, 32(6):625–640.

Prosser, C. L. (1967). Ionic analyses and effects of ions on contractions of sponge tissues. *Zeitschrift für vergleichende Physiologie*, 54(2):109–120.

Raupach, M. R., Marland, G., Ciais, P., Le Quéré, C., Canadell, J. G., Klepper, G., and Field, C. B. (2007). Global and regional drivers of accelerating co2 emissions. *Proceedings of the National Academy of Sciences*, 104(24):10288–10293.

Raven, J., Caldeira, K., Elderfield, H., Hoegh-Guldberg, O., Liss, P., Riebesell, U., Shepherd, J., Turley, C., and Watson, A. (2005). *Ocean acidification due to increasing atmospheric carbon dioxide*. The Royal Society.

Reaka-Kudla, M. L. (1997). The global biodiversity of coral reefs: a comparison with rain forests. *Biodiversity II: Understanding and protecting our biological resources*, 2:551.

Redfield, A. C. (1963). The influence of organisms on the composition of seawater. *The sea*, 2:26–77.

Riebesell, U., Fabry, V. J., Hansson, L., and Gattuso, J.-P. (2011). *Guide to best practices for ocean acidification research and data reporting*. Office for Official Publications of the European Communities.

Roche, D. G., Binning, S. A., Bosiger, Y., Johansen, J. L., and Rummer, J. L. (2013). Finding the best estimates of metabolic rates in a coral reef fish. *Journal of Experimental Biology*, 216(11):2103–2110.

Roff, G. and Mumby, P. J. (2012). Global disparity in the resilience of coral reefs. *Trends in Ecology and Evolution*, 27(7):404–413.

Rützler, K. (1971). Bredin-Archbold Smithsonian Biological Survey of Dominica: Burrowing sponges, Genus Siphonodictyon Bergquist, from the Caribbean. *Smithsonian Contributions to Zoology*.

Rützler, K. (1975). The role of burrowing sponges in bioerosion. *Oecologia*, 19(3):203–216.

Rützler, K. (2002). Impact of crustose clionid sponges on Caribbean reef corals.

Rützler, K. and Rieger, G. (1973). Sponge burrowing: fine structure of Cliona lampa penetrating calcareous substrata. *Marine Biology*, 21(2):144–162.

Sabine, C. L., Feely, R. A., Gruber, N., Key, R. M., Lee, K., Bullister, J. L., Wanninkhof, R., Wong, C., Wallace, D. W., Tilbrook, B., et al. (2004). The oceanic sink for anthropogenic co2. *science*, 305(5682):367–371.

Schönberg, C. H., Fang, J. K., Carreiro-Silva, M., Tribollet, A., and Wisshak, M. (2017). Bioerosion: The other ocean acidification problem. *ICES Journal of Marine Science*, 74(4):895–925.

Schönberg, C. H. L. (2000). Sponges of the ´Cliona viridis complex‘ - a key for species identification. *Proc. 9th Int. Coral Reef Symp.*, (May):1–6.

Schönberg, C. H. L. (2008). A history of sponge erosion: from past myths and hypotheses to recent approaches. In *Current developments in bioerosion*, pages 165–202. Springer.

Schönberg, C. H. L. and Suwa, R. (2007). Why bioeroding sponges may be better hosts for symbiotic dinoflagellates than many corals. *Porifera Research: Biodiversity, Innovation and Sustainability. Publ Museu Nac Rio de Janeiro*, (May 2014).

Schönberg, H. L. and Ortiz, J. C. (2008). Is sponge bioerosion increasing. In *Proceedings of the 11th International Coral Reef Symposium*, volume 8, pages 7–11. International Society for Reef Studies Fort Lauderdale, FL.

Shaw, E. C., Phinn, S. R., Tilbrook, B., and Steven, A. (2014). Comparability of slack water and lagrangian flow respirometry methods for community metabolic measurements. *PloS one*, 9(11):e112161.

Shaw, E. C., Phinn, S. R., Tilbrook, B., and Steven, A. (2015). Natural in situ relationships suggest coral reef calcium carbonate production will decline with ocean acidification. *Limnology and Oceanography*, 60(3):777–788.

Silbiger, N. and Donahue, M. (2015). Secondary calcification and dissolution respond differently to future ocean conditions. *Biogeosciences*, 12(2):567–578.

Silverman, J., Lazar, B., and Erez, J. (2007). Effect of aragonite saturation, temperature, and nutrients on the community calcification rate of a coral reef. *Journal of Geophysical Research: Oceans*, 112(5):1–14.

Smith, A. S. V., Key, G. S., Limnology, S., and May, N. (1975). Carbon Dioxide and Metabolism in Marine Environments Carbon dioxide and metabolism in marine environments '. *Limnology*, 20(3):493–495.

Smith, S. (1978). Coral-reef area and the contributions of reefs to processes and resources of the world's oceans. *Nature*, 273(5659):225.

Solomon, S., Qin, D., Manning, M., Averyt, K., Marquis, M., and Tignor, M. M. (2007). *Climate change 2007-the physical science basis: Working group I contribution to the fourth assessment report of the IPCC*, volume 4. Cambridge university press.

Sommerville, L. and Hartshorne, D. (1986). Intracellular calcium and smooth muscle contraction. *Cell Calcium*, 7(5-6):353–364.

Spalding, M., Burke, L., Wood, S. A., Ashpole, J., Hutchison, J., and Zu Ermgassen, P. (2017). Mapping the global value and distribution of coral reef tourism. *Marine Policy*, 82:104–113.

Spalding, M. and Grenfell, A. (1997). New estimates of global and regional coral reef areas. *Coral reefs*, 16(4):225–230.

Spalding, M., Spalding, M. D., Ravilious, C., Green, E. P., et al. (2001). *World atlas of coral reefs*. Univ of California Press.

Sullivan, B. W., Faulkner, D. J., Matsumoto, G. K., He, C. H., and Clardy, J. (1986). Metabolites of the burrowing sponge Siphonodictyon coralliphagum. *The Journal of Organic Chemistry*, 51(24):4568–4573.

Takeshita, Y., Mcgillis, W., Briggs, E. M., Carter, A. L., Donham, E. M., Martz, T. R., Price, N. N., and Smith, J. E. (2016). Oceans coral reef using a boundary layer approach. *Journal of Geophysical Research*, pages 5655–5671.

Tansik, A. L., Fitt, W. K., and Hopkinson, B. M. (2017). Inorganic carbon is scarce for symbionts in scleractinian corals. *Limnology and Oceanography*, 62(5):2045–2055.

Teppema, L. J., Bijl, H., Gourabi, B. M., and Dahan, A. (2006). The carbonic anhydrase inhibitors methazolamide and acetazolamide have different effects on the hypoxic ventilatory response in the anaesthetized cat. *The Journal of physiology*, 574(2):565–572.

Uku, J. and Björk, M. (2005). Productivity aspects of three tropical seagrass species in areas of different nutrient levels in kenya. *Estuarine, Coastal and Shelf Science*, 63(3):407–420.

van Duyl, F. C. and Gast, G. J. (2001). Linkage of small-scale spatial variations in doc, inorganic nutrients and bacterioplankton growth with different coral reef water types. *Aquatic Microbial Ecology*, 24(1):17–26.

van Heuven, S. M. A. C., Webb, A. E., Bakker, D. M. D., Meesters, E., Duyl, F. C. V., Reichart, G.-j., and Lennart, J. (2018). In-situ incubation of a coral patch for community-scale assessment of metabolic and chemical processes on a reef slope. *PeerJ*, pages 1–24.

Vega Thurber, R. L., Burkepile, D. E., Fuchs, C., Shantz, A. A., McMinds, R., and Zaneveld, J. R. (2014). Chronic nutrient enrichment increases prevalence and severity of coral disease and bleaching. *Global change biology*, 20(2):544–554.

Vermeij, M. J., Van Moorselaar, I., Engelhard, S., Hörnlein, C., Vonk, S. M., and Visser, P. M. (2010). The effects of nutrient enrichment and herbivore abundance on the ability of turf algae to overgrow coral in the caribbean. *PloS one*, 5(12):e14312.

Veron, J. E. (2011). Ocean acidification and coral reefs: an emerging big picture. *Diversity*, 3(2):262–274.

Warburton, F. E. (1958). The manner in which the sponge Cliona bores in calcareous objects. *Canadian Journal of Zoology*, 36(4):555–562.

Webb, A. E., Pomponi, S. A., van Duyl, F. C., Reichart, G.-J., and de Nooijer, L. J. (2019). pH regulation and tissue coordination pathways promote calcium carbonate bioerosion by excavating sponges. *Scientific reports*, 9(1):758.

Webb, A. E., van Heuven, S. M. A. C., de Bakker, D. M., van Duyl, F. C., Reichart, G.-J., and de Nooijer, L. J. (2017). Combined effects of experimental acidification and eutrophication on reef sponge bioerosion rates. *Frontiers in Marine Science*, 4:311.

Weisz, J. B., Massaro, A. J., Ramsby, B. D., and Hill, M. S. (2010). Zooxanthellar symbionts shape host sponge trophic status through translocation of carbon. *Biological Bulletin*, 219(3):189–197.

Wild, C., Huettel, M., Klueter, A., Kremb, S. G., Rasheed, M. Y., and Jørgensen, B. B. (2004). Coral mucus functions as an energy carrier and particle trap in the reef ecosystem. *Nature*, 428(6978):66.

Wilkinson, C. (2004). Status of coral reefs of the world (australian institute of marine science, townsville, australia). *línea: http://www. aims. gov. au/pages/research/coralbleaching/scr2004/index. html*.

Wisshak, M., Schönberg, C. H. L., Form, A., and Freiwald, A. (2012). Ocean acidification accelerates reef bioerosion. *PloS one*, 7(9):e45124.

Wisshak, M., Schönberg, C. H. L., Form, A., and Freiwald, A. (2013). Effects of ocean acidification and global warming on reef bioerosion-lessons from a clionaid sponge. *Aquatic Biology*, 19(2):111–127.

Wisshak, M., Schönberg, C. H. L., Form, A., and Freiwald, A. (2014). Sponge bioerosion accelerated by ocean acidification across species and latitudes? *Helgoland marine research*, 68(2):253.

Wisshak, M. and Tapanila, L. (2008). *Current developments in bioerosion*. Springer Science & Business Media.

Wood, B. L. (1967). Geology of the cook islands. *New Zealand journal of geology and geophysics*, 10(6):1429–1445.

Yates, K. K. and Halley, R. B. (2003). Measuring coral reef community metabolism using new benthic chamber technology. *Coral Reefs*, 22(3):247–255.

Yeakel, K. L., Andersson, A. J., Bates, N. R., Noyes, T. J., Collins, A., and Garley, R. (2015). Shifts in coral reef biogeochemistry and resulting acidification linked to offshore productivity. *Proceedings of the National Academy of Sciences*, 112(47):14512–14517.

Zundelevich, A., Lazar, B., and Ilan, M. (2007). Chemical versus mechanical bioerosion of coral reefs by boring sponges-lessons from Pione cf. vastifica. *Journal of experimental biology*, 210(1):91–96.

Summary

For coral reefs to persist, the rate of $CaCO_3$ production must be greater than the rate of erosion to enable positive growth. Negative impacts of global change (ocean acidification and warming) and local stressors (eutrophication, overfishing) on accretion co-occur with positive effects of these changes on bioerosion capacity and chemical dissolution by excavating euendolithic organisms. Although the effects of environmental pressures on calcification are well documented, their impact on bioerosion remains somewhat elusive. This is especially relevant for reefs characterised with low calcifying rates as they will tip faster into net loss. As many reefs of the Caribbean region and Gulf of Mexico suffered from a decrease by up to 80% in scleractinian coral cover in the past 50 years, their configuration bears very little resemblance with reefs pre-1980s, in terms of benthic composition, coral cover and structural complexity. Areas covered by sand, rubble, cyanobacteria, turf, macroalgae and excavating sponges have increased at the expense of the declining coral. Specifically, excavating sponges can contribute up to 90% of the total macroborer activity on coral reefs and their rates of bioerosion have been shown to increase as a function of pCO_2. The overarching aim of this thesis was to quantify and understand the accretion and loss terms of coral reef communities with a focus on the interactions of anthropogenic ocean acidification and eutrophication with bioerosion by coral-excavating sponges.

The use of incubations was central in this piece of work. Changes in the chemical composition of the water overlying excavating sponges and reef communities indicate the relative contribution of various metabolic processes such as net calcification/dissolution and net respiration/production. However, to first determine the underlying mechanisms of $CaCO_3$ dissolution, the use of fluorescence microscopy revealed that excavating sponges promote $CaCO_3$ dissolution by actively decreasing pH at the sponge/coral interface. The high $[H^+]$ at this site is achieved through delivery

of low-pH vesicles by the etching cells resulting in $CaCO_3$ dissolution. The dissolution of calcite neutralizes the released protons and elevates pH, after which the increased concentrations of Ca^{2+} and HCO_3^- are removed before new acidic vesicles are emptied at the sponge-calcite interface. The mechanism by which Ca^{2+} and HCO_3^- ions are transported away from the site of dissolution will inherently determine the rate at which $CaCO_3$ is dissolved. We tentatively inferred that excess Ca^{2+} may be used to instigate the contraction of conductive cell pathways enabling the transport of $CaCO_3$ chips out of the sponge tissue. The enzyme carbonic anhydrase (CA), which is responsible for significantly increasing the speed of the reversible reaction $H_2O + CO_2 \leftrightarrow H^+ + HCO3^-$, has been shown to be associated to the sponge's etching processes and is therefore thought to play a role in the dissolution of $CaCO_3$. By blocking its activity whilst incubating bioeroding sponges and analysing the rate of dissolution, CA was found to play an important role in speeding up protonation of HCO_3^- ions at the dissolution site, enabling CO_2 to diffuse out of the etching area. CA activity increases at night to overcome the build-up of CO_2 outside the dissolution site due to sponge and symbiont respiration. Excavating sponges that host symbiotic zooxanthellae bore faster into coral skeleton during the day, likely caused by an enhanced CO_2 gradient due to symbiont photosynthesis. Incubations performed under different pCO_2 ranges showed that CA activity is comparable across pCO_2 levels, while chemical dissolution increases as a function of pCO_2. This indicates that although the enzyme can exert a strong influence on dissolution rates, it does not determine the basic $CaCO_3$ dissolution reaction.

At high pCO_2, faster dissolution rates are the result of the reduced ΩAr, with less protons being required to dissolve calcium carbonate. Light-enhanced bioerosion, however, does not occur at high pCO_2 levels, in fact, night-time chemical bioerosion rates become comparable or even higher than day-time rates. This indicates that the acquired energy from photosynthesis does no longer enhance dissolution at high pCO_2 levels. We hypothesise that this could either be explained by 1) both sponge bioerosion and symbiont photosynthesis competing for the same source of dissolved inorganic carbon, or/and 2) the pCO_2 gradient utilised to remove protonated bicarbonate ions cannot be intensified further, even with enhanced photosynthesis, as sponge tissue pCO_2 concentration is too high.

Incubations performed at the community level around Saba and Curaçao yielded net community calcification (NCC) rates which were lower than those reported for reef flats worldwide. In fact, two out of the five 20m reef patch incubations around Saba resulted in net dissolution. Still, Saba coral reefs are considered relatively pristine sites compared to the average within the wider Caribbean. Around Curaçao, incubations on reef assemblages dominated by coral yielded even lower NCC rates. Incubations of

other benthic assemblages that currently characterized shallow Caribbean reef substrate (such as bioeroding sponges, benthic cyanobacterial mats and sand) all resulted in net dissolution. For both Saba and Curaçao, integrating net community production over 24 hours yielded rates that were all skewed towards net respiration, indicating that these study sites were net heterotrophic during the survey period. Results suggest that reef calcification on these sites is barely able to compensate the $CaCO_3$ losses due to dissolution from other opportunistic benthic residents. Events of reef dissolution appear to coincide with shifts to net heterotrophic metabolism. With the ongoing global and local pressures, the delicate balance between $CaCO_3$ accretion and loss is likely to tip. The Caribbean reefs of today give an insight into tomorrow's reefs worldwide, in which community assemblages have changed, structural complexity has lessened and waters are moving away from oligotrophy.

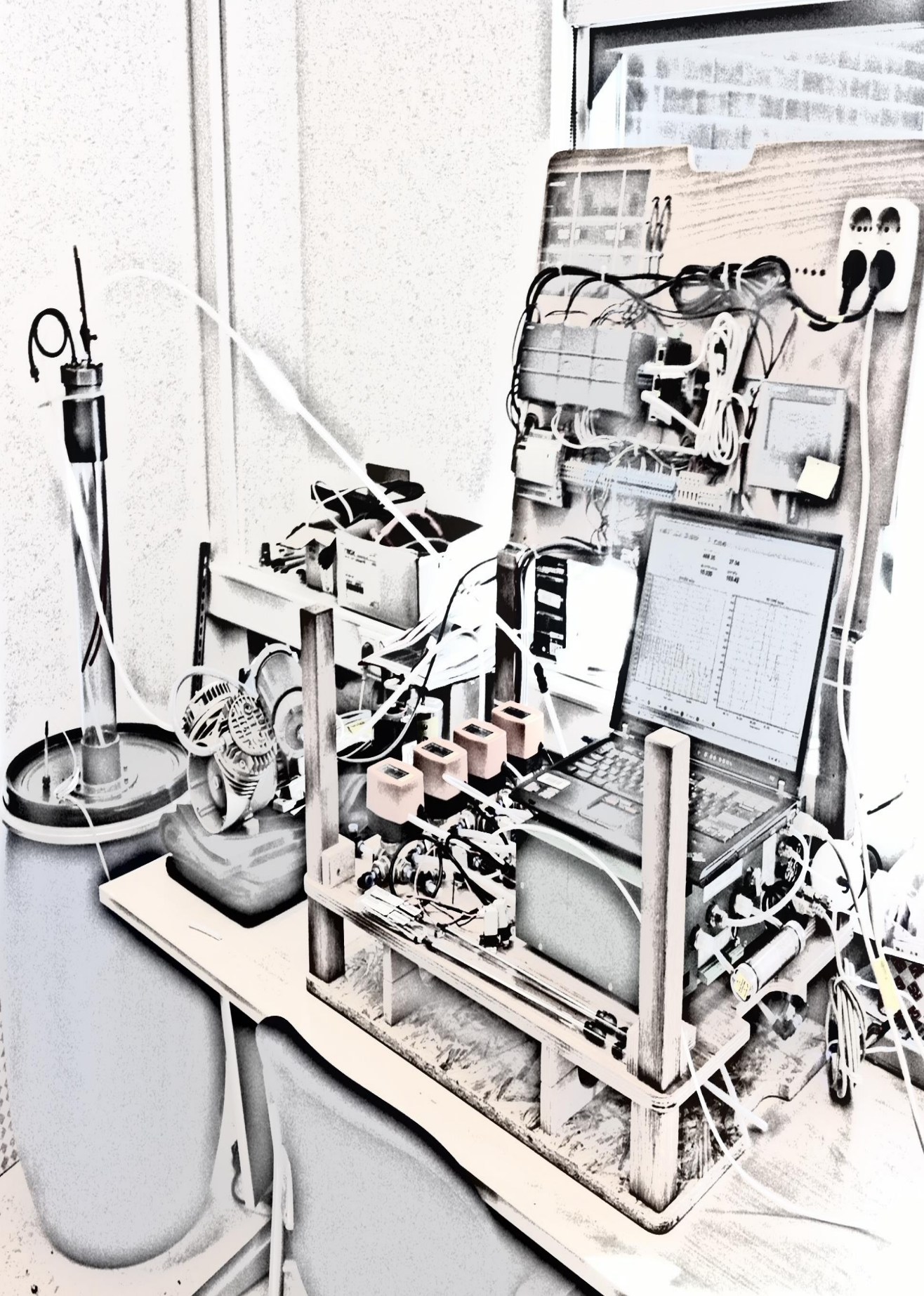

Samenvatting

Voor het voorbestaan van koraalriffen moet de productie van $CaCO_3$ groter zijn dan de erosie om op die manier verticale rifgroei te garanderen. De negatieve impact van zowel wereldomvattende klimaatsverandering (oceaanverzuring en opwarming van het oppervlakte water) als van lokale stressoren (eutrofiëring en overbevissing) op rifaangroei gaat samen met een positief effect van deze ontwikkelingen op de bioeroderende capaciteit van borende euendolithische organismen. Terwijl de effecten van een veranderend milieu op verkalking goed gedocumenteerd zijn, blijft de impact hiervan op bioerosie enigszins onderbelicht. Toch is bioerosie zeer relevant, met name op riffen die al gekenmerkt worden door een lage calcificatie snelheid, aangezien de balans op deze riffen het risico loopt te kantelen naar netto erosie. Aangezien de bedekking van het overgrote deel van de rifvormende koralen binnen het Caribisch gebied en de golf van Mexico in de afgelopen 50 jaar met tot wel 80% is afgenomen, vertonen hedendaagse configuraties weinig gelijkenis meer met dezelfde riffen rond de jaren zeventig. Meer specifiek, zijn er duidelijke veranderingen zichtbaar wat betreft de benthische samenstelling, koraalbedekking en structurele complexiteit. Zand, puin, cyanobacteriën, turfalgen, macroalgen en boorsponzen zijn toegenomen als bodembedekkers ten koste van het verdwijnende koraal. In deze nieuwe omstandigheden, kunnen boorsponzen verantwoordelijk zijn voor tot wel 90% van de totale erosie van koraalriffen door substraatpenetrerende macro-organismen aangezien hun boorsnelheid toeneemt als een functie van pCO_2. Het overkoepelende doel van dit proefschrift was het kwantificeren en uitgebreider interpreteren van de aangroei- en afbraak elementen van koraalrifgemeenschappen met een focus op de interacties van antropogene oceaanverzuring en eutrofiëring op bioerosie door boorsponzen.

De implementatie van incubaties staat centraal in dit boek. Veranderingen in de chemische samenstelling van het de waterlaag boven sponzen en rifgemeenschappen

onthullen de verhoudingen binnen verschillende metabolische processen zoals netto calcificatie/chemische afbraak en netto dissimilatie/ productie. Om echter eerst de onderliggende mechanismen van $CaCO_3$-oplossing te bepalen, bleek uit het gebruik van fluorescentiemicroscopie dat boorsponzen $CaCO_3$-oplossing bevorderen door de pH op het spons/koraal-grensvlak actief te verlagen. De hoge $[H^+]$ op dit grensvlak wordt bereikt door afgifte van blaasjes met een lage pH door etscellen, een proces dat resulteert in $CaCO_3$-oplossing. Op het spons-calcietgrensvlak neutraliseert de oplossing van calciet de vrijgemaakte protonen en verhoogt de pH, waarna de verhoogde concentraties Ca^{2+} en $HCO_3{}^-$ worden verwijderd voordat het zuur uit nieuwe blaasjes wordt geleegd. Het mechanisme waarmee Ca^{2+} en $HCO_3{}^-$ ionen van de plaats van oplossing worden getransporteerd, zal inherent de snelheid bepalen waarmee $CaCO_3$ wordt opgelost. Een voorlopige conclusie van deze thesis is dat het overtollig Ca^{2+} kan worden gebruikt om de samentrekking van geleidende celpaden die het transport van $CaCO_3$-chips uit het sponsweefsel mogelijk maken te initiëren. Het enzym koolzuuranhydrase (CA), dat verantwoordelijk is voor het katalyseren van de omkeerbare reactie $H_2O + CO_2 \leftrightarrow H^+ + HCO3^-$ is aantoonbaar geassocieerd met de etsprocessen van de spons en wordt daarom verondersteld een rol te spelen bij het oplossen van $CaCO_3$. Door de activiteit van CA te blokkeren tijdens de incubatie van boorsponzen en vervolgens het meten van boorsnelheden, hebben we kunnen aantonen dat CA een belangrijke rol speelt bij het versnellen van protonering van bicarbonaat-ionen op de het grensvlak van oplossing, waardoor CO_2 uit het etsgebied kan diffunderen. 's Nachts neemt de CA-activiteit toe om de opeenhoping van CO_2 buiten de oplosplaats als gevolg van spons- en symbiontdissimilatie te boven te komen. Boorsponzen met symbiotische zooxanthellae boren overdag sneller in het koraalskelet dan symbiontloze sponzen. Dit wordt waarschijnlijk veroorzaakt door een gunstigere CO_2-gradiënt als gevolg van fotosynthese door de symbionten. Incubaties uitgevoerd onder verschillende pCO_2- scenario's laat zien dat de activiteit van CA niet verandert, terwijl chemische oplossing wel toeneemt als functie van pCO_2. Dit geeft aan dat, hoewel het enzym een sterke invloed kan uitoefenen op de oplossnelheid, het niet leidend is in het bepalen van de basale $CaCO_3$-oplossingsreactie.

De verhoogde snelheid van kalkoplossing bij een hoge pCO_2 is het resultaat van de verlaging van de ΩAr, hierdoor zijn er minder protonen nodig om calciumcarbonaat op te lossen. Een verhoging van de boorsnelheid overdag komt echter niet voor bij de hogere pCO_2-niveaus, nacht-erosie snelheden zijn in dit geval gelijk of zelfs hoger dan de chemische boorsnelheden die overdag worden gemeten. Onze hypothese is dat dit kan worden verklaard door 1) sponsbioerosie en symbiont fotosynthese concurreren om dezelfde bron van opgeloste anorganische koolstof, en/of 2) de gradiënt in pCO_2 die wordt gebruikt om geprotoneerde bicarbonaationen te verwijderen niet verder

kan worden geïntensiveerd, zelfs niet met verbeterde fotosynthese, omdat de pCO_2-concentratie in weefsel van de spons te hoog is.

Incubaties uitgevoerd op rifgemeenschapsniveau rond Saba en Curaçao leverden netto calcification budgetten van de rifgemeenschappen (NCC) die lager uitkwamen dan eerder gerapporteerde budgetten van rifplateaus wereldwijd. Twee van de vijf rifincubaties op 20 m diepte rond Saba lieten zelf netto afbraak van het rif zien. Desalniettemin worden de koraalriffen van Saba beschouwd als relatief ongerept in vergelijking met de rest van het Caribisch gebied. Rond Curaçao leverden incubaties op koraalriffen gedomineerd door koraal inderdaad nog lagere NCC-snelheden op. Incubaties van andere benthische gemeenschappen die momenteel het ondiepe Caribisch rifsubstraat kenmerken (zoals boorsponzen, benthische cyanobacteriële matten en zand) lieten allemaal netto erosie van riffen zien. Voor zowel Saba als Curaçao leverde de integratie van de netto gemeenschapsproductie over 24 uur snelheden op die wijzen op dissimilatie, wat suggereert dat deze onderzoeklocaties netto heterotroof waren ten tijden van de onderzoeksperiode. De resultaten suggereren verder dat rifgroei door calcificerende organismen op deze locaties de afbraak van $CaCO_3$ als gevolg van erosie door andere meer opportunistische benthische biota nauwelijks kan compenseren. Het lijkt erop dat rifafbraak samen valt met een verschuiving naar een netto heterotroof metabolisme van de rifgemeenschap. Door de voortdurende impact van wereldwijde en lokale stressoren zal het fragiele evenwicht tussen aangroei en verlies van $CaCO_3$ hoogstwaarschijnlijk steeds vaker kantelen ten faveure van netto rifafbraak. Het is de verwachting dat dergelijke ontwikkelingen op de Caribische riffen van vandaag, waarbij rifgemeenschappen zijn veranderd, de structurele complexiteit is afgenomen en water eutrofer is geworden, indicatief zijn voor de wereldwijde riffen van morgen.

Acknowledgements

I would like to thank You. In no particular order. I'll use the power of association. But first! Lennart. In all the surging seas of supervisors, I got you and this was likely the core success of this piece of work. I enjoyed profoundly our many exchanges throughout these years whether they regarded science or any other topic we came to discuss. I am incredibly grateful for the liberty you continuously gave me. From the depth of my heart, brain and liver, thank you. I would also like to start by thanking you Fleur, the Caribbean lady, thank you so much for sharing your insightful knowledge on reefs and sponges with me throughout these years, it was always a breath of fresh air going from my department to your office. Gert-Jan, thank you for your time spent reading and reviewing our manuscripts. I am very grateful for all your comments and remarks that were always delivered with a pinch of wit and humour.

I am also very thankful to the reading committee. Jean Pierre Gattuso, Jasper de Goeij, Karline Soetaert, Jelle Reumer and Jack Middelburg, thank you for reading our work, for your constructive comments and your support.

And now I am sitting near to you Sofia, so I'll start here. My darling Swedish hurricane, you arrived into my office and life at the end of my PhD and I could not have wished for a better second round of officemates. Thank you for your enthusiasm, Swedish self-singing and humour which have made my last moments at NIOZ much more entertaining than I expected. Regarding entertainment, I would also like to thank Siham, my PhD little sister, whose constant energy and undulating movements have kept me awake and on the ball till the end. I will never forget the image of you dressed up as a fish bouncing around the 2018 Christmas ball. About fish, I remember swimming in and out of that gigantic fish mass in Curaçao with me Caribbean babies Inge and Didier. Inge, you are one of my favourite Dutch discoveries (with bitterballen), you are f*****g mad and I love your dark humour that you seem

to only divulge to chosen ones. I am honoured to be one of them. Thank you for all your support throughout these years. Didier, Dids', Desiderius, what a wonderful colleague, friend, ally, you have been these past 4 years. This thesis is a product of our combined effort, and extremely "organised" underwater adventures. I cannot imagine a better partner in crime to work with and of course enjoy oh so many beers. Thank you so much for your unwavering friendship. There is no one I feel happier and safer underwater with. I hope our future work will be filled with ever so more aquatic adventures, rum, laughter and maybe even sponges. On the subject of sponges, I would like to thank the Harbour Branch Institute crew, Shirley, Don, Megan and Stephanie, thank you so much for all those great moments in Florida with you. What an amasingly fun and fruitful collaboration. Shirley, I hope I can remain one of the sponge girls for years to come. Furu, thanks for your support and unconditional help with everything. Still on sponges, thank you so much to the Damsco gang, Jasper, Ben, Martijn and Niklas for all the nice beers, banter and science talk. Science talk has obviously been quite present during these past 9 months and 4 years but not as present as just random non-scientific talking, and for that I cannot go without thanking Esmee, Esmage, my soulmate, such an incredible creature. How many words we have shared. They would probably make a much more riveting book than this one, although probably difficult to publish. I love you. Thank you so much for listening better that anyone I know and providing wonderful advice for every aspect of my life. You are one of the main reasons I feel at home in these lands. I am sure our friendship will never fade even as you become the most recognise artist of the Seven Seas. Vis-à-vis of seas, thank you to the Pelagia crew, Peter, Iwan, Bert, Inno, Jan Dirk for making every cruise such a wonderful expedition. Thank you to all the amasing diving Saba team 2015 and 2018: Erik, Lisa, Frank, Jimmy, Jean Phillip, Brett, Tobia, Ayumi, Janine, Ingrid, Sarah, Kristen, Ewan, Sarah, Sil, Yun, Marin, Myriam, Tamara, Matthijs, Rob, Tuna, Michael, Lodewijk, Bas, Jarnot, Dahlia, Bert, Sherwood. These cruises were a wonderful combination of exploration, hard-core diving and fun. Wonderful memories! A big kiss to Superdiver and Frank for all the great French chat on board. To my French comrade, Julie. Ma doud, what a wonderful exchange we have had in the last 2 years, you trying to organise me, and I trying to de-organise you. We both failed and succeeded beautifully. Your closeness has made me incredibly happy and grateful. Living in Den Helder without you would have been like butter without big fat crystals of salt... Pointless! Love you. Den Helder was also vastly improved by fencing at the KIM with the wonderful Joris, Rob, Peter, Koen, Zoa, Jacob and Bart. Fencing with you guys was such a source of fun and a great way to shake off all PhD related frustrations at the end of the day. Thank you.

I would like to thank the whole OCS department for all the nice coffees, drinks, lunches, dinners and department outings. To the PhD OCS girls, Linda, Ulrike, Eveline, Coral, and the dusty Michelle and Laura, thank you so much for the nice moments in the NIOZ corridors and rare but very entertaining evenings. Thank you to Wim, Luce, Geeert-Jan, Jan-Berend, Piet, Henko, Rob, Rijneke, Peter, Femke, Jan and all the OCS members for making the basis of a great department to evolve but mostly revolve in. On the subject of NIOZ peeps, Bob, da Bob, thank you for all the nice things you twisted, shaped and created in the context of my project. I am so grateful for the help you provided throughout my years at NIOZ. I can also not thank enough Sharyn and Karel, somehow I felt like we were a little team (well especially regarding carbonate chemistry) and for that I am very thankful. You guys helped and supported me so much, every single chapter in this book is the product of our combined work. Thank you for everything. Sharyn, best container ally evaaaaaaa! Thank you for all the great Welsh banter and your sparkle for life (and wine, and gin). I recall all of our moments with much much fondness. Steven, I wonder what chapter titles I would have had if you would not have taken this job (well half of it). I learned so much from you and I enjoyed every single moment we spent together in the lab/container/office/bar/boat/water. Most importantly, thank you for making me discover "Tuinslang" by Donnie. It changed my life and the life of many others. A massive thank you to Rick for all our nice moments whether they were at NIOZ or outside playing, around the world, in your "van" Frans and later in van Damme with Céline. I would like to also thank Matthijs for the few but lovely moments we shared and mainly for making me discover the existence of E-Life and Sci Hub, which have become indispensable to me. Thank you to the MMB girls Zeynep, Laura, Marijke, Clara, Christine, Saara, Diana and Sigrid for all our enjoyable encounters at NIOZ and in bars. A special thank you to Darci, Nicole and Yvo for all the laughter, good mood and very fun nights. Also Gabs', for all our drunken steps into PhDhood together, thank you for those great moments. I would also like to thank the NIOZ workshop, you guys were essential in developing all the equipment that escorted me throughout my fieldwork. Johan and Roel, thank you so much for your help and humour. A big thank you to the bird boy and girls as well, Jan, Suzanna and Irene for the few but enjoyable drinks and chats we had.

These PhD years were punctuated by wonderful fieldwork intermezzos, mostly in the Caribbean. I recall with much enjoyment my time at Carmabi with the gang, Valerie, Thomas, Bert, Mark, Kelly, Kristen, Megan, Roy, Lisanne, Jeroen, Friso and Lisette, thank you for making it so much fun. Lucas, my smiling-eyed rapping yoga mousquetaire, you were a wonderful encounter, thanks for all the laughing. I know many many beers are still to come in your beautiful company. Michelle and Renee,

thank you for your everlasting hospitality and great banter. Needless to say, you are welcome wherever I randomly land. The time in Statia was also very memorable and for that I would like to thank Johan and Masru. Gernot and Jelle, learning to catch Foraminifera in both Statia and Curacao with you guys was brilliant, thanks a lot for giving me the opportunity to join your Foram team.

I would like to finish by thanking my family and old friends, the geographical distance between us has certainly not impaired your caring and good vibes. Antoine, Pioupiou and Raf thank you so much for all the flute, Catan, wonderful cocktails and dreams from youth to present. I love you guys. Theus, mon chou, your support and kindness has warmed me up since I can remember. Thank you for always challenging my thoughts and ideas and encouraging me to think further.

Olga, Henri, Madeleine, Peter, Ralf and Bernadette thank you for enabling Julie and I to carry out many writing retreats in your little French paradise and for all your loveliness.

Julia and Ian, I see you both way to little but every time it's bloody great. Thank you to the St Andrews crew, Mali, El Chamb, Fenner, Hannah, Judith, Lea, Tackler, Callum, Beth, Bella and German Hannah, for always welcoming me at every gathering and for all the absolutely fabulous banter and games. Symke, our renewed friendship has meant the world to me, thank you for your insight and sympathy. Master MER peeps, Didi, Lucas, Cyril, Erwan, PO, Eva, Celine, thank you so much wherever you are for the many adventures we have had together and for all of those to come.

Mum and Dad thank you so much for having shared with me your love and passion for every little thing that makes life awesome, whether it is bees, Ian Dury, flowers, spiders, home grown vegetables, tunicates, good food, Chelsea, good wine and most importantly good friends. Thank you for inspiring me to simply follow my feet. Laura, thank you for your support and wisdom during my time in the Netherlands and always welcoming me into your home. Elsa, thank you for letting me into the secrets and the pleasures of a non-academia driven life and all your kind and supporting chat. Guillaume thanks for always putting beers in your fridge when you knew I was coming to visit, that means the world to me! Robin, thank you so much for the cover of this thesis, I really love it! Burny, merci a toi, Florence, Caroline et Gwenn for all the love you have given our family since Jane and Dennis moved to France. The wonderful times spent in your company by the sea was at the origin, I am sure, of my desire to never venture too far away from the ocean and for that I am eternally grateful.

Lastly, thank you to all my girls from home, Alice, Camille, Julie, Mathilde, Marthe and Sophie, for our beautiful little alliance ;) and absolutely unforgettable times we have had together ranging from youth till present. You are all indisputably mad. Thank you.

About the author

Alice Webb was born and raised in Rennes, France. Her youth in Brittany was punctuated by eating crab and sometimes while watching *Free Willy*. This synergistic experience is likely to have been at the origin of her desire to study the aquatic world. This she did in Scotland, at the University of St Andrews, where she obtained an honours BSc degree in Marine biology (2010) and her first experience, as well as her last, with deep-fried Mars bars. She pursued her studies in the shape of a joint European Masters at the universities of Bordeaux, Bilbao and Southampton and acquired an MSc in Oceanography in 2012. During her BSc, Alice studied the decline of grey seal population in Great Britain since the 1950s as a function of their proximity to fisheries. She had hoped to study orcas but far more punctual students got there first so she settled for seals. During her MSc, Alice conducted a project on the seasonal biochemical variations in the Bay of Villefranche sur Mer, leaving the marine mammal world for good through the realisation that *Free Willy* already kind of said it all. In 2013, she went on to work as a research assistant on the project eFOCE (European Free Ocean Carbon dioxide Enrichment Experiment) where she developed an online platform to view continuously generated data from underwater mesocosms. Following this job, she worked on Heron Island, Australia with the University of Queensland on coral physiology and ocean acidification. In 2015, Alice started her PhD at NIOZ (Royal Netherlands Institute for Sea Research) where she investigated rates and mechanisms of coral dissolution by bioeroding sponges and reef communities. During this period, Alice led three projects in the Dutch Caribbean (at CNSI, St Eustration and Carmabi, Curaçao) and one project at the Harbour Branch institute in Florida. She also participated to three scientific cruises aboard the Pelagia and two scientific diving cruises aboard the Caribbean Explorer II.

List of publications

Webb, A. E., Pomponi, S. A., van Duyl, F. C., Reichart, G. J., and de Nooijer, L. J. (2019). pH Regulation and Tissue Coordination Pathways Promote Calcium Carbonate Bioerosion by Excavating Sponges. *Scientific reports*, 9(1), 758.

Webb, A. E., van Heuven, S. M., de Bakker, D. M., Meesters, E., van Duyl, F. C., Reichart, G. J., and de Nooijer, L. J. (2018). In-situ incubation of a coral patch for community-scale assessment of metabolic and chemical processes on a reef slope. *PeerJ*, 6, e5966.

De Bakker, D. M., **Webb, A. E.**, van den Bogaart, L. A., van Heuven, S. M., Meesters, E. H., and van Duyl, F. C. (2018). Quantification of chemical and mechanical bioerosion rates of six Caribbean excavating sponge species found on the coral reefs of Curaçao. *PloS ONE*, 13(5), e0197824.

Webb, A. E., van Heuven, S. M.A, de Bakker, D. M., van Duyl, F. C., Reichart, G. J., and de Nooijer, L. J. (2017). Combined effects of experimental acidification and eutrophication on reef sponge bioerosion rates. *Frontiers in Marine Science*, 4:311.

Under review or in preparation for submission

Webb, A. E., de Bakker, D. M., da Costa, T. van Heuven, S. M., van Duyl, F. C., Reichart, G. J., and de Nooijer, L. J. Carbonate dissolution mediated by key benthic communities on a degrading coral reef. *(in prep.)*.

Webb, A. E., de Bakker, D. M., van Heuven, S. M., van Duyl, F. C., Reichart, G. J., and de Nooijer, L. J. Diurnal Variability in Carbonic Anhydrase Activity for CaCO3 Dissolution by Excavating Sponges. *(In review at the Journal of Experimental Biology).*

De Goeyse, S., **Webb, A. E.**, Reichart, G. J., and de Nooijer, L. J. Carbonic anhydrase is invilved in benthic foraminiferal calcification. *(In review at Biogeosciences).*

De Bakker, D. M., Van Duyl, F. C., De Froe, E., Velila, E., Zanke, F., Nietzel, S., Piek, S., Veillat, S. J., Scholten, Y. J. H., Meijs, R., **Webb, A. E.**, and Meesters, E. H. Temporal consistency and spatial variability on the shallow reefs of Bonaire. *(in prep.).*

'Mourir pour des idées l'idée est excellente
Moi j'ai failli mourir de ne l'avoir pas eue
Car tous ceux qui l'avaient, multitude accablante,
En hurlant à la mort me sont tombés dessus.
Ils ont su me convaincre et ma muse insolente
Abjurant ses erreurs se rallie à leur foi
Avec un soupçon de réserve toutefois,
Mourons pour des idées, d'accord, mais de mort lente
D'accord, mais de mort lente.'

G. Brassens, 1972